2012

Apatite U-Th/He Thermochronometry in Slowly Eroding Landscapes: Addressing Age Dispersion to Understand Appalachian Topographic Development

Ryan Edward McKeon
Lehigh University

APATITE U-Th/He THERMOCHRONOMETRY IN SLOWLY ERODING LANDSCAPES: ADDRESSING AGE DISPERSION TO UNDERSTAND APPALACHIAN TOPOGRAPHIC DEVELOPMENT

by

Ryan Edward McKeon

A Dissertation

Presented to the Graduate and Research Committee

of Lehigh University

in Candidacy for the Degree of

Doctor of Philosophy

in

Earth and Environmental Sciences

Lehigh University

May 21, 2012

Approved and recommended for acceptance as a dissertation in partial fulfillment of the requirements for the degree of Doctor of Philosophy

Ryan Edward McKeon

Apatite U-Th/He Thermochronometry in Slowly Eroding Landscapes:
Addressing Age Dispersion to Understand Appalachian Topographic Development

April 16th, 2012

Defense Date

Dissertation Director
Dr. Peter K. Zeitler

Approved Date

Committee Members:

Dr. Frank J. Pazzaglia

Dr. David J. Anastasio

Dr. Peter W. Reiners (external)

ACKNOWLEDGMENTS

The research that is presented in this dissertation was the product of numerous contributions from many people and in no way represents a solitary quest by me.

This research would not have been possible without the financial support from a Geological Society of America Student Research Grant and multiple Palmer Research Grants from the Department of Earth and Environmental Sciences. Additionally I never would have had the opportunity to build collaborations with some of the people mentioned below if I did not receive additional support from the Department of Earth and Environmental Sciences to travel to many conferences during my tenure here at Lehigh University.

To my advisor Peter, I am grateful for the freedom and encouragement he provided to explore ideas and for building collaborations with other members of our scientific community. His tolerance of my inability to hit self-imposed deadlines and not comment or read me the riot act was impressive, but also taught me that the motivation needs to come from within, which is something any procrastinator must address at some point. From Frank I learned the true meaning of what a testable hypothesis really is, a clarifying view of scientific exploration that has and will continue to benefit me greatly as I move forward. I also would be remiss if I did not acknowledge the many hours of his time that I took with my classic leading question "Do you have a hot second"?

To my colleagues in the trenches of grad student life, I am eternally indebted for helping me maintain a healthy dose of the seemingly paradoxical combination of self-

confidence and humility that guides us all through the various stages of the game we call grad school. Specifically, I would like to thank the members of STEPS 580, Jo, Alex, and Michael for tolerating my wild swings between confidence and self-doubt, my tendency to offer my two-cents when it was not requested nor appreciated, and generally helping me maintain some form of sanity during a process that was more difficult than I might have previously appreciated. A special nod goes to Julie for always appearing to have her eyes on the prize and in so doing, motivating the competitive side of me to not let her graduate with out me doing the same. I still owe Chris B. a six-pack for holding my hand through the early stages of learning MATLAB and for all of my annoying "short" questions that I have asked him since.

My quality of life in the department has been greatly enhanced by the ability of Nancy and Laura to tolerate my goofy questions and poor attempts at organization along with my general ability to waste their time… many thanks guys.

I will be forever impressed by the ability of Bruce Idleman to keep a straight face as he learned of my latest attempt at destroying the lab facilities he so carefully built. I truly am not sure how he does it. I would also like to thank the people who allowed me visit and work in their labs during my time here at Lehigh. Thank yous go Peter Reiners, David Shuster, and Ken Farley for allowing me to invite myself to their worlds and play with their toys.

Outside of Lehigh and the world of thermochronology, I would like to acknowledge the sage-like advice, commiseration, and great friendships of my fellow Ph.D. aspirants Daniel Chaffee and Charles Rathkopf, not to mention the excursions to the mountains. To my family, I can never really articulate how much their unyielding

support and encouragement has helped me along this road, without them I simply would not have been able to do this. Finally, I am forever grateful for the generosity and tolerance of Tricia, whom listened to me whine about all of the little mundane problems as though they were titanic struggles and never pointed out that she was getting her degree and working full-time to boot… Sanders and my life have been better for her efforts and understanding.

TABLE OF CONTENTS

LIST OF FIGURES

LIST OF TABLES

ABSTRACT

The persistence of rugged topography and considerable relief in the Appalachian Mountains of eastern North America is difficult to explain in the context of an old and long-decaying mountain range. Despite an influential history of tectonic and geomorphic investigation an explanation of the drivers of long-term evolution of the Appalachian landscape has remained elusive. Along their length, the relationship between bedrock geology, tectonic history, and relief varies widely, suggesting that the modern topography is decoupled in space and time from the collisional orogenies of the Paleozoic and rifting in the Mesozoic. This dissertation addresses the use of U-Th/He thermochronometry on the mineral apatite to constrain the low-temperature cooling history of the Appalachian region in order to understand the processes responsible for the long-term preservation or rejuvenation of the Appalachian landscape.

Chapter 1 addresses the problem of intra-sample age dispersion in apatite U-Th/He thermochronometry, which is frequently encountered in slowly eroding regions like the Appalachians. Using protocols developed for grain abrasion it was found that the sources responsible for causing the age dispersion could be mitigated or deciphered in the context of other acknowledged sources. One such source is radiation damage, which impedes He diffusion and results in the ages of different grains from the same sample being dependent on the cooling rate and the grain specific concentration of U and Th. In Chapters 2 and 3 I use different sampling techniques to explore the low-temperature thermal history information that the age dispersion caused by radiation damage provides to address pace and variability of erosion throughout the Appalachian landscape. This

research gives the first evidence of unsteady erosion of the southern portion of the range and in so doing suggests a more nuanced history that until now has not been detectable through other geochronological tools.

CHAPTER 1

Effects of physical and chemical abrasion on AHe thermochronometry

Ryan E. McKeon*
Peter K. Zeitler
Bruce D. Idleman

Department of Earth and Environmental Sciences, Lehigh University, Bethlehem, PA 18015
* rem208@lehigh.edu

For Submission to *Geochimica et Cosmochimica Acta*
Keywords: U-Th/He Thermochronometry, Abrasion, Apatite, Zonation, Age Dispersion

CHAPTER ABSTRACT

Intra-sample age dispersion in apatite U-Th/He thermochronology that exceeds analytical uncertainty of laboratory measurements can be caused by a number of factors, making the identification and mitigation of a single or combination of sources of dispersion difficult using the standard analysis protocol. We explored the use of grain abrasion as a means of addressing observed dispersion using rapidly cooled samples from sediment cores collected offshore from Bermuda and slowly cooled samples from Proterozoic gneiss from western North Carolina in the southern Appalachians of eastern North America. We removed a minimum of 25 μm from the surface of individual apatite grains physically using an air abrasion cell and experimented with a potentially more efficient chemical abrasion protocol using dilute nitric acid. Using our established protocols, we found that chemical abrasion replicated the positive effects of physical abrasion for the Bermuda samples, which are known from previous studies to suffer from He implantation from external sources. For the slowly cooled Appalachian samples, abrasion by both methods did not significantly decrease age dispersion, however, it uncovered a 5X greater range of eU concentrations (eU = [U] + 0.235*[Th]) than was observed for untreated grains, which we interpret as evidence of sometimes severe, but not pervasive core-rich zonation of U and Th. We show how core-rich zonation of this magnitude can produce wide age dispersion with no correlation to eU concentration if the whole grain is analyzed using standard AHe protocols. We illustrate that useful and compelling low-temperature thermal history information can be derived from the eU-age relationship of the abraded grains by exploiting the age dispersion using known effects from radiation damage. We

argue that for datasets that suffer from age dispersion, grain abrasion by either method provides an effective and rapid means to assess the sources of age dispersion without resorting to time and resource-intensive studies that are unrealistic to apply to a large sample suite.

1.1 INTRODUCTION

Apatite U-Th/He thermochronometry (AHe) is a low-temperature thermochronometer widely applied by investigations interested in processes affecting the uppermost few kilometers of the crust. (e.g. House et al., 1998; House et al., 2002; Reiners et al., 2003; Ehlers et al., 2006; Stock et al., 2006; Berger et al., 2008; Flowers et al., 2008; Ault et al, 2009) As use of the technique has increased, so too has the number of studies reporting dispersion of data that exceed the analytical uncertainty of the laboratory measurements. Commonly this problem is associated with samples from regions with very slow cooling histories resulting from low long-term erosion rates in cratonic or stable continental margin settings (Belton et al., 2004; Spotila et al., 2004; Green et al., 2006; Fitzgerald et al., 2006; Danišík et al., 2008), however, rapidly cooled samples have also illustrated similar issues (Spiegel et al., 2009).

The proposed sources of age dispersion in AHe thermochronology fall into three categories: 1) internal and external impurities, 2) assumptions about U, Th, and Sm homogeneity, and 3) kinetic complexities and have been thoroughly reviewed by Farley (2002), Ehlers and Farley (2003), and Fitzgerald et al. (2006). The reality is that these

problems can occur in combination, making identification and mitigation of the sources of age dispersion difficult when using the standard analysis protocols (e.g. Farley, 2002). Grain size reduction through abrasion can address several potential sources of age dispersion. The removal of the outer portion of the grain prevents contamination from helium implanted into the grain from external sources as explained by Farley (2002) and illustrated by Spiegel et al (2009). Additionally, analysis of the abraded cores of apatite grains in conjunction with untreated grains from the same sample gives an indication of the variability of U, Th, and Sm zonation, which is unknown following traditional analysis protocols.

Following from the demonstration of the benefits of grain abrasion in reducing age dispersion (Danišík et al., 2008; Spiegel et al., 2009), we present protocols for physical and chemical abrasion of apatite for the controlled reduction of grain size. We present results from chemical abrasion of Durango apatite, an accepted age standard, and rapidly cooled apatites from the Bermuda Rise (Spiegel et al., 2009) to test the validity of this technique. We then apply both techniques to slowly-cooled apatites from the southern Appalachians that demonstrate the kind of problematic age dispersion that does not correlate specifically to any one source, similar to the observations of other studies from regions characterized by slow long-term erosion rates. Using these methods we demonstrate that abrasion can be an effective and easily implemented tool that for some samples can reveal the causes of age dispersion and potentially extract added constraints on low-temperature thermal histories.

1.2 SAMPLES

We conducted experiments on both chemical and physical abrasion. To test chemical abrasion as a means of grain-size reduction, we conducted experiments using an accepted analytical standard (Durango apatite) as well as samples from sediment cores from the Bermuda Rise for which physical abrasion has been documented to decrease age dispersion (Spiegel et al., 2009). Durango apatite has a simple, rapid, and well constrained cooling history that is bracketed through $^{40}Ar/^{39}Ar$ dating of feldspars from volcanic rocks that date the emplacement of the Durango apatite deposit at 31.44 ± 0.18 Ma (2σ) (McDowell et al., 2005). Although it is used as an analytical standard, Durango apatite has an unusually high Th/U ratio and also documented heterogeneity of U and Th concentrations (Boyce and Hodges, 2005). Aliquots of Durango apatite used for chemical abrasion experiments were taken from our lab age standard supply, which are 180 – 220 μm internal shards derived from a single large crystal. To test our chemical and physical abrasion protocols we used the same apatite separates as Spiegel et al. (2009). These samples from the Bermuda Rise were derived from DSDP leg 43, site 386, located about 140 km southeast of Bermuda. The apatites were collected from turbiditic sandstones at a burial depth of less than 200 m with vitrinite reflectance and fission track length analysis giving no evidence for significant reheating following deposition (Spiegel et al., 2009). The apatites are volcanic in origin and are thought to have experienced rapid cooling, transport, and burial. Thus the AHe age should be equivalent with the stratigraphic age of the two turbidites used in this study: 43-2 (26.5 ± 3.5 MA) and 43-3 (29.5 ± 2.5 Ma) determined though calcareous nannoplankton (Okada and Thierstein,

1979). Spiegel et al. (2009) found large age dispersion and generally too-old ages from untreated grains that were corrected for He ejection (resulting from the energetic decay of U, Th, and Sm) using the F_T correction (Farley et al., 1996), whereas uncorrected physically abraded grains yielded ages that fit the geologic constraints and had much lower dispersion. They interpreted these results to illustrate that the low concentration of U, Th, and Sm (henceforth collectively referred to as effective uranium or eU, where eU = [U] + 0.235[Th] (Shuster et al. 2006)) of the apatites made them susceptible to contamination from implanted He making F_T corrected ages too old, the effects of which were mitigated through physical abrasion.

We also used apatites from the southern Appalachian bedrock to explore abrasion as a means of identifying the sources of age dispersion in regions characterized by slow cooling. During slow cooling, ages become dispersed between different aliquots that experienced the same thermal history as a result of variations in grain size (Farley, 2000; Reiners and Farley, 2001) and diffusion kinetics from the accumulation of radiation damage as a function of the eU concentration (Shuster et al., 2006; Flowers et al., 2009). These characteristics impact age dispersion when the sample is in the Partial Retention Zone (PRZ), where the transition from complete diffusive loss to total retention of He is made between ~40 – 80˚C (Stockli et al., 2000). The rate at which a sample is exhumed through the PRZ dictates the amount of age dispersion that will occur as a result of these combined effects, which has been successfully exploited to constrain low temperature cooling histories in regions of slow cooling (Flowers et al., 2007; Flowers, 2009; Flowers and Kelley, 2011).

We focused on two samples derived from Proterozoic gneiss of North American affinity that outcrops in the rugged topography of western North Carolina. These samples were collected as part of a broader investigation aimed at constraining the exhumation history of the highest and most rugged portion of the southern Appalachians, the results of the broader dataset and the geologic implications this work will be discussed a separate article (McKeon et al., - Chapter 2). Apatite fission track ages from the region suggest steady slow cooling corresponding to a long-term average exhumation rate of ~20 m/Myr (Naeser et al., 2004). The samples discussed here represent end-member locations in the modern landscape, a ridge top sample (SY-2) from Waterrock Knob at 1775 m and a valley bottom sample (SY-13) near the Little Tennessee River at 512 m. Multi-grain AHe ages for both samples produced extreme age dispersion (McKeon et al., - Chapter 2). For SY-2, ages ranged from 111 to 183 Ma (n = 4); for SY-13, ages ranged from 89 to 131 Ma (n = 6) with neither sample displaying any correlation to acknowledged kinetic complexities or the presence or absence of inclusions when using more rigorous hot HF dissolution protocols typically reserved for zircon digestion, motivating this exploration of grain abrasion to address the causes of age dispersion.

1.3 METHODS

1.3.1 Abrasion Protocols

1.3.1.1 Physical Abrasion: Physical abrasion was carried out using a stainless steel air abrasion chamber similar to the design of (Krogh, 1982) with several milligrams of 220-grit aluminum oxide added for abrasive media. Abrasion of greater than one alpha stopping distance of the outer portion of the grain removes the potential contamination of helium implantation from external sources and the need to correct the resulting age for helium loss through alpha ejection. Grain size reduction during abrasion was calibrated by abrading grains individually and documenting the size reduction of the three principle grain axes through measurement using digital images. During abrasion, grain morphologies evolved from hexagonal prisms to oblate ellipsoids, with the original long axis experiencing the greatest reduction in size and the overall volume loss from pre-abrasion to post-abrasion being 85% ± 3.3 (1σ, n = 11). Tracking the location of inclusions relative to the grain surface during abrasion suggests that grain size reduction is uniform for each individual grain axis, such that both sides of the same axis are abraded equally, though the different axes experience different amounts of total size reduction (Figure 1.1). It was found that the speed of grain size reduction was strongly dependent on the air pressure, however, similar abraded grain morphologies resulted from both slow (1 psi for 65 min) or fast (3 psi for 6 min) abrasion protocols. It should be noted that the protocol necessary for the confident removal of at least one alpha stopping distance from a grain will be specific to the individual abrasion chamber and

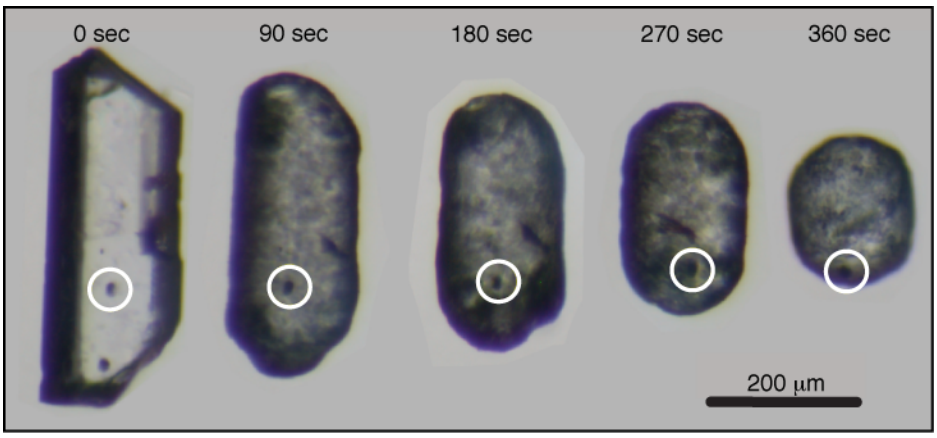

Figure 1.1: Images showing the evolution of grain size and morphology of a single grain as a result of physical abrasion. The time above each image reflects the cumulative duration of abrasion to that point. The white circle tracks the location of a single mineral inclusion within the grain and illustrates that the reduction in grain size through physical abrasion is uniform for each individual grain axis, such that both sides of the same axis are abraded equally, though the different axes experience different amounts of total size reduction. This grain is from Bermuda sample 43-2 and was not dated.

thus must be calibrated for effective application of the abrasion technique. For specific details on how we calibrated grain size reduction see Appendix A1. Once the conditions for grain size reduction were calibrated to remove a minimum of 25 μm from both sides of the three principle axes, grains from an individual sample were abraded in batches of up to 15 grains. Not all grains survived the abrasion process; we suspect this is a result of grains breaking up along fractures or partings that were not visible during the optical selection process.

1.3.1.2 Chemical Abrasion: We experimented with using weak nitric acid as a potentially less labor-intensive and more reproducible means of achieving the necessary grain size reduction. Published dissolution rates from digestion of Durango apatite (Guidry and Mackenzie, 2003) were used as a starting point for calibrating the necessary temperature and duration of immersion to attain the desired abrasion extent. In an effort

to achieve a uniform reduction in grain size we used a weak 1:1000 nitric acid solution (pH ~1.8, 0.0158 M) to slow chemical attack of the grain surface. Repeated single-grain trials indicated that immersion in 10 mL of 1:1000 nitric acid solution at 50˚C for 4.25 hours (stirring every 45 min) resulted in greater than or equal to the necessary grain-size reduction of 25 μm from all three axes of the grain. To maintain the temperature and prevent evaporation of the acid solution, beakers containing the grains and acid solution were covered with aluminum foil and placed in a convection oven set to 50˚C. During these calibration trials the post-abrasion surface texture of grains from different samples varied widely (Figure 1.2), however, the extent of grain size reduction was found to be relatively consistent. Exactly what causes the variation in surface morphology following chemical abrasion is beyond the scope of this investigation, however we speculate that it could be related to eU concentration, dislocation density in the crystal lattice, or other grain specific characteristics such as chemical composition. Similar to our implementation of physical abrasion, grain size reduction was calibrated using single grains and then once the protocol for reproducibly removing 25 μm from all axes was established we chemically abraded grains in batches of up to 15 grains.

1.3.2 AHe Thermochronometry

For all samples analyzed in this study, grains were selected for AHe analysis using standard optical selection criteria (e.g. Farley, 2002; Ehlers and Farley, 2003) to be free of inclusions, fractures, and grain coatings, and when possible, euhedral prior to any

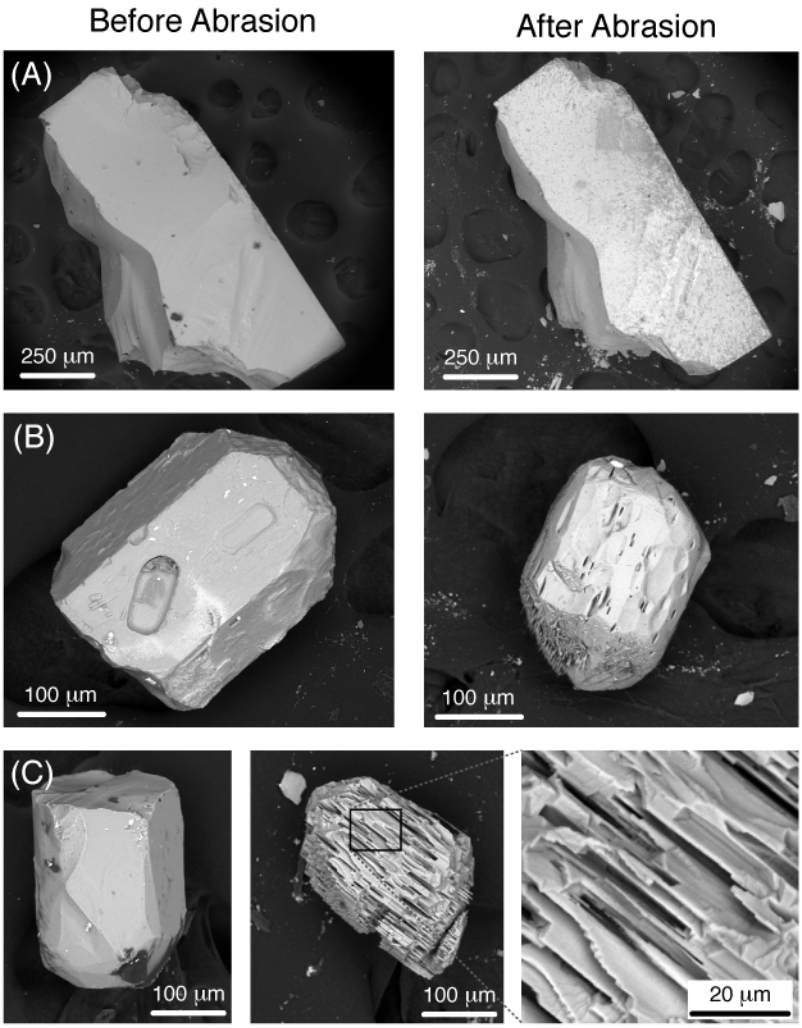

Figure 1.2: Before and after electron backscatter images illustrating the range of surface textures that resulted from chemical abrasion of apatite. These images were collected from grains used during the calibration process and were not used in this study. The abrasion conditions were very similar for these three grains and the extent of grain-size reduction was also quite similar. (A) Large shard of Durango apatite that experienced grain-size reduction from chemical abrasion while showing little change to surface texture. (B) Large grain from crystalline basement gneiss from southwestern Colorado showing relatively little change in surface texture with extensive grain size reduction. (C) Medium grain from diorite sample from northern Pakistan near Nanga Parbat showing an extreme change in surface texture with extensive grain size reduction. Black box shows the location of the higher magnification image of the pitted surface texture.

abrasion treatment. For Durango apatite, we chose internal shards from our lab age standard supply based on geometry, preferring blocky shapes to blade-like shapes in an attempt to decrease the chance of losing any portion of the shard due to breakage during handling between the multiple steps of the analysis. For the Bermuda rise samples, we obtained apatite separates used by Spiegel et al. (2009) and chose individual grains based on standard selection criteria. For the Appalachian samples, apatites were separated from bedrock samples using traditional crushing, sieving, magnetic, and density sorting techniques. Apatites from these samples contained abundant mineral inclusions and grains were picked under isopropyl alcohol or refractive oil to assist in identifying grains of suitable clarity for dating. Subsets of selected grains from all three samples were chemically abraded following the protocol outlined above. Similarly, a subset of selected grains from the Bermuda and Appalachian samples were physically abraded following our protocol. Untreated grains from all three sample pools were analyzed as a control to observe the affect of abrasion. Abraded and untreated grains from all samples were loaded individually in Nb micro-tube carriers for He, U, Th, and Sm analysis. Sample preparation and He analysis was conducted at the Noble Gas Geochronology Lab at Lehigh University and U, Th, Sm analysis was conducted at the Arizona Radiogenic Helium Dating Lab at the University of Arizona or the Caltech Noble Gas Laboratory (as indicated on Tables 1.1 – 1.3). Further discussion of analytical methods for measurement of He, U, Th, and Sm, calculating the F_T correction, and eU concentration are described in Appendix A2.

1.4 RESULTS

1.4.1 Chemical Abrasion Calibration

Figure 1.3 and Table 1.1 show how chemical abrasion of internal shards of Durango apatite systematically produced younger ages with higher Th/U ratios than untreated shards that were run as age standards throughout this experiment. Chemically abraded shards of Durango yielded ages ranging from 26.36 to 31.22 Ma (n=16; mean of 28.50 ± 1.42 (all errors and standard deviations reported are 1σ unless otherwise indicated)) Ma and Th/U ratios ranging from 21.0 to 24.0 (mean of 22.60 ± 1.05). By comparison, 15 untreated shards dated during the chemical abrasion experiment yielded ages from 30.49 to 32.63 Ma (mean of 31.52 ± 0.69 Ma) with Th/U ratios from 18.6 to 21.6 (mean of 20.23 ± 0.89).

For the fast-cooled samples from Bermuda, our analysis of untreated, physically, and chemically abraded grains replicate the results of Spiegel et al. (2009), where ages from abraded samples (by either method) show decreased age dispersion and are more plausible given geologic constraints (Figure 1.4 and Table 1.2). Note that ages for all abraded grains reported herein are not corrected for alpha loss with the F_T correction because of the removal of the portion of the grain where ejection is possible. For simplicity, we combine the published data from Spiegel et al. (2009) with our datasets of untreated and physically abraded aliquots for comparison to the chemically abraded grains for both samples. For sample 43-2 the stratigraphic age is 26.5 ± 3.5 Ma and the

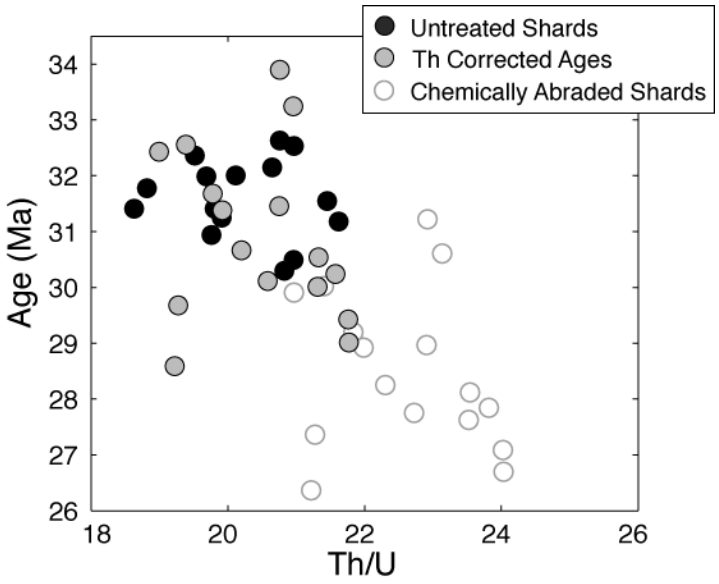

Figure 1.3: Results of chemical abrasion of Durango apatite. The plot shows the relationship between the measured Th/U ratio and age for chemically abraded shards of Durango apatite (open circles) compared with untreated shards (black circles) analyzed as analytical standards during the chemical abrasion experiment. This plot illustrates how chemically abraded shards are systematically enriched in Th and produce younger ages than the untreated shards. When this Th enrichment is corrected for (gray circles – see discussion (1.5.1) for description of the correction), the Th/U ratios and ages become more consistent with the accepted age of Durango apatite. Error bars are not visible because the uncertainty is smaller than the size of the symbols.

means of untreated, physically abraded, and chemically abraded aliquots were 35.80 ± 3.68 Ma, 31.90 ± 5.96 Ma, and 27.54 ± 4.08 Ma respectively. For sample 43-3 the stratigraphic age is 29.5 ± 2.5 Ma and the means of untreated, physically abraded, and chemically abraded aliquots were 33.64 ± 4.86 Ma, 28.56 ± 1.72 Ma, and 28.34 ± 0.66 Ma respectively, with one young and geologically implausible outlier removed from the chemical abrasion pool. For both samples chemical abrasion successfully replicated the results of physical abrasion and resulted in ages that fit the presumed geologic history.

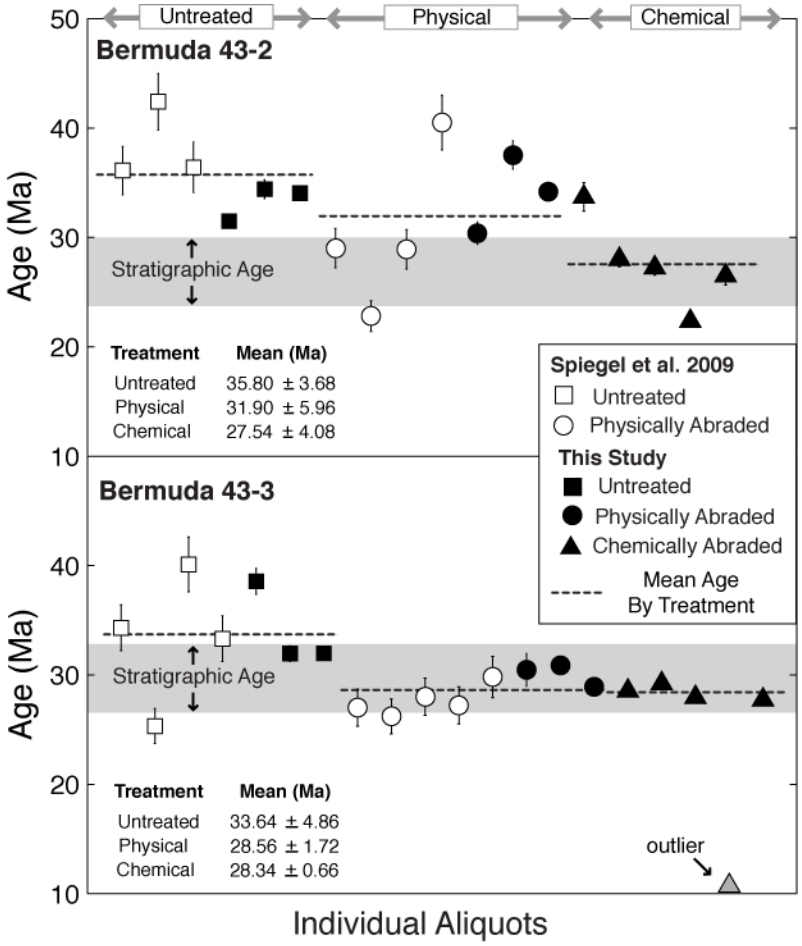

Figure 1.4: Results of physical and chemical abrasion from this study (filled symbols) compared with Spiegel et al. (2009) (open symbols) of two samples of volcanic apatites from turbidite deposits from offshore of Bermuda. For both samples, chemically abraded grains replicate the results from physically abraded grains where AHe ages are younger than untreated grains and fall within the range of the stratigraphic age of the unit they were derived from. (A) Results from sample 43-2 where more dispersion was found in physically abraded grains versus chemically abraded grains which correlate with the stratigraphic age. (B) Results from sample 43-3 where both physical and chemical abrasion drastically decrease age dispersion and fit well with the stratigraphic age. Where error bars are not visible, the uncertainty is smaller than the size of the symbol.

1.4.2 Appalachian Samples

Figure 1.5 and Table 1.3 summarize the results of nearly 80 aliquots from our attempts to understand the sources of age dispersion through physical and chemical abrasion of two

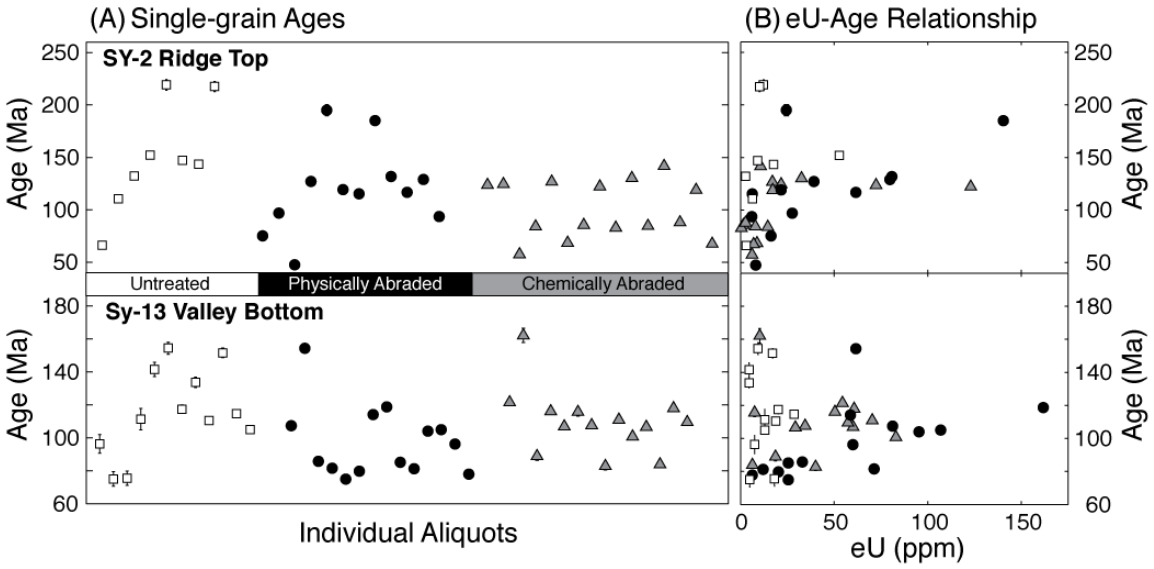

Figure 1.5: Results of untreated (open squares), physically (black circles), and chemically (gray triangles) abraded grains from two slowly cooled samples from the Southern Appalachians of western North Carolina. Panel A illustrates the wide age dispersion observed from untreated and abraded single-grain aliquots from samples SY-2 and SY-13 (note the different vertical scales for the two samples). Error bars represent the 1σ analytical age uncertainty for each aliquot, where error bars are not visible the range of uncertainty is smaller than the symbol. Panel B shows the eU-age relationship for all the aliquots presented in panel A for both samples. Of particular note is the generally low eU and lack of correlation between eU and age for the untreated grains (open squares) when compared with the strong correlation between eU and age observed from the abraded grains (circles and triangles) for both samples.

slowly cooled Appalachian samples. Untreated single-grain aliquots from both samples produced wide age dispersion with no correlation to eU concentration or grain size (reported here as the radius of a sphere with an equivalent F_T correction after 1.ham et al. (2011)), reflecting the results of the multi-grain aliquots from earlier work (McKeon et al, in prep). For SY-2 (ridge top sample) ages ranged from 111 to 219 Ma with one grain producing an age of 66 Ma, eU ranged from 2 to 16 ppm, and grain size from 72 to 93 μm. For SY-13 (valley bottom sample) ages ranged from 75 to 154 Ma, eU ranged from 2 to 7 ppm and grain size from 68 to 163 μm. Abrasion by either method produced a modest reduction in age dispersion and interestingly revealed a large increase in the range

of eU concentrations observed in both samples (Figure 5). For SY-13, ages from physically abraded grains (n = 14) ranged from 74.9 to 154.3 Ma and were positively correlated with a range of eU concentrations from 6 to 162 ppm. Chemically abraded grains (n = 14) displayed similar ranges for age (82.9 – 162.2 Ma) and eU (6 – 70 ppm) and were also positively correlated. SY-2 produced similar results for physical (47.6 – 185.0 Ma, 6 – 140 ppm, n = 12) and chemical abrasion (57.5 – 141.7 Ma, 3 – 123 ppm, n = 15) with age and eU also being positively correlated.

1.5 DISCUSSION

1.5.1 Chemical Abrasion

Chemical abrasion successfully replicated the results of physical abrasion for samples from widely varying thermal histories, but it was found that high Th apatites showed a systematic tendency to produce younger than expected ages. The ages of chemically abraded grains from the Bermuda (Figure 1.4) and Appalachian (Figure 1.5) samples were indistinguishable from ages of physically abraded grains, indicating that although chemical abrasion produces variable and sometimes startling surface textures (Figure 1.2), it does not appear to have systematically impacted the results from these samples. However, chemically abraded shards of Durango apatite were systematically younger than the accepted age and numerous untreated shards that were analyzed during the same experiment (Figure 1.3). To produce ages younger than expected, either He must be preferentially leached from the abraded shard, which seems unlikely, or U, Th, or Sm

must be somehow enriched during the abrasion process. In addition to being systematically younger, the abraded shards were also systematically enriched in Th relative to the untreated pool (Figure 1.3), which we interpret as a result of Th reprecipitating on the surface of the shard during abrasion while U and Sm do not. To explore this hypothesis we corrected for the suspected Th enrichment of the abraded shards by multiplying their observed Th concentration by the ratio of the mean Th/U observed from the untreated and abraded sample pools (Table 1.1). This correction decreased the Th concentration of the abraded grains producing older ages. When using the corrected Th concentration, the mean age for abraded shards becomes 30.93 ± 1.42 Ma relative to 31.52 ± 0.69 Ma for the untreated shards, compared to a mean of 28.50 Ma for the uncorrected chemically abraded shards (Figure 1.3). In this light, it is interesting to note that the only chemically abraded grain (C43-2D) from the Bermuda samples that was younger than the stratigraphic age of the rock it was derived from had a Th/U ratio equivalent to Durango apatite and was the highest Th/U ratio for all of the Bermuda samples analyzed for this study. Further refinement of the abrasion protocol is needed to address issues with Th fractionation, it is possible that this issue could be avoided by rinsing chemically abraded samples in a stronger nitric acid solution before packaging them for analysis. Overall, our results suggest that chemical abrasion holds promise as a viable and efficient option for grain size reduction that does not appear to impact the helium concentration of the treated grain.

1.5.2 Physical Abrasion and Age Dispersion

The results of physically abraded grains from the Bermuda and Appalachian samples illustrate that grain size reduction and the elimination of the F_T correction can decrease age dispersion for some samples, but for others wide age dispersion will persist. For the Bermuda samples, our untreated and physically abraded single-grain analyses nicely replicate the results of multi-grain analyses by Spiegel et al. (2009) (Figure 1.4). Our results corroborate their observation that abrasion is an effective means to address suspected contamination from He implantation resulting from U and Th rich grain coatings, neighboring minerals, or migrating fluids and validate the protocol for physical abrasion outlined above. For the Appalachian samples, modest decreases in age dispersion were observed for both samples as a result of physical abrasion, however, age dispersion from single grains still greatly exceeded analytical uncertainty following grain size reduction (Figure 1.5). Taken together, our results suggest that for fast-cooled samples physical abrasion addresses first-order sources of age dispersion such as He implantation and the assumption of homogeneously distributed U, Th, and Sm for the F_T correction. Whereas, for slowly cooled samples, these sources play a lesser or more complex role in the sourcing of age dispersion and will be considered in detail below.

1.5.3 Zonation and Radiation Damage

The most interesting result to come from our work with abrasion by either method was the dramatic increase in the range of eU concentrations observed in the abraded grains from the Appalachian samples and the positive correlation between the eU concentration and the age that the abraded samples displayed (Figure 1.5). The nearly 5X increase in

eU concentration observed in the abraded grains suggests the presence of strong core-rich zonation in these Appalachian apatites; however, the presence of very low eU grains in the abraded pool also suggest that it is not be a pervasive pattern. Zonation is an often-cited source for unconstrained age dispersion due to the fact that traditional analytical methods assume eU homogeneity when determining the F_T correction. The subject has recently received thorough consideration through the development of LA-ICP-MS mapping of 2-D U and Th concentrations within individual apatite grains (Farley et al., 2011, Flowers and Kelley, 2011, and Ault and Flowers, 2012). While the dispersion rooted in the incorrect application of the F_T correction may average to a small impact over a large suite of samples (Ault and Flowers, 2012), for any single analysis the actual age can vary from 21% too old, to 39% too young for the end-member cases where all parent nuclides are either in the center of a grain or along its edge (assuming a radius of 80 μm). Furthermore, the dilution of the eU concentration through the presence of a large volume low eU rim surrounding a low volume high eU core can completely change how one views the data in context of well documented and explainable kinetic controls on AHe ages resulting from radiation damage during slow cooling (Shuster et al., 2006; Flowers et al., 2009).

To illustrate this point, we used eleven grains from SY-2 and SY-13 for which the pre- and post-abrasion geometry and eU concentration of the abraded core were measured. We made the simplifying assumption of severe core-rich zonation, such that all of the U, Th, and Sm in the pre-abrasion grain was sequestered within the abraded core. We then calculated the change in volume using the pre- and post-abrasion geometries and use that

to dilute the eU concentration as if the intact pre-abrasion grain was digested and analyzed following standard U, Th, and Sm analysis protocol. Finally, we applied an appropriate F_T correction to the age for the pre-abrasion geometry, as is standard practice for any non-abraded grain. The results of this thought experiment (Figure 1.6) illustrate how the dilution of the eU concentration and the unnecessary application of the F_T correction for alpha loss that did not occur, create widely dispersed ages with no correlation to eU and appear surprisingly similar to the observed eU-Age relationship of the untreated grains from the Appalachians (Figure 1.5).

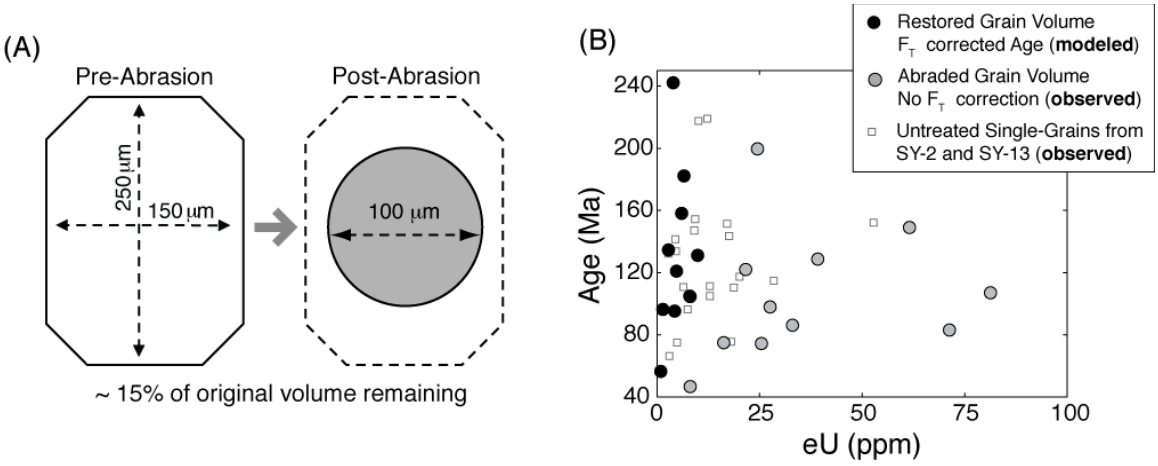

Figure 1.6: A) Cartoon illustrating the reduction in size from physical abrasion of an apatite grain, which was observed to result in an average volume loss of 85% +/- 3.3% 1σ. B) Plot of eU vs. age observed for 11 abraded grains from the two Appalachian samples (gray circles), modeled Ft corrected ages using the pre-abrasion volume and the observed eU concentration from the abraded core (black circles), and untreated single-grain aliquots (open gray squares). This plot illustrates how severe core-rich zonation of U and Th can dramatically impact the eU-age relationship that is observed in unabraded vs. abraded grains. In this thought experiment where all eU is sequestered in the core of the grain, the eU of an untreated grain is moved along the X axis to low eU values through dilution caused by the low concentration rim and the age is increased through the F_T correction for alpha ejection that never occurred. Analysis uncertainty is not show for the observed samples on this plot for clarity.

The Radiation Damage Accumulation and Annealing Model (RDAAM - Flowers et al, 2009) predicts that differences in eU concentration will lead to increasingly dispersed

ages as the rate of cooling slows down. Thus, an eU-age correlation as seen in the abraded grains from both Appalachian samples, can be interpreted in the context of the thermal history required to produce the observed age dispersion, provided that thermal history fits within the context of other known constraints. We used the RDAAM model within the kinetic model HeFTy (Ketcham, 2005) to predict the ages for a range of eU concentrations (1 - 175 ppm) and grain sizes (radii of 60 – 100 μm) for a long-term average erosion rate of 20 m/Myr and an assumed geothermal gradient of 20˚C/km for a long-term cooling rate of 0.4˚C/Myr. We find that while there is still modest dispersion of the ages from abraded grains, the general shape of the eU-age trend from both samples closely mimics that of the RDAAM predicted forward model data for slow long-term erosion (Figure 1.7), which corroborates regional apatite fission track data (Naeser et al, 2004) and is in stark contrast to the untreated grains. These results suggest that strong core-rich zonation concentrates radiation damage within the core of the grain, progressively altering the kinetics of He diffusion during slow cooling through the PRZ. This relationship suggests that in this scenario the core could be more retentive than the rest of the grain and as a result of the kinetic differences, different parts of the grain could effectively close to He diffusion at different points in the cooling history.

1.5.4 Implications of Abrasion for AHe Thermochronometry

A simple argument against abrasion is that as a bulk thermochronometric technique, AHe cooling ages are derived by measuring all of the He within the natural diffusive profile of a grain, which accumulates as a function of the thermal history. Thus, as has recently

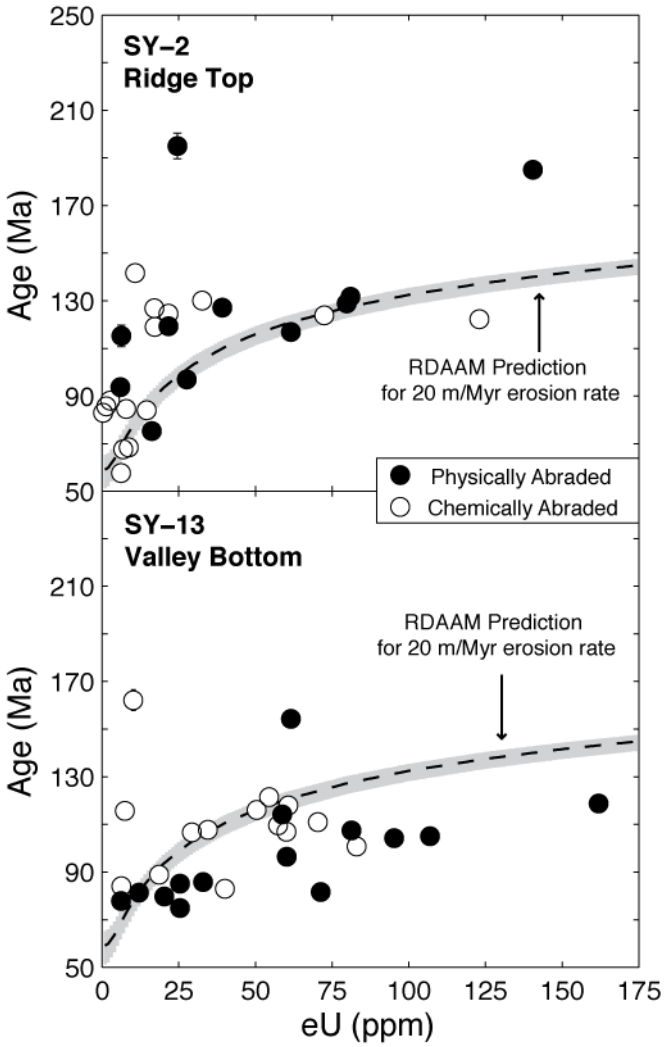

Figure 1.7: Plots comparing the eU-age relationship of the Appalachian samples to that predicted by radiation damage for a long-term average erosion rate of 20 m/Myr that matches apatite fission track data for the region. The dashed black line represents a grain size of 80 um and the gray shading shows the range in age for a grain radius of 60 to 100 um. Forward modeling of the affects of radiation damage and grain size where accomplished using the RDAAM in HeFTy.

been pointed out for the dating of fractured grains (Brown et al., 2011), any tampering with the natural ^{4}He concentration profile through abrasion will affect the age derived from that grain. For rapidly cooled samples the impact is negligible because the diffusive profile is essentially flat. However, for slowly cooled samples with uniform distributions of U, Th, and Sm, the age calculated from an abraded grain would be older than the age would have been if the whole grain were analyzed due to the loss of the low concentration rim (Farley, 2002). In spite of this reality, we would argue that the beneficial constraints on the thermal history that can be derived from the analysis of

abraded grains illustrated above outweigh the cost of the loss of low temperature information that is stored along outer edge of the diffusive concentration profile. Furthermore, if one was interested to do so, calculating a dimension-modified closure temperature through modeling the ingrown diffusive profile and then integrating over the non-abraded portion that was analyzed could address the discrepancy between abraded and untreated ages.

The implications of abrasion with respect to zonation of U, Th, and Sm and alpha redistribution are similar to the F_T correction for untreated grains. Correcting the measured age for He ejection improves the accuracy of AHe age determinations (Farley et al., 1996), however, the assumptions of U, Th, and Sm homogeneity within the grain and a zero concentration of He producing elements outside the grain are implicit in the use of the F_T correction and have been shown to introduce dispersion due to zonation (Farley et al., 2011; Ault and Flowers, 2012) and implantation (Spiegel et al., 2009). While abrasion removes the portion of the grain that is subject He ejection and implantation, by abrading a zoned grain He redistribution within the grain can cause similar problems to F_T correcting an untreated zoned grain, only the relationship is reversed. Abrading and not correcting a rim-enriched grain will produce too old an age due to more He being redistributed into the core much the way that F_T correcting an untreated core-enriched grain would produce too old an age from over-correcting the alpha loss. Similarly, abrading and not correcting a core-enriched grain will produce too young an age because a greater amount of He is redistributed into the rim, in the same manner that F_T correcting an untreated rim-enriched grain will under-correct for alpha

loss. The ideal would be to measure the zonation pattern and date the same grain and thus know the correct way to deal with alpha redistribution or ejection prior to any treatment. However, current methods for measuring the spatial variation of U, Th, and Sm concentration are destructive to the grain and preclude this style of dual analysis. As a result, the safest assumption for untreated grains is that alpha loss occurred and therefore the age should be corrected. Similarly, for abraded grains, the safest assumption is that alpha redistribution occurred, where He lost from the core is balanced by He contributed from the removed rim, and therefore no correction should be applied to the age determined for abraded core.

A simple argument in support of abrasion is that most applications of AHe thermochronometry require the analysis of large number of samples (not to mention replicate aliquots) to effectively capture the complexity that transient topography, changes in relief, and the rate of erosion impose upon shallow isotherms (e.g. Braun, 2002; Reiners et al., 2003; Ehlers et al., 2006). Thus, detailed characterization of every sample quickly becomes unrealistic due to the time and resources required. It is interesting that the majority of studies reporting problems with age dispersion are from regions characterized by slow cooling (e.g. Belton et al., 2004; Green et al., 2006; Fitzgerald et al., 2006; Danišík et al., 2008, McKeon et al, in prep). This is an unfortunate predicament because it is the very nature of slow long-term cooling, resulting from small magnitudes of exhumation, that creates a dependence on the low temperature sensitivity of AHe thermochronometry to investigate interactions between tectonic and erosive processes in these settings. We have illustrated how the combination of U, Th,

and Sm zonation, the F_T correction, and the impact of radiation damage on the kinetics of He diffusion can severely impact the ages acquired by traditional bulk AHe analysis, making an understanding of the zonation of U, Th, and Sm a beneficial data set when interpreting AHe data from these regions. We would argue that for datasets that display wide age dispersion, abrasion is an effective means to quickly and cheaply assess the dominant characteristic responsible for the dispersion observed, from which valuable information constraining the thermal history can be derived.

1.6 CONCLUSIONS

Here we have presented protocols for abrasion of apatite using physical abrasion in an air abrasion chamber and chemical abrasion using dilute nitric acid. We find that chemical abrasion can replicate the results of physical abrasion from rapidly cooled samples, corroborating the findings of Spiegel et al. (2009) using single grain analysis and from slowly cooled samples from the Appalachians. However, following chemical abrasion ages of Durango apatite are systematically younger than the accepted age and have higher Th/U ratios. We interpret these results to be caused by reprecipitation of Th on the grain surface during abrasion and suggest that further refinement of the chemical abrasion protocol will address and remediate this result.

For the slowly cooled Appalachian samples, through abrasion we found dramatic increases in eU concentration relative to untreated grains and interpret this as evidence of severe, but not pervasive core-rich zonation of U, Th, and Sm. We show how core-rich

zonation of this magnitude can produce wide age dispersion with no correlation to grain size or eU if the whole grain is analyzed using standard AHe protocols. We illustrate that useful and compelling low-temperature thermal history information can be derived from the eU-age relationship of the abraded grains by exploiting the age dispersion using known effects from radiation damage. Finally, we argue that grain abrasion by either method provides an effective and rapid means to assess the sources of age dispersion without resorting to time and resource-intensive studies that are difficult to apply to a large sample suite.

1.7 ACKNOWLEDGEMENTS

Cornelia Spiegel (University of Bremen) and Barry Kohn (University of Melbourne) are thanked for providing apatite separates from the Bermuda Rise. This research was supported by a Geological Society of America Student Research Grant and multiple Palmer Research Grants from the Department of Earth and Environmental Sciences of Lehigh University to R.E. McKeon. Samples from the Appalachians were collected as part of NSF-EAR 9909393 to P.K. Zeitler and B.D. Idleman.

1.8 REFERENCES

Ault, A.K., and Flowers, R.M., 2012, Is apatite U-Th zonation information necessary for accurate interpretation of apatite (U-Th)/He thermochronometry data?: Geochimica et Cosmochimica Acta, v. 79, no. C, p. 60–78, doi: 10.1016/j.gca.2011.11.037.

Ault, A.K., Flowers, R.M., and Bowring, S.A., 2009, Phanerozoic burial and unroofing history of the western Slave craton and Wopmay orogen from apatite (U–Th)/He thermochronometry: Earth and Planetary Science Letters, v. 284, no. 1, p. 1–11.

Belton, D., Brown, R.W., Kohn, B.P., Fink, D., and Farley, K.A., 2004, Quantitative resolution of the debate over antiquity of the central Australian landscape : implications for the tectonic and geomorphic stability of cratonic interiors: Earth and Planetary Science Letters, v. 219, p. 21–34, doi: 10.1016/S0012-821X(03)00705-2.

Berger, A.L., Gulick, S.P.S., Spotila, J.A., Upton, P., Jaeger, J.M., Chapman, J.B., Worthington, L.A., Pavlis, T.L., Ridgway, K.D., and Willems, B.A., 2008, Quaternary tectonic response to intensified glacial erosion in an orogenic wedge: Nature Geoscience, v. 1, no. 11, p. 793–799.

Boyce, J., and Hodges, K.V., 2005, U and Th zoning in Cerro de Mercado (Durango, Mexico) fluorapatite: Insights regarding the impact of recoil redistribution of radiogenic 4He on (U-Th)/He thermochronology: Chemical Geology, v. 219, p. 261–274, doi: 10.1016/j.chemgeo.2005.02.007.

Braun, J., 2002, Estimating exhumation rate and relief evolution by spectral analysis of age–elevation datasets: Terra Nova, v. 14, no. 3, p. 210–214.

Brown, R.W., Beucher, R., Roper, S., Gallagher, K., Persano, C., Stuart, F., Fitzgerald, P.G., Swift, D.A., 2011, Exploiting the natural dispersion of single crystal fragment (U-Th)/He age determinations using a new inverse approach to deriving thermal history information, Abstract V31G-06 presented at 2011 Fall Meeting, AGU, San Francisco, CA, 5-9 Dec.

Danišík, M., Sachsenhofer, R.F., Privalov, V.A., Panova, E.A., Frisch, W., and Spiegel, C., 2008, Low-temperature thermal evolution of the Azov Massif (Ukrainian Shield–Ukraine)—Implications for interpreting (U–Th)/He and fission track ages from cratons: Tectonophysics, v. 456, no. 3, p. 171–179.

Ehlers, T.A., and Farley, K.A., 2003, Apatite (U–Th)/He thermochronometry: methods and applications to problems in tectonic and surface processes: Earth and Planetary Science Letters, v. 206, no. 1, p. 1–14.

Ehlers, T.A., Farley, K.A., Rusmore, M.E., and Woodsworth, G.J., 2006, Apatite (U-Th)/He signal of large-magnitude accelerated glacial erosion, southwest British Columbia: Geology, v. 34, no. 9, p. 765, doi: 10.1130/G22507.1.

Farley, K.A., 2002, (U-Th)/He dating: Techniques, calibrations, and applications: Reviews in Mineralogy and Geochemistry, v. 47, no. 1, p. 819–844.

Farley, K.A., 2000, Helium diffusion from apatite: General behavior as illustrated by Durango fluorapatite: Journal of Geophysical Research, v. 105, no. B2, p. 2903–2914.

Farley, K.A., Shuster, D.L., and Ketcham, R.A., 2011, U and Th zonation in apatite observed by laser ablation ICPMS, and implications for the (U-Th)/He system: Geochimica et Cosmochimica Acta, v. 75, no. 16, p. 4515–4530, doi: 10.1016/j.gca.2011.05.020.

Farley, K.A., Wolf, R.A., and Silver, L.T., 1996, The effects of long alpha-stopping distances on (U-Th)/He ages: Geochimica et Cosmochimica Acta, v. 60, no. 21, p. 4223–4229.

Fitzgerald, P., Baldwin, S., Webb, L., and O'Sullivan, P., 2006, Interpretation of (U-Th)/He single grain ages from slowly cooled crustal terranes: A case study from the Transantarctic Mountains of southern Victoria Land: Chemical Geology, v. 225, p. 91–120, doi: 10.1016/j.chemgeo.2005.09.001.

Flowers, R.M., 2009, Exploiting radiation damage control on apatite (U–Th)/He dates in cratonic regions: Earth and Planetary Science Letters, v. 277, p. 148–155.

Flowers, R.M., and Kelley, S.A., 2011, Interpreting data dispersion and "inverted" dates in apatite (U-Th)/He and fission-track datasets: An example from the US midcontinent: Geochimica et Cosmochimica Acta, v. 75, no. 18, p. 5169–5186, doi: 10.1016/j.gca.2011.06.016.

Flowers, R.M., Ketcham, R.A., Shuster, D.L., and Farley, K.A., 2009, Apatite (U-Th)/He thermochronometry using radiation damage accumulation and annealing model: Geochimica et Cosmochimica Acta, v. 73, no. 8, p. 2347–2365, doi: 10.1016/j.gca.2009.01.015.

Flowers, R., Shuster, D., Wernicke, B., and Farley, K., 2007, Radiation damage control on apatite (U-Th)/He dates from the Grand Canyon region, Colorado Plateau: Geology, v. 35, no. 5, p. 447, doi: 10.1130/G23471A.1.

Flowers, R., Wernicke, B., and Farley, K., 2008, Unroofing, incision, and uplift history of the southwestern Colorado Plateau from apatite (U-Th)/He thermochronometry: Geological Society of America Bulletin, v. 120, no. 5-6, p. 571–587.

Green, P., Crowhurst, P., Duddy, I., Japsen, P., and Holford, S., 2006, Conflicting (U–Th)/He and fission track ages in apatite: Enhanced He retention, not anomalous annealing behaviour: Earth and Planetary Science Letters, v. 250, no. 3-4, p. 407–427, doi: 10.1016/j.epsl.2006.08.022.

Guidry, M.W., and Mackenzie, F.T., 2003, Experimental study of igneous and sedimentary apatite dissolution: Control of pH, distance from equilibrium, and temperature on dissolution rates: Geochimica et Cosmochimica Acta, v. 67, no. 16, p. 2949–2963, doi: 10.1016/S0016-7037(03)00265-5.

House, M.A., Wernicke, B.P., and Farley, K.A., 1998, Dating topography of the Sierra Nevada, California, using apatite (U–Th)/He ages: Nature, v. 396, no. 6706, p. 66–69.

House, M., Kohn, B., Farley, K., and Raza, A., 2002, Evaluating thermal history models for the Otway Basin, southeastern Australia, using (U-Th)/He and fission-track data from borehole apatites: Tectonophysics, v. 349, no. 1-4, p. 277–295.

Ketcham, R.A., 2005, Forward and inverse modeling of low-temperature thermochronometry data. in Reiners, P.W., and Ehlers, T.A., (eds.) Low-Temperature themrochronology: Techniques, Interpretations, and Applications, Reviews in Mineralogy and Geochemistry v. 58, p. 315-350.

Ketcham, R.A., Gautheron, C., and Tassan-Got, L., 2011, Accounting for long alpha-particle stopping distances in (U-Th-Sm)/He geochronology: Refinement of the baseline case: Geochimica et Cosmochimica Acta, v. 75, no. 24, p. 7779–7791, doi: 10.1016/j.gca.2011.10.011.

Krogh, T., 1982, Improved accuracy of U-Pb zircon ages by the creation of more concordant systems using an air abrasion technique: Geochimica et Cosmochimica Acta, v. 46, no. 4, p. 637–649.

McDowell, F., McIntosh, W., and Farley, K., 2005, A precise 40Ar-39Ar reference age for the Durango apatite (U-Th)/He and fission-track dating standard: Chemical Geology, v. 214, p. 249–263.

Naeser, N. D., Naeser, C. W., Southworth, C. S., Morgan, B. A., and Schultz, A. P., 2004, Paleozoic to Recent tectonic and denudation history of rocks in the Blue Ridge Province, central and southern Appalachians; evidence from fission-track thermochronology: Geological Society of America, Abstracts with Programs, 36, 114.

Okada, H., Thierstein, H., 1979. In: Tucholke, B. Vogt, P. (Eds.), Calcareous Nannoplankton - Leg 43, Deep Sea Drilling Project: Initial Reports of the Deep Sea Drilling Project, vol. 43, p. 507-574.

Reiners, P.W., and Farley, K.A., 2001, Influence of crystal size on apatite (U–Th)/He thermochronology: an example from the Bighorn Mountains, Wyoming: Earth and Planetary Science Letters, v. 188, no. 3, p. 413–420.

Reiners, P.W., Ehlers, T.A., Mitchell, S.G., and Montgomery, D.R., 2003, Coupled spatial variations in precipitation and long-term erosion rates across the Washington Cascades: Nature, v. 426, no. 6967, p. 645–647, doi: 10.1038/nature02111.

Shuster, D., Flowers, R., and Farley, K., 2006, The influence of natural radiation damage on helium diffusion kinetics in apatite: Earth and Planetary Science Letters, v. 249, no. 3-4, p. 148–161, doi: 10.1016/j.epsl.2006.07.028.

Spiegel, C., Kohn, B., Belton, D., Berner, Z., and Gleadow, A., 2009, Apatite (U–Th–Sm)/He thermochronology of rapidly cooled samples: The effect of He implantation: Earth and Planetary Science Letters, v. 285, no. 1-2, p. 105–114, doi: 10.1016/j.epsl.2009.05.045.

Spotila, J.A., Bank, G.C., Reiners, P.W., Naeser, C.W., Naeser, N.D., and Henika, B.S., 2004, Origin of the Blue Ridge escarpment along the passive margin of Eastern North America: Basin Research, v. 16, no. 1, p. 41–63.

Stock, G.M., Ehlers, T.A., and Farley, K.A., 2006, Where does sediment come from? Quantifying catchment erosion with detrital apatite (U-Th)/He thermochronometry: Geology, v. 34, no. 9, p. 725–728.

Stockli, D.F., Farley, K.A., and Dumitru, T.A., 2000, Calibration of the apatite (U-Th)/He thermochronometer on an exhumed fault block, White Mountains, California: Geology, v. 28, no. 11, p. 983–986.

APPENDIX - A

A1: Calibrating Grain-size Reduction

For both abrasion techniques, our goal was to establish protocols that reliably removed a minimum of 25 μm globally from the surface of the grain and to do so for batches of grains so that abrasion could be conducted on many grains from one sample, not just a single grain at a time. Here we describe the tests that we used to test our ability to accomplish these goals.

A1.1. Physical Abrasion:

During the calibration of the correct air pressure, abrasive media amount and grit size, and duration of abrasion we conducted numerous abrasion trails using apatites from a

variety of locales and spanning varying ranges of grain size. We did not find any significant variations to the rate of grain size reduction on the part of the apatite grains. Air pressure was found to dramatically effect the duration necessary to attain the desired 25 μm of grain size reduction, however, the resulting morphology of the abraded grain was not affected. Once establishing a general protocol, 12 grains from the two Appalachian samples were abraded individually. Digital images for tracking grain size reduction were captured frequently during single grain abrasion trials as a second check on the variability of the rate of grain size reduction. We were careful about this point because we did not want to systematically bias our data if only large grains survived while smaller grains were withered away in the time necessary for all grains to attain the desired size reduction. Finally, to test if having multiple grains in the abrader at one affected the size reduction we had observed in single grain trials we used three grains of nearly identical size for each of the three principle grain axes. The three grains were measured before and after abrasion and due to the change in morphology no abraded core could be linked to the original grain. Thus any of the post-abrasion measurements of length and the two width axes could have come from any of the pre-abrasion measurements. As a worst-case test, the smallest dimension of each pre-abrasion axis for the three grains was compared to the largest post-abrasion measurement of the same axis, such that in this hypothetical case, the smallest original grain was abraded the least, leaving the largest post abrasion core. For all axes it was found for the worst-case that a minimum of 20 μm was removed. Follow this demonstration and our numerous, well-documented single-grain abrasion trials we felt confident abrading grain in batches of up to 15 grains at once.

A1.2. Chemical Abrasion:

The calibration of chemical abrasion followed a similar pattern to that of physical abrasion. Initially a wide variety of apatite separates and grain sizes were used to assess how grains reacted to prolonged exposure to weak nitric acid solutions. It was during this period where the wide range of surface textures resulting from chemical abrasion was observed. Once the general conditions for acid strength, duration, and temperature were established, multiple trials were conducted using the same conditions but different samples to address differences in the rate of size reduction. Finally, as a test of the reproducibility of grain size reduction, 17 grains were individually abraded as part of a single trial. Of these 17 grains, 14 were recovered and comparison of before and after measurements confirmed the reproducibility of the desired grain size reduction using chemical abrasion.

A2. Apatite U-Th/He Thermochronometry

Apatite grains were selected for analysis under isopropyl alcohol using a stereographic microscope and are selected to be clear, euhedral, and free of inclusions and fractures. (e.g. Farley, 2002). Once selected for analysis, grains were photographed and measured along three principle axes to determine the F_T correction for each grain (Farely et al., 1996). For analysis, individual apatite grains are packed in 1 mm Nb stents, loaded into

an all-metal vacuum extraction line and heated at 1150˚C for 15 minutes in a resistance furnace. After gettering, the evolved gas was analyzed using a Balzer's Prisma quadrupole mass spectrometer, with abundances being determined two ways: via a ^{3}He spike calibrated for mass discrimination using a 1:1 $^{4}He/^{3}He$ mix, and manometrically using the ^{4}He beam observed in the calibration shots, which were run before, in the midst of, and after the analysis of each batch of unknowns. Agreement between spiked and manometric data was usually within 1%, and where these values deviate, the cause appears to be interference at mass 3 due to the presence of high hydrogen loads. As a result, all data reported in this paper are based on the manometric calibration. Following degassing, grains were recovered and sent to the Arizona Radiogenic Helium Dating Laboratory at the University of Arizona or the Noble Gas for U, Th, and Sm analysis. There, stents containing degassed apatite grains are placed in Teflon vials and spiked with ^{233}U, ^{229}Th, and ^{147}Sm in solution and the apatite is dissolved directly from the stent using dilute (~20%) warm nitric acid. Radiogenic isotope concentrations are measured using ICP-MS. Effective uranium (eU) concentrations (Shuster et al., 2006) are calculated using the volume from the geometric approximation of the grain from the F_T correction to calculate a mass of the grain, which is then used in conjunction with the measured amounts of U and Th (in ng) to derive a concentration of eU in ppm. At Caltech, U, Th, and Sm are also calculated through isotope dilution using ICP-MS, the only notable difference being the use of ^{51}V as a tracer for the measurement of Ca, from which the mass of the dissolved grain was estimated for converting measured U and Th into concentrations. Agreement between the eU calculated using the F_T volume

approximation or ^{51}V tracer for Ca to convert to concentrations was within several percent.

A2.1 Calculating the F_T correction

The F_T correction is calculated using the measured axes and either a cylindrical (including flattened cylinder), ellipsoidal (including sphere), or tetragonal prism geometry dependent upon which best approximates the shape of the grain. The tetragonal prism geometry can accommodate the sharp tips of some grain morphologies (e.g. zircon grains) that have been shown to improve the accuracy of the FT corrections (Hourigan et al., 2005). Instead of using the surface-to-volume ratio of an equivalent sphere to calculate the F_T correction for a non-spherical grain (Meesters and Dunai, 2002), we instead use a Monte-Carlo method that causes decays of all alpha producing isotopes at random x, y, and z coordinates within the input geometric approximation of the grain. The new point created by the decay (the alpha particle's stopping point) is then determined to be in or out of the grain. This is then repeated for 10^7 decays and the ratio of alphas that are "in" to the total number of alphas created is the F_T correction for that grain geometry.

Additional References:

Farley, K.A., 2002, (U-Th)/He dating: Techniques, calibrations, and applications: Reviews in Mineralogy and Geochemistry, v. 47, no. 1, p. 819–844.

Farley, K.A., Wolf, R.A., and Silver, L.T., 1996, The effects of long alpha-stopping distances on (U-Th)/He ages: Geochimica et Cosmochimica Acta, v. 60, no. 21, p. 4223–4229.

Hourigan, J.K., Reiners, P.W., and Brandon, M., 2005, U-Th zonation-dependent alpha-ejection in (U-Th)/He chronometry: Geochimica et Cosmochimica Acta, v. 69, no. 13, p. 3349–3365, doi: 10.1016/j.gca.2005.01.024.

Meesters, A.G.C.A., and Dunai, T.J., 2002, Solving the production-diffusion equation for finite diffusion domains of various shapes Part I. Implications for low-temperature (U-Th)/He thermochonology: Chemical Geology, v. 186, p. 333–344.

Shuster, D., Flowers, R., and Farley, K., 2006, The influence of natural radiation damage on helium diffusion kinetics in apatite: Earth and Planetary Science Letters, v. 249, no. 3-4, p. 148–161, doi: 10.1016/j.epsl.2006.07.028.

Table 1.1: Apatite U-Th/He data for Durango chemical abrasion experiment.

Aliquot ID	Age (Ma)	± 1σ[a] (Ma)	eU[b] (ppm)	F_T[c]	Radius[d] (µm)	^{4}He (pmol)	U (pmol)	Th (pmol)	Sm (pmol)	Th/U
Untreated Age Standards										
10dur-22	32.63	0.29	61.63	*NA*	*NA*	1.85E-13	7.60E-13	1.58E-11	1.26E-11	20.76
10dur-23	31.55	0.27	62.58	*NA*	*NA*	2.61E-13	1.08E-12	2.32E-11	1.60E-11	21.45
10dur-24	31.18	0.26	63.68	*NA*	*NA*	2.59E-13	1.08E-12	2.33E-11	1.59E-11	21.62
10dur-25	31.78	0.28	70.99	*NA*	*NA*	3.93E-13	1.79E-12	3.38E-11	2.20E-11	18.82
10dur-26	30.49	0.28	68.00	*NA*	*NA*	3.07E-13	1.34E-12	2.80E-11	1.98E-11	20.96
10dur-27	31.41	0.28	78.89	*NA*	*NA*	2.90E-13	1.28E-12	2.54E-11	1.67E-11	19.81
10dur-28*	32.36	0.57	*NA*	*NA*	*NA*	2.42E-13	1.05E-12	2.05E-11	2.23E-11	19.52
10dur-29*	31.41	0.54	*NA*	*NA*	*NA*	5.88E-13	2.73E-12	5.09E-11	6.41E-11	18.63
10dur-30*	31.99	0.46	*NA*	*NA*	*NA*	4.72E-13	2.06E-12	4.06E-11	6.13E-11	19.69
10dur-31	30.30	0.21	61.67	*NA*	*NA*	1.70E-13	7.49E-13	1.56E-11	1.34E-11	20.82
10dur-32	32.53	0.20	60.31	*NA*	*NA*	1.54E-13	6.29E-13	1.32E-11	1.24E-11	20.96
10dur-33	31.25	0.16	76.35	*NA*	*NA*	2.35E-13	1.04E-12	2.08E-11	1.49E-11	19.91
10dur-34	32.01	0.36	60.08	*NA*	*NA*	1.20E-13	5.15E-13	1.04E-11	1.02E-11	20.11
10dur-36	32.15	0.20	59.77	*NA*	*NA*	1.30E-13	5.44E-13	1.12E-11	9.57E-12	20.65
10dur-37	30.94	0.14	72.66	*NA*	*NA*	2.64E-13	1.19E-12	2.35E-11	1.65E-11	19.76
									Mean Th/U Ratio (Used for Th Correction) =	*20.23*
Chemically Abraded Durango										
10DUR-A22	31.22	0.30	63.50	*NA*	*NA*	1.18E-13	4.65E-13	1.07E-11	8.62E-12	22.92
10DUR-A23	27.75	0.25	74.96	*NA*	*NA*	1.68E-13	7.51E-13	1.71E-11	1.08E-11	22.72
10DUR-A24	27.09	0.24	69.96	*NA*	*NA*	1.63E-13	7.14E-13	1.71E-11	1.13E-11	24.02
10DUR-A25	28.12	0.24	78.96	*NA*	*NA*	2.18E-13	9.33E-13	2.20E-11	1.30E-11	23.54
10DUR-A26	29.91	0.27	60.46	*NA*	*NA*	1.49E-13	6.63E-13	1.39E-11	1.10E-11	20.96
10DUR-A27	30.02	0.25	72.31	*NA*	*NA*	3.68E-13	1.60E-12	3.43E-11	1.90E-11	21.40
10DUR-A28	28.97	0.24	76.97	*NA*	*NA*	2.72E-13	1.16E-12	2.66E-11	1.76E-11	22.91
10DUR-A29	26.36	0.22	81.47	*NA*	*NA*	2.74E-13	1.37E-12	2.90E-11	1.78E-11	21.22
10DUR-A30	27.36	0.23	85.10	*NA*	*NA*	2.10E-13	1.01E-12	2.15E-11	1.35E-11	21.27
10DUR-A31	30.61	0.30	66.35	*NA*	*NA*	1.11E-13	4.45E-13	1.03E-11	8.14E-12	23.13
10DUR-A32	27.84	0.25	71.55	*NA*	*NA*	1.69E-13	7.23E-13	1.72E-11	1.29E-11	23.81
10DUR-A33	27.63	0.18	68.25	*NA*	*NA*	1.94E-13	8.46E-13	1.99E-11	1.34E-11	23.52
10DUR-A34	28.25	0.22	76.75	*NA*	*NA*	1.10E-13	4.93E-13	1.10E-11	8.81E-12	22.30
CDUR-1	28.92	0.32	81.66	*NA*	*NA*	1.36E-13	6.01E-13	1.32E-11	8.38E-12	21.99
CDUR-2	26.70	0.13	81.71	*NA*	*NA*	2.04E-13	9.04E-13	2.17E-11	1.23E-11	24.03
CDUR-3	29.20	0.18	73.43	*NA*	*NA*	1.27E-13	5.57E-13	1.22E-11	8.19E-12	21.83
									Mean Th/U Ratio (Used for Th Correction) =	*22.60*

[a] **± 1σ** Analytical uncertainty from propagated error of He, U, Th, and Sm analyses along with F_T and blank measurements

[b] **eU** Effective Uranium = [U] + 0.235*[Th]

[c] **F_T** Alpha-loss correction factor from monte carlo simulation - Not Applicable to Durango shards.

[d] **Radius** F_T equivalent spherical radius of the grain (Ketcham et al., 2012) - Not Applicable to Durango shards.

NA Not Analyzed

* U, Th, Sm analyzed at U. Arizona, all other Durango aliquots analyzed at Caltech.

Table 1.2: Apatite U-Th/He data for Bermuda samples*.

Aliquot ID	Age (Ma)	± 1σ[a] (Ma)	eU[b] (ppm)	F_T[c]	Radius[d] (μm)	^{4}He (mol)	U (mol)	Th (mol)	Sm (mol)	Th/U
Untreated										
43-2A	31.48	0.57	13.03	0.84	87.3	2.23E-14	5.25E-13	5.68E-13	2.47E-12	1.08
43-2B	34.41	0.86	9.83	0.77	61.4	7.17E-15	1.65E-13	1.97E-13	6.32E-13	1.20
43-2C	34.04	0.67	3.13	0.88	114.5	1.55E-14	2.68E-13	5.69E-13	5.03E-12	2.12
43-3A	38.55	1.19	3.68	0.77	59.4	2.38E-15	2.92E-14	1.39E-13	1.73E-12	4.77
43-3B	31.94	0.71	6.74	0.74	57.2	5.59E-15	6.71E-14	4.91E-13	3.20E-12	7.32
43-3C	31.97	0.59	7.50	0.82	83.1	1.87E-14	1.82E-13	1.58E-12	7.47E-12	8.65
Physically Abraded										
P43-2A	30.38	1.02	1.88	*NA*	*NA*	3.39E-15	7.97E-14	2.46E-14	1.70E-12	0.31
P43-2B	37.53	1.30	1.78	*NA*	*NA*	3.05E-15	4.71E-14	6.54E-14	1.30E-12	1.39
P43-2C	34.18	0.46	42.36	*NA*	*NA*	5.04E-14	3.44E-13	3.45E-12	6.99E-12	10.03
P43-3A	30.46	1.50	3.63	*NA*	*NA*	8.19E-16	9.37E-15	4.77E-14	6.62E-13	5.09
P43-3B	30.87	0.66	8.98	*NA*	*NA*	5.37E-15	4.96E-14	3.62E-13	2.61E-12	7.31
P43-3C	28.92	0.69	6.40	*NA*	*NA*	3.43E-15	3.23E-14	2.53E-13	1.98E-12	7.86
Chemically Abraded										
C43-2A	33.69	1.30	2.24	*NA*	*NA*	2.30E-15	4.41E-14	3.58E-14	9.76E-13	0.81
C43-2B	27.99	0.68	6.94	*NA*	*NA*	6.81E-15	1.30E-13	2.45E-13	3.23E-12	*1.88*
C43-2C	27.22	0.66	6.29	*NA*	*NA*	6.60E-15	1.29E-13	2.56E-13	9.87E-13	1.99
C43-2D	22.33	0.27	48.94	*NA*	*NA*	4.82E-14	2.93E-13	5.98E-12	6.71E-12	20.42
C43-2E	26.49	0.85	5.80	*NA*	*NA*	3.92E-15	1.06E-13	4.06E-14	4.22E-13	0.38
C43-3A	28.53	0.42	10.26	*NA*	*NA*	1.00E-14	7.24E-14	8.52E-13	4.82E-12	11.76
C43-3B	29.19	0.43	9.94	*NA*	*NA*	8.46E-15	4.61E-14	7.64E-13	3.63E-12	16.58
C43-3C	27.94	0.50	9.86	*NA*	*NA*	6.34E-15	6.60E-14	4.67E-13	3.23E-12	7.07
C43-3D	10.73	0.19	18.09	*NA*	*NA*	2.63E-15	6.74E-14	5.31E-13	1.39E-12	7.87
C43-3E	27.71	0.49	29.34	*NA*	*NA*	8.22E-15	1.07E-13	5.31E-13	1.42E-12	4.96

* U, Th, and Sm analyzed at Caltech for all Bermuda aliquots.

[a] **± 1σ** Analytical uncertainty from propagated error of He, U, Th, and Sm analyses along with F_T and blank measurements

[b] **eU** Effective Uranium = [U] + 0.235*[Th]

[c] **F_T** Alpha-loss correction factor from monte carlo simulation - Not Applicable to abraded grains.

[d] **Radius** F_T equivalent spherical radius of the grain (Ketcham et al., 2012) - Not Applicable to abraded grains.

NA Not Analyzed

Table 1.3: Apatite U-Th/He data for Appalachian samples.

Aliquot ID	Age (Ma)	± 1σ[a] (Ma)	eU[b] (ppm)	F_T[c]	Radius[d] (μm)	^{4}He (mol)	U (mol)	Th (mol)	Sm (mol)	Th/U
Sample SY-2 - Ridge Top										
Untreated										
NC-SY-2AB (2)	66.33	1.92	3.0	0.84	86.5	1.50E-14	1.97E-13	4.63E-14	9.84E-14	0.23
SY2-1	110.67	2.55	6.4	0.84	85.0	4.31E-14	3.40E-13	7.66E-14	8.82E-13	7.90
SY2-2	132.23	3.15	2.7	0.85	92.7	2.09E-14	1.27E-13	6.60E-14	1.69E-12	6.07
SY2-3	152.17	3.44	52.8	0.85	92.8	4.89E-13	2.76E-12	6.27E-13	6.47E-12	5.64
SY2-4	219.09	4.95	12.25	0.84	85.0	1.21E-13	4.76E-13	1.12E-13	3.08E-12	3.94
SY2-5	147.07	3.49	9.1	0.82	76.7	6.65E-14	4.14E-13	3.91E-14	1.73E-12	6.22
SY2-6	143.52	3.33	17.6	0.81	72.4	8.32E-14	5.30E-13	8.49E-14	1.89E-12	6.38
SY2-8	217.52	4.98	10.1	0.84	88.1	1.86E-13	7.40E-13	1.48E-13	1.98E-12	3.98
Physically Abraded*										
sy2-pa01	75.31	3.31	16.25	*NA*	*NA*	2.90E-15	2.61E-14	1.53E-14	2.27E-13	9.01
sy2-pa02	96.86	2.76	27.6	*NA*	*NA*	1.91E-14	1.42E-13	4.33E-14	7.14E-13	7.43
sy2-pa03	47.55	1.96	8.1	*NA*	*NA*	2.42E-15	3.62E-14	1.28E-14	4.46E-13	14.97
sy2-pa04	127.05	3.34	39.2	*NA*	*NA*	3.49E-14	2.05E-13	2.93E-14	9.23E-13	5.86
sy2-pa05	195.03	5.34	24.5	*NA*	*NA*	4.36E-14	1.60E-13	4.73E-14	3.73E-13	3.67
sy2-pa06	119.34	1.90	21.65	*NA*	*NA*	1.32E-13	8.40E-13	5.87E-14	2.21E-12	6.35
sy2-pa07	115.19	4.50	6.25	*NA*	*NA*	7.51E-15	4.82E-14	7.67E-15	5.09E-13	6.41
sy2-pa08	184.96	2.28	140.45	*NA*	*NA*	3.51E-13	1.41E-12	2.05E-13	2.22E-12	4.01
sy2-pa09	131.78	1.93	80.95	*NA*	*NA*	1.75E-13	9.91E-13	1.38E-13	2.26E-12	5.66
sy2-pa10	116.78	2.58	61.6	*NA*	*NA*	5.55E-14	3.56E-13	4.41E-14	1.22E-12	6.41
sy2-pa11	128.89	2.49	79.75	*NA*	*NA*	8.75E-14	4.99E-13	9.77E-14	1.87E-12	5.71
sy2-pa12	93.72	3.69	5.95	*NA*	*NA*	6.18E-15	4.95E-14	5.80E-15	1.11E-13	8.02
Chemically Abraded										
SY2-A1	123.78	2.20	72.4	*NA*	*NA*	2.04E-13	1.19E-12	3.16E-13	3.48E-12	5.86
SY2-A2	124.57	2.29	21.7	*NA*	*NA*	6.51E-14	3.88E-13	6.48E-14	6.58E-13	5.95
SY2-A3	57.54	1.11	6.1	*NA*	*NA*	9.35E-15	1.17E-13	3.52E-14	8.31E-13	12.55
SY2-A4	84.04	1.67	14.55	*NA*	*NA*	2.31E-14	2.06E-13	2.86E-14	3.99E-13	8.91
SY2-A5	126.78	2.37	17	*NA*	*NA*	2.39E-13	1.38E-12	3.28E-13	4.44E-12	5.75
SY2-A6	68.49	1.39	8.7	*NA*	*NA*	1.01E-14	1.09E-13	1.77E-14	3.21E-13	10.89
SY2-A8	85.58	2.45	1.4	*NA*	*NA*	7.56E-15	6.49E-14	1.46E-14	1.61E-13	8.58
SY2-A9	122.20	2.07	123.05	*NA*	*NA*	1.92E-13	1.15E-12	2.42E-13	3.16E-12	6.01
SY2-A10	82.90	2.56	0.4	*NA*	*NA*	3.19E-15	2.63E-14	1.46E-14	9.04E-14	8.26
SY2-A11	130.21	2.50	32.6	*NA*	*NA*	1.90E-13	1.08E-12	1.66E-13	1.60E-12	5.71
SY2-A12	84.57	1.65	7.8	*NA*	*NA*	1.86E-14	1.63E-13	2.74E-14	2.25E-13	8.80
SY2-A13	141.67	2.76	10.7	*NA*	*NA*	5.97E-14	3.16E-13	3.51E-14	2.12E-13	5.30
SY2-A14	88.01	2.29	2.6	*NA*	*NA*	4.52E-15	3.61E-14	1.47E-14	3.94E-13	7.98
SY2-A15	118.94	2.08	17.15	*NA*	*NA*	3.26E-14	1.72E-13	1.70E-13	7.87E-13	5.27
SY2-A17	67.56	1.37	6.9	*NA*	*NA*	4.21E-14	4.71E-13	4.82E-14	1.32E-12	11.19
Sample SY-13 - Valley Bottom										
Untreated										
NC SY 13 400(1)	96.31	5.59	7.5	0.92	163.3	4.02E-13	3.43E-12	3.23E-13	*NA*	0.09
NC-SY-13 2	75.03	4.35	4.9	0.87	102.1	5.36E-14	6.06E-13	1.11E-13	7.76E-13	0.18
NC-SY-13 3	75.51	4.38	18.1	0.87	103.2	1.18E-13	1.27E-12	4.97E-13	1.17E-12	0.39

NC-SY-13 1	111.26	6.45	12.9	0.83	78.7	8.89E-14	6.95E-13	1.85E-13	9.92E-13	0.27
SY13-1	141.51	4.25	4.5	0.79	66.6	1.60E-14	8.69E-14	9.94E-14	1.69E-12	5.42
SY13-2	154.38	3.66	9.3	0.82	75.2	5.49E-14	3.15E-13	8.11E-14	2.17E-12	5.74
SY13-3	117.38	2.58	20.1	0.85	95.2	1.96E-13	1.30E-12	8.65E-13	1.40E-11	6.64
SY13-4	133.67	3.17	4.6	0.80	71.5	1.96E-14	1.18E-13	9.36E-14	1.98E-12	6.01
SY13-5	110.42	2.25	18.7	0.80	73.0	7.19E-14	4.47E-13	7.64E-13	5.42E-12	6.23
SY13-6	151.50	2.93	17.1	0.78	68.3	7.18E-14	2.71E-13	8.26E-13	6.68E-12	3.78
SY13-7	114.72	2.42	28.5	0.81	74.4	1.21E-13	7.83E-13	9.75E-13	6.69E-12	6.45
SY13-8	104.92	2.06	12.9	0.81	80.1	6.08E-14	3.21E-13	9.69E-13	7.26E-12	5.28
Physically Abraded										
PA-SY13-1	107.43	1.65	81.3	*NA*	*NA*	5.78E-14	3.17E-13	4.18E-13	2.76E-12	5.49
PA-SY13-2	154.28	1.95	61.55	*NA*	*NA*	8.94E-14	2.04E-13	1.04E-12	5.20E-12	2.28
PA-SY13-3	85.75	1.68	33	*NA*	*NA*	2.65E-14	2.34E-13	1.66E-14	1.50E-12	8.84
PA-SY13-4	81.64	1.27	71.3	*NA*	*NA*	2.42E-14	1.78E-13	2.23E-13	4.04E-13	7.35
PA-SY13-5	74.89	1.31	25.45	*NA*	*NA*	9.64E-15	7.47E-14	1.06E-13	7.42E-13	7.75
PA-SY13-6	79.77	1.40	20.3	*NA*	*NA*	1.12E-14	9.31E-14	5.89E-14	2.91E-12	8.30
PA-SY13-7	114.08	1.48	58.7	*NA*	*NA*	5.12E-14	1.73E-13	7.46E-13	3.45E-12	3.37
PA-SY13-8	118.69	1.73	161.85	*NA*	*NA*	2.31E-13	1.11E-12	1.69E-12	3.26E-12	4.81
PA-SY13-9	85.24	1.30	25.4	*NA*	*NA*	2.07E-14	1.33E-13	2.36E-13	1.26E-12	6.41
PA-SY13-10	81.34	2.24	12.05	*NA*	*NA*	3.21E-15	2.15E-14	3.62E-14	8.85E-13	6.71
PA-SY13-11	104.15	1.76	95.25	*NA*	*NA*	9.07E-14	6.16E-13	2.29E-13	5.01E-12	6.80
PA-SY13-12	105.02	1.85	106.9	*NA*	*NA*	8.48E-14	5.61E-13	2.58E-13	4.84E-12	6.61
PA-SY13-13	96.30	1.66	60.15	*NA*	*NA*	3.21E-14	2.37E-13	8.56E-14	1.52E-12	7.38
PA-SY13-14	77.83	2.04	6.15	*NA*	*NA*	4.09E-15	3.72E-14	1.24E-14	8.60E-13	9.09
Chemically Abraded										
SY13-A1	121.48	2.03	54.4	*NA*	*NA*	1.89E-13	8.39E-13	1.57E-12	3.42E-12	4.43
SY13-A2	162.15	4.36	10.2	*NA*	*NA*	1.60E-14	4.50E-14	1.33E-13	4.88E-13	2.81
SY13-A3	88.95	2.54	18.6	*NA*	*NA*	2.44E-14	2.06E-13	2.66E-14	1.34E-12	8.41
SY13-A5	116.11	2.11	50.4	*NA*	*NA*	1.28E-13	6.69E-13	7.58E-13	1.09E-11	5.22
SY13-A6	106.92	1.79	60.1	*NA*	*NA*	1.11E-13	5.45E-13	1.11E-12	1.51E-12	4.92
SY13-A7	115.70	2.53	7.5	*NA*	*NA*	1.93E-14	1.07E-13	7.46E-14	5.61E-12	5.56
SY13-A8	107.69	1.63	34.5	*NA*	*NA*	1.26E-13	4.75E-13	1.85E-12	3.43E-12	3.77
SY13-A9	82.85	2.30	40.1	*NA*	*NA*	2.38E-14	2.10E-13	5.30E-14	9.61E-13	8.80
SY13-A10	110.94	1.80	70.4	*NA*	*NA*	4.85E-14	1.58E-13	7.75E-13	1.56E-12	3.26
SY13-A101	100.75	1.55	83	*NA*	*NA*	1.70E-13	9.68E-13	1.45E-12	4.86E-12	5.69
SY13-A102	106.61	1.53	29.3	*NA*	*NA*	4.04E-14	1.83E-13	4.65E-13	2.95E-12	4.54
SY13-A103	83.95	1.56	6.3	*NA*	*NA*	1.08E-14	8.41E-14	5.35E-14	3.80E-12	7.81
SY13-A104	117.95	2.18	60.7	*NA*	*NA*	8.51E-14	5.40E-13	6.25E-14	2.92E-12	6.35
SY13-A105	109.49	1.52	57.4	*NA*	*NA*	1.53E-13	6.25E-13	1.96E-12	7.86E-12	4.08

[a] **± 1σ** Analytical uncertainty from propagated error of He, U, Th, and Sm analyses along with F_T and blank measurements

[b] **eU** Effective Uranium = [U] + 0.235*[Th]

[c] **F_T** Alpha-loss correction factor from monte carlo simulation - Not Applicable to abraded grains.

[d] **Radius** F_T equivalent spherical radius of the grain (Ketcham et al., 2012) - Not Applicable to abraded grains.

NA Not Analyzed

* U, Th, Sm analyzed at Caltech, all other Appalachian aliquots analyzed at U. Arizona.

CHAPTER 2

DECAY OF AN OLD OROGEN: INFERENCES ABOUT APPALACHIAN LANDSCAPE EVOLUTION FROM LOW-TEMPERATURE THERMOCHRONOLOGY

Ryan E. McKeon[1]*
Peter K. Zeilter[1]
Frank J. Pazzaglia[1]
Bruce D. Idleman[1]
Eva Enkelmann[2]

[1] Department of Earth and Environmental Sciences, Lehigh University, Bethlehem, PA 18015, USA
[2] Universität Tübingen Institut für Geowissenschaften, Wilhelmstr. 56, 72074 Tübingen Germany
* Corresponding Author: rem208@lehigh.edu

For Submission to *Geological Society of America Bulletin*

Keywords: Appalachians, Landscape Evolution, Apatite U-Th/He, Thermochronology, Radiation Damage, Age Dispersion

CHAPTER ABSTRACT

The Appalachians are the archetypal old, long-decaying orogen from which major theories for the drivers and patterns of long-term landscape evolution have been derived. However, the modern topography of the range bears no connection to the regional tectonic history and the along strike variability of maximum elevation and relief make it difficult to describe the range in the context of an old and uniformly decaying landscape. Long-term estimates of erosion rates from apatite fission-track match short-term estimates from cosmogenic nuclide data and suggest slow and steady erosion at 20 m/Myr. Intermediate data like sediment accumulation rates and river incision point to unsteadiness, which we assess using apatite U-Th/He thermochronology. We collected samples from the central Appalachian hinterland in Pennsylvania and New Jersey and from the rugged Blue Ridge Mountains of western North Carolina. All cooling ages were pre-Cenozoic, precluding significant exhumation in connection with the large pulse of Miocene sediment observed offshore. Considerable age dispersion was observed between and within samples that did not correlate with known sources of dispersion for apatite U-Th/He thermochronology. Using two "bad actor" samples from the southern Appalachians we found through abrasion of the grain surface that our observed dispersion was rooted in U and Th zonation, which masked the dispersion expected from radiation damage given the evidence for slow cooling. By taking advantage of the known closure temperature variation caused by grain-specific radiation damage using the abraded grains we are able to show unsteady cooling histories for our two bad actors suggesting that Appalachian landscape evolution is more nuanced than previously documented.

2.1 INTRODUCTION – The Enigma of Appalachian Topography

Topography is an important signal in geodyamics. However, compared to young or active settings, the topographic signal in old orogens can be more enigmatic than telegraphic. Along their length, the Appalachians are a good example of this. Often set forth as a classic mountain belt, the Appalachians are quite curious in their topographic expression (Pazzaglia and Brandon, 1996). Along strike, relief in the Appalachians varies considerably, from 1500 meters in the southern Appalachians to less than 200 meters in Pennsylvania. Independent of the magnitude of relief, the location of highest elevations and relief varies in its tectonic setting: the highest values in the southern Appalachians are developed in the Grenville-aged crystalline rocks of the Blue Ridge, compared to the topographic inversion seen in the central Appalachians, where elevations in the orogenic core have been reduced to sea level and the highest elevations occur in the foreland thrust belt. Finally, Mesozoic rift basins, the youngest major tectonic feature in the region, are strung along the length of eastern North America, yet their boundaries are not defined by any noticeable change in local relief. In summary, the modern Appalachian Mountains do not simply equate to the Appalachian compressional or extensional orogen.

Appalachian landscapes are also enigmatic in their evolution, which is not consistent with simple erosional decay of an original orogenic welt. Data that can constrain this long evolution are surprisingly sparse for a region that has played such a central role in the origin of ideas about landscape development (e.g., Davis, 1889, 1899; Hack, 1960). For

much of the unglaciated Appalachians, long-term inference of erosion rates from low-temperature thermochronology gives very low rates of erosion, on the order of 20 to 40 meters per million years averaged over the past ~100 Myr (e.g. Blackmer et al., 1994; Boettcher and Milliken, 1994; Miller and Duddy, 1989; Naeser et al., 2004; Roden and Miller, 1989; Roden, 1991). At face value these rates are perplexingly similar to shorter-term values obtained by cosmogenic methods averaged over past several tens of thousands of years (Pavich et al., 1985; Matmon et al., 2003; Hancock and Kirwan, 2007; Portenga and Bierman, 2011 and references therein). The conundrum here is that if landscape evolution has been driven by the progressive isostatic consumption of an orogenic root, where slope and relief dictate the erosion rate (Ahnert, 1970), it is hard to see how older and presumably greater relief (resulting from a thicker crustal root) was being removed at the same slow rate that pertained during relatively recent (yet glaciated) times, especially if the buoyancy of the crustal root can decrease through time (Fischer, 2002). Moreover, the low rates are observed over a wide range of localities in different topographic settings, and seem at odds with the observed variations in topography, stratigraphic evidence for pulses of higher sediment-sourcing rates (Pazzaglia and Brandon, 1996), and evidence in some areas for a considerably active landscape, e.g., the dynamics of the New River (Ward et al., 2005) and drainage capture along the Blue Ridge escarpment (Prince et al, 2011). In particular, through summarizing the earlier work of Poag and Sevon (1989) among others, Pazzaglia and Brandon (1996) documented a Miocene pulse of sediment accumulation in the Baltimore Canyon Trough that amounts to some 1000 meters of erosion apportioned over an area stretching from Virginia to New Hampshire, an event that fits in no obvious way with either simple post-

orogenic decay of a Late Paleozoic orogen, or relaxation following Mesozoic reactivation of Appalachian orogenic lithosphere by Atlantic rifting.

In this study we combine new apatite U-Th/He data with previous thermochronological data to investigate the spatial and temporal variability of exhumation in the central and southern Appalachians. The original motivation of this work stemmed from the Pazzaglia and Brandon (1996) observation of pulsed Miocene sedimentation, which raised the possibility that the very low closure temperatures associated with U-Th/He dating of the mineral apatite might allow us to locate the source of this sediment through bedrock dating in the Appalachian landscape. We begin by reporting the general patterns of the data we collected and the large intra-sample age dispersion that we encountered. Next we describe our detailed experiments involving two samples that were aimed at identifying and mitigating the source(s) of the age dispersion we observed. We discuss our results in the context of known sources of age dispersion, updating reviews (Farley, 2002; Ehlers and Farley, 2003; Fitzgerald et al., 2006) with recent advances. Finally, we demonstrate that despite wide age dispersion, interpretable results can be derived from apatite U-Th/He dating in some areas that have experienced slow cooling and provide the first evidence for unsteady erosion of the southern Appalachians.

2.2 THE APPALACHIAN LANDSCAPE AND PREVIOUS WORK

2.2.1 The Modern Appalachian Landscape

The general bedrock geology and topographic characteristics of the central and southern Appalachians can be grouped into five physiographic provinces that are parallel to the strike of range (Figure 2.1). Starting to the east, the Coastal Plain is flat, near sea level, and composed of Cretaceous to Quaternary clastic sediment shed off of the higher topography to the west. The Piedmont province is composed of Paleozoic metamorphic and igneous rocks that represent the core of the Paleozoic Appalachians, thought to have been Andean in scale (Slingerland and Furlong, 1989), now characterized by very low relief and low elevation. The Blue Ridge escarpment, a topographic step of 300 - 500 m along its ~500 km length, separates the Piedmont from the Grenville-aged gneisses and late Proterozoic through early Cambrian metasediments of the Blue Ridge province. The highest elevations and greatest relief of the modern Appalachians is found in the southern Blue Ridge province in the mountains of western North Carolina, which has recently been described as isostatically compensated by a 45-55 km thick crustal root (Hawman et al., 2012). Stepping further west, the Valley and Ridge province is composed of deformed Paleozoic sedimentary rocks of the Appalachian fold-and-thrust belt and the Appalachian Plateau furthest to the west is the undeformed foreland basin of the Paleozoic Appalachian. Elevation and relief in the Valley and Ridge and Appalachian Plateau vary considerably along strike, from subdued topography in Pennsylvania and the southern Appalachians to higher elevations and relief in area of the New River of West

Virginia. Finally, the Baltimore Canyon Trough offshore of Maryland is the largest passive margin sedimentary basin along eastern North America, which has collected an average thickness of 10 km of clastic sediment in unsteady pulses of rapid deposition most recently during the late Cretaceous and the Miocene (Pazzaglia and Brandon, 1996).

2.2.2 Low-Temperature Thermochronology

2.2.2.1 Fission-Track dating. Extensive apatite fission-track analysis from the Appalachian landscape provides a baseline for the pattern of long-term exhumation. Apatite fission-track (AFT) ages reflect cooling through 90 - 110˚C, which translates to approximately 4 km depth within the crust assuming a post-orogenic geothermal gradient of ~20 ˚C/km. All AFT ages from throughout the Appalachian landscape are pre-Cenozoic, which places an upper limit on the extent of recent exhumation that can explain the observed pulse of Miocene sediment in offshore basins. Generally speaking, the oldest AFT ages in the Appalachian region are found in the sedimentary units of the former Appalachian foreland basin now exposed in the Appalachian Plateau and the Valley and Ridge provinces of the central portion of the modern Appalachian Mountains, ranging from 100 to >200 Ma (Blackmer et al., 1994; Boettcher and Milliken, 1994; Miller and Duddy, 1989; Roden and Miller, 1989; Roden, 1991). AFT ages are youngest in Northern New England (Roden-Tice, and Tice, 2005; Roden-Tice et al., 2009) and the Adirondack region (Roden-Tice and Tice, 2005; Taylor and Fitzgerald, 2011) ranging from ~80 to 150 Ma, which are interpreted to be a result of thermal doming and incision caused by passage of that region over the Great Meteor hotspot during the early

Cretaceous. In the southern Appalachians Naeser et al. (2001) describe a pattern of the oldest AFT ages from the Valley and Ridge (~ 200 Ma), younger and more varied ages from the Blue Ridge (95 - 185 Ma), and intermediate ages from the Piedmont province (130 – 200 Ma). Samples from the high relief region of the Blue Ridge in western North Carolina show an age-elevation relationship that suggests prolonged slow cooling at an average rate of 20 m/Myr since the Jurassic (Naeser et al, 2004).

2.2.2 U-Th/He dating. Previous application of Apatite U-Th/He Thermochronology (AHe) within the central and southern Appalachians is limited to a single study by Spotila et al. (2004). Using a combination of AHe and AFT data from the Piedmont and Blue Ridge physiographic provinces of Virginia they found relatively old AHe ages with most ranging from 90 – 200 Ma. They observed the oldest ages from the high topography of the Blue Ridge province, the youngest at the base of the escarpment that separates the Blue Ridge from the Piedmont province, and increasing ages progressively southeast towards the center of the low elevation and low relief Piedmont. They interpreted this pattern to represent the slow and systematic northwestward retreat of a rift flank escarpment across the Piedmont province after it was generated during Mesozoic rifting, explaining both the existence and position of the modern topographic break and the distribution of ages they observed. It should be noted that AHe ages for this study were determined on fairly large composites of many grains and for those samples where replicate aliquots were analyzed; age dispersion exceeding analytical uncertainty was common.

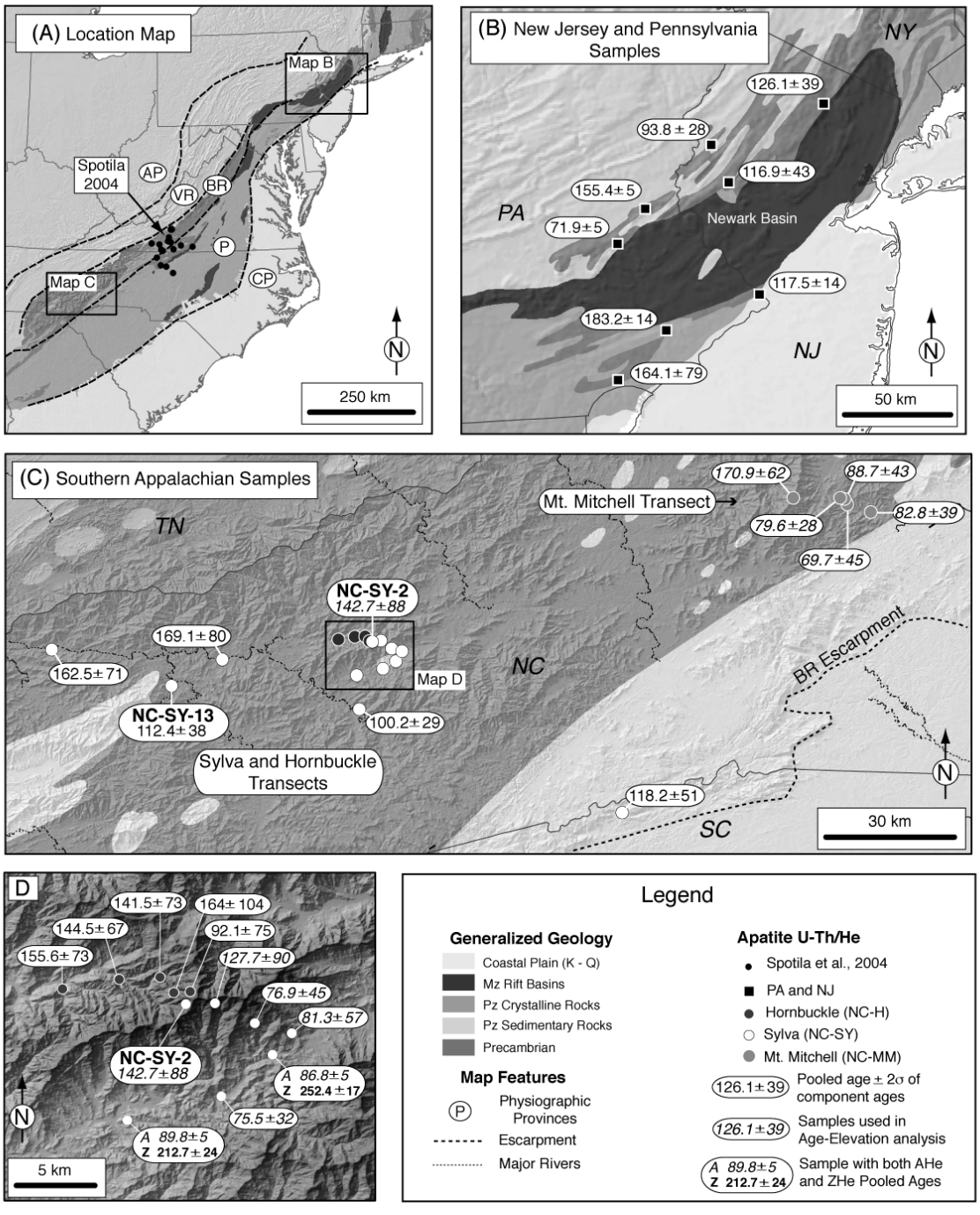

Caption on Next Page

2.3 APATITE U-TH/HE THERMOCHRONOLOGY

Apatite U-Th/He (AHe) thermochronology is based on the production of alpha particles (^{4}He) from the decay of U and Th (and to a minor degree Sm) and the thermally controlled retention of that He within individual grains. The closure temperature (Dodson, 1973) of the AHe system is dependent upon the cooling rate and defined by a zone of partial retention (PRZ) of He from ~35-90 °C (Stockli et al., 2000, House et al., 2002; Flowers et al., 2009). At slow cooling rates, similar to those found in decaying orogens, helium diffusion in apatite can remain active at temperatures below 40˚C, and bulk closure for helium could be as low as 50˚C (Shuster et al. 2006), which enables detection and quantification of small magnitudes of exhumation that are not possible with deeper thermochronologic systems. It has been shown that grain specific characteristics of size (Farley 2000) and effective uranium concentration (henceforth referred to as eU where eU = [U] + 0.235 * [Th]) (Shuster el al., 2006; Flowers et al., 2009) impact the closure temperature. Thus, as result of slow cooling through the PRZ, grains experiencing the same thermal history can produce different ages from which more detailed thermal

Figure 2.1: (A) Map showing the location of central and southern Appalachian study areas in the context of the bedrock geology and physiographic provinces of the Appalachian landscape of eastern North America. (B) Map showing the location and results of AHe thermochronology in the central Appalachians surrounding the Mesozoic Newark rift basin overlaid over the bedrock geology. (C) Shaded-relief map with bedrock geology showing the location and results of AHe and zircon U-Th/He (ZHe) thermochronology from the southern Appalachians of western North Carolina. All of the samples were collected from the rugged topography of the Blue Ridge province to the northwest of the escarpment that separates the Blue Ridge from the Piedmont province. (D) Detailed shaded-relief map of the location and results from the Sylva (open circles) and Hornbuckle (filled circles) transects sampling east and west respectively from Waterrock Knob. Of note is the contrast in the age-elevation relationship of these two transects, where the Sylva samples show a positive correlation, but the Hornbuckle samples on the western side of the ridge show no correlation and much older ages at low elevation.

history information can be derived (e.g. Reiners and Farley, 2001; Flowers et al, 2007; Flowers, 2009). It is important to note that thermochronologic data measures cooling rates, which are interpreted to represent erosion rates through a temperature for depth transformation using a (typically assumed) geothermal gradient. For the southern Appalachians the modern geothermal gradient is ~15 ˚C/km (Nathenson and Guffanti, 1988). Presumably the gradient was higher immediately following the orogenies of the Paleozoic and has been relaxing since. For comparisons of erosion rates using our results and modeling exercises we assume a constant geothermal gradient of 20˚C/km, which we feel is a plausible assumption of the long-term geothermal gradient for this post-orogenic region.

2.3.1 Sampling

With the goal of identifying the spatial and temporal variability of exhumation and perhaps a locality that gave young ages and might thus be a source of Miocene sediment, we examined two Appalachian regions that had not yet been subject to bedrock sampling for U-Th/He dating, the southern Blue Ridge Mountains in the southern Appalachians and a broader swath across the central Appalachians largely in southeastern Pennsylvania. For the New England Appalachians, in another publication we report the results of alternative method, U-Th/He dating of detrital apatites sampled from modern drainages (McKeon et al., Chapter 3).

In the central Appalachians where relief is low, we used a reconnaissance approach to search for any regions that might give anomalously young ages. Samples were collected from outcrops of Precambrian crystalline rock surrounding the Mesozoic Newark rift basin of New Jersey and Pennsylvania. In the southern Appalachians, we focused sampling on two areas of high relief in the Blue Ridge province of western North Carolina. Samples were collected from Mt. Mitchell, the highest point in the Appalachians, and from the Waterrock Knob along the Blue Ridge Parkway near the Great Smoky Mountains. We collected samples along crude vertical transects in the hopes that age-elevation relationships and the ages of the lowest-elevation samples might be informative about more recent landscape evolution. Sample locations are given in Table 2.1 and can be seen in Figure 2.1.

2.3.2 Methods.

As we discuss below, our results are quite complex and we found slowly cooled bedrock apatites from the Appalachians to be analytically challenging. We expended considerable effort over a number of years in trying to understand the origin of this complexity, and as a result the analytical methods we used evolved during this time span. Technical details about analytical methods are given in Appendix 1; in general these methods are similar to those used in most U-Th/He laboratories (e.g. Farley, 2002).

2.3.2.1 General Methods. Conventional mineral-separation procedures were used to extract apatite from bedrock samples from which grains were selected for AHe analysis

using standard optical selection criteria (e.g. Farley, 2002; Ehlers and Farley, 2003) to be free of inclusions, fractures, and grain coatings, and when possible, euhedral. Apatites from these samples contained abundant mineral inclusions and grains were frequently picked under isopropyl alcohol or refractive oil to assist in identifying grains of suitable clarity for dating. Some analyses, particularly those made early in the project, used multiple grains per aliquot, up to as many as 20 or more, but many of our analyses were done on single grains (Supplemental Table 1). Alpha-loss (F_T) corrections (Farley et al., 1996) were calculated for each grain using 2D measurements and then pooled for multi-grain aliquots. Selected grains were loaded in to Pt or Nb micro-tube carriers for He, U, Th, and in later years Sm analysis. Sample preparation and He analysis was conducted at the Noble Gas Geochronology Lab at Lehigh University. U, Th, and Sm analysis was conducted using ICP-MS isotope dilution at Yale University and later the Arizona Radiogenic Helium Dating Lab at the University of Arizona.

2.3.2.2 Data Reduction. Uncertainties on the ages reported for individual analyses are based on a blanket 2.9% error (1s) derived from Monte Carlo simulation that propagated uncertainties in the lab's long-term reproducibility on the Durango apatite standard, typical uncertainties in U and Th measurements, and a 1% error in the F_T alpha-correction factor. We feel this is the best measure of overall precision for these analyses made earlier in the history of our laboratory. For purposes of general discussion about our conventional results, we choose to report pooled ages (Vermeesch, 2008) as the best representation of the age of our samples. This choice is justified by the fact that the component analyses for each sample involved both single- and multi-grain analyses and

due to the wide intra-sample age dispersion we encountered they are the simplest means to compare between samples and with the results of Spotila et al (2004). For pooled ages, the uncertainty represents the propagated uncertainty of the individual component ages. Because it is based only on the fairly good analytical precision, the pooled-age uncertainty will be quite low, so as a qualitative indicator for the actual dispersion between individual analyses that contributed to the pooled ages, we also report the 2s standard deviation of the component ages.

2.3.3. Results

Figure 2.1 and Table 2.1 summarize the results using pooled ages for 30 samples from the central and southern Appalachians. Individual component ages (from more than 200 aliquots) and analytical data can be found in Supplemental Table B1.

2.3.3.1 Data Quality and Dispersion. In the form of pooled ages, our results are relatively consistent, as can be seen in Figure 1. However, more locally among some adjacent samples and especially internally, within samples for which we analyzed a number of aliquots, the age dispersion can be very large, certainly greater than that predicted from analytical uncertainties (Table 2.1; Supplementary Table B1). For example, 10 single- and multi-grain aliquots from sample NC-SY-13 produced a range of F_T-corrected ages from 75 to 131 Ma, where the pooled analytical uncertainty (2σ) was 1.9 Ma, but the 2s standard deviation of the component ages was 38.2 Ma. This sort of behavior is often seen in older slowly cooled apatites (e.g. Belton et al., 2004; Spotila et al., 2004; Green et

al., 2006; Fitzgerald et al, 2006; Danisik et al., 2008). We conducted a number of experiments to explore the cause for this internal dispersion, which we describe and discuss below.

2.3.3.2 Central Appalachians. Pooled ages from this region range widely between 70 and 185 Ma, with no direct indication of Cenozoic cooling related to significant exhumation from this region. Ages tend to be younger on the western, footwall side of the Newark rift basin, with all ages post-dating extensional deformation. These results are consistent with available fission-track apatite ages from Newark Basin sedimentary rocks (Roden and Miller, 1991), which range from 129 to 196 Ma.

2.3.3.3 Southern Appalachians. Pooled ages from this portion of the southern Appalachians are also relatively old, ranging from 70 to 171 Ma. Pooled ages from the rugged topography of the Blue Ridge province show complex relationships with elevation and landscape position, such that neither is a universal predictor of the age observed. For the Mt. Mitchell and Sylva transects, ages are oldest at the highest elevations and then decrease towards the valleys (Figure 2.2), however, the Hornbuckle transect, which descends the opposite side of the ridge from the Sylva transect, shows no correlation between age and elevation (Figure 2.1) with all ages being quite old (~ 150 Ma). Similarly, all three transects locally display a younger to the southeast, older to the northwest trend, but this trend does not appear to be influenced by position relative to the Blue Ridge escarpment as was described by Spotila et al (2004) for samples further to the north (Figure 2.2). Given the complexity of the pooled ages and the wide intra-sample

age dispersion we observed, these results motivated our detailed experiments described below.

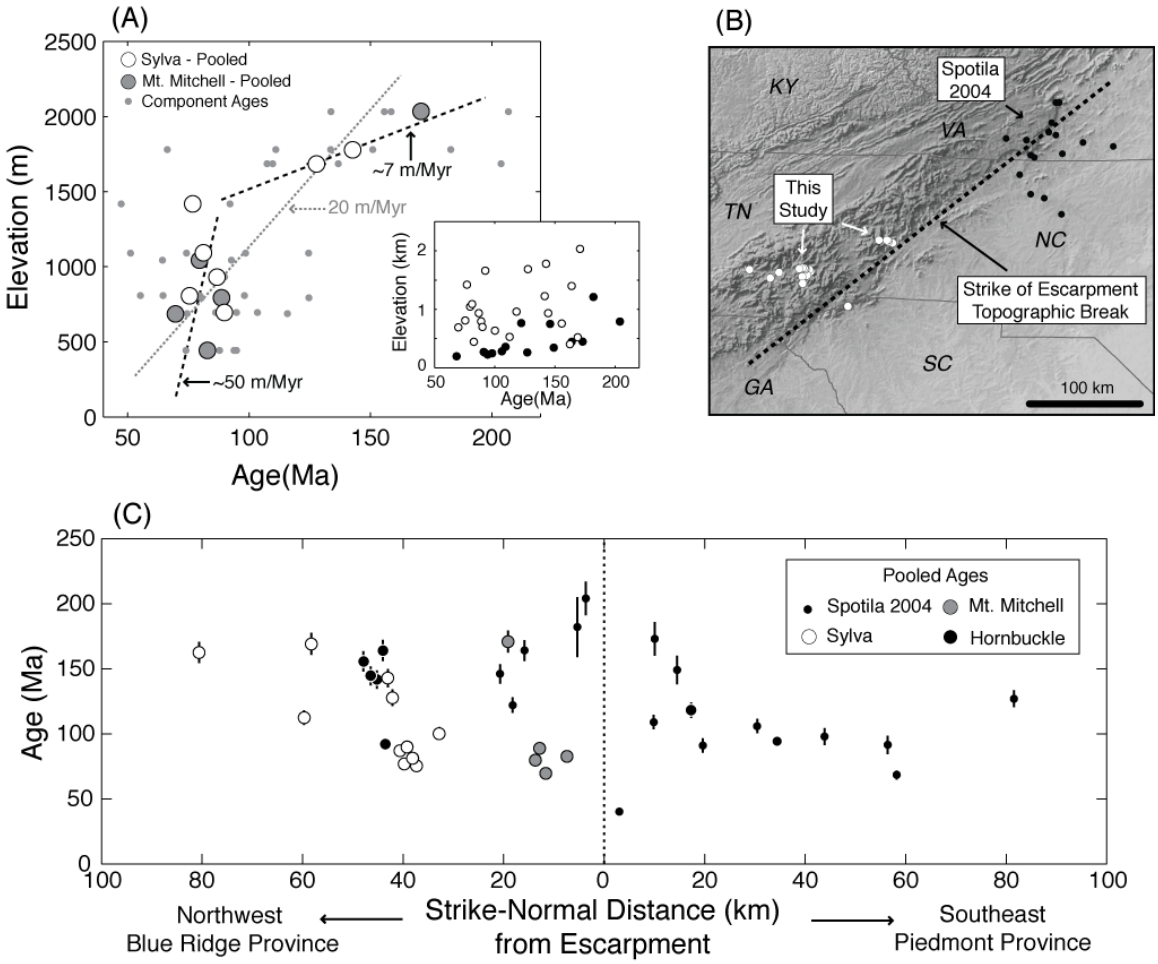

Figure 2.2: Results of pooled AHe ages from the southern Appalachians and the data from Spotila et al. (2004) plotted against elevation and landscape position. (A) Inset plot of Age-elevation relationship for all AHe samples from the southern Appalachians (open circles from this study, filled circles from Spotila et al. (2004)) and selected samples from the Sylva and Mt. Mitchell transects (large circles) with their component ages showing the intra-sample dispersion (small gray circles) on the main plot. These plots collectively illustrate that potentially intriguing information about exhumation rate unsteadiness may be stored in the cooling history of these rocks; however, the regional data set suggests significant complexity. (B) Shaded-relief map of the southern Appalachian region showing the location of the samples relative to the strike of the escarpment topographic brake used in (C). (C) Plot of pooled age vs. strike normal distance from the escarpment topographic brake (black dashed line in (B)) that separates the Piedmont from the Blue Ridge physiographic provinces. Error bars illustrate the 2σ analytical uncertainty of the pooled age, not the dispersion of the component ages. Of note is that locally our samples show a similar pattern of younger samples to the southeast and older ages to the northwest, as was observed by Spotila et al., however, this trend shows no correlation with distance from the escarpment for our samples.

2.4 ADDRESSING AGE DISPERSION

2.4.1 Constraining Internal and External Impurities.

Previous studies have also acknowledged problems with age dispersion when using AHe thermochronology in regions characterized by slow cooling (Belton et al., 2004; Spotila etal., 2004; Green et al., 2006; Fitzgerald et al, 2006; Danisik et al., 2008). As a result we conducted several experiments to constrain possible sources of dispersion from internal and external impurities using two "bad actor" samples from the southern Appalachians that displayed wide age dispersion. Because of the energetic decay of U and Th, He can be implanted into an apatite grain from neighboring U and Th bearing minerals or pour fluids, however, this problem can be mitigated through physical abrasion of outer portion of the apatite grain (Spiegel et al., 2009; McKeon et al. - Chapter 1). We dated additional single grain aliquots of untreated and physically abraded apatite grains from NC-SY-2 (ridge top sample) and NC-SY-13 (valley bottom sample) in an attempt to constrain age dispersion sourced from external impurities. Grains were abraded with several milligrams of aluminum oxide abrasive media in an air abrasion cell similar to the design of Krogh (1982) and grain size reduction was documented through digital imagery. Grains were abraded until greater than 25 μm was removed from all sides of the grain to remove the entire portion of the grain that could be affected by helium ejection due to energetic decay or helium implantation from external sources. Abraded apatite grains were loaded individually in Nb micro-tubes and analyzed for He, U, Th, and Sm as per the untreated grains.

U and Th bearing mineral inclusions are often cited as a potential source for age dispersion (Farley 2002; Ehlers and Farley, 2003; Fitzgerald et al., 2006, Vermeesch et al., 2007) because they implant all of their helium into the host grain, but are not dissolved using the standard nitric acid dissolution protocol and therefore produce too old ages because of the "parentless" helium. Due to the tendency of apatites from this region to contain both large (up to 25 μm) and small mineral inclusions (1-5 μm), we selected 14 inclusion-bearing grains from NC-SY-13 of suitable morphology and analyzed half using the standard nitric acid dissolution protocol and half with the more rigorous hot Hydrofluoric acid dissolution protocol for digesting zircons (Reiners, 2005) in order to fully digest the grain and its inclusions. In addition, 5 inclusion-free grains that were representative of those used for untreated and abraded aliquots were also digested using hot HF to test for the presence of impurities that could not be detected using optical grain selection techniques. For this experiment with inclusions, samples were loaded individually in Nb micro-tubes and He, U, Th, and Sm analyses were all conducted at Arizona Radiogenic Helium Dating Lab at University of Arizona.

2.4.2 Results of Abrasion and Inclusion Experiments

Our inclusion and abrasion experiments were an attempt to understand the dispersion in our data. In this paper we summarize the results of additional untreated single-grain analyses and physically abraded grains from "bad-actor" samples NC-SY-2 (ridge top)

and NC-SY-13 (valley bottom) that were reported in McKeon et al. (Chapter 1) and we report results of our inclusions experiment from NC-SY-13. Both "bad-actor" samples displayed wide age dispersion for additional single-grain analyses. None of these ages could *a priori* be dismissed as geologically unreasonable, nor were they easily interpretable in the context of known sources of age dispersion related to slow cooling such as grain size (here defined as the radius of a sphere with an equivalent F_T correction after Ketcham et al. (2011)) or eU (Figure 2.3).

2.4.2.1 Abrasion results. Physically abraded grains from both samples displayed nearly the same wide range of ages as untreated aliquots; however, abraded grains were observed to have a much wider range of eU concentrations than their untreated counterparts (McKeon et al., Chapter 1). Due to the removal of the portion of the grain that is subject to alpha particle ejection, ages reported for physically abraded grains are not F_T corrected. For physically abraded grains, age was positively correlated with eU for both samples, a relationship that is predicted through the accumulation of radiation damage during slow cooling (Shuster et al. 2006; Flowers et al., 2009), but was not observed in the untreated aliquots (Figure 2.3) or the pooled ages (Table 2.1).

2.4.2.2 Inclusion results. For sample NC-SY-13, neither the presence of inclusions nor the protocol used for dissolving apatite grains was found to impact the observed age dispersion (Figure 2.3). Ages of inclusion-bearing grains that received the standard nitric acid dissolution protocol ranged from 79.9 to 129.8 Ma versus 98.2 to 132.0 Ma for grains digested with the more rigorous hot HF dissolution protocol. Five inclusion-free

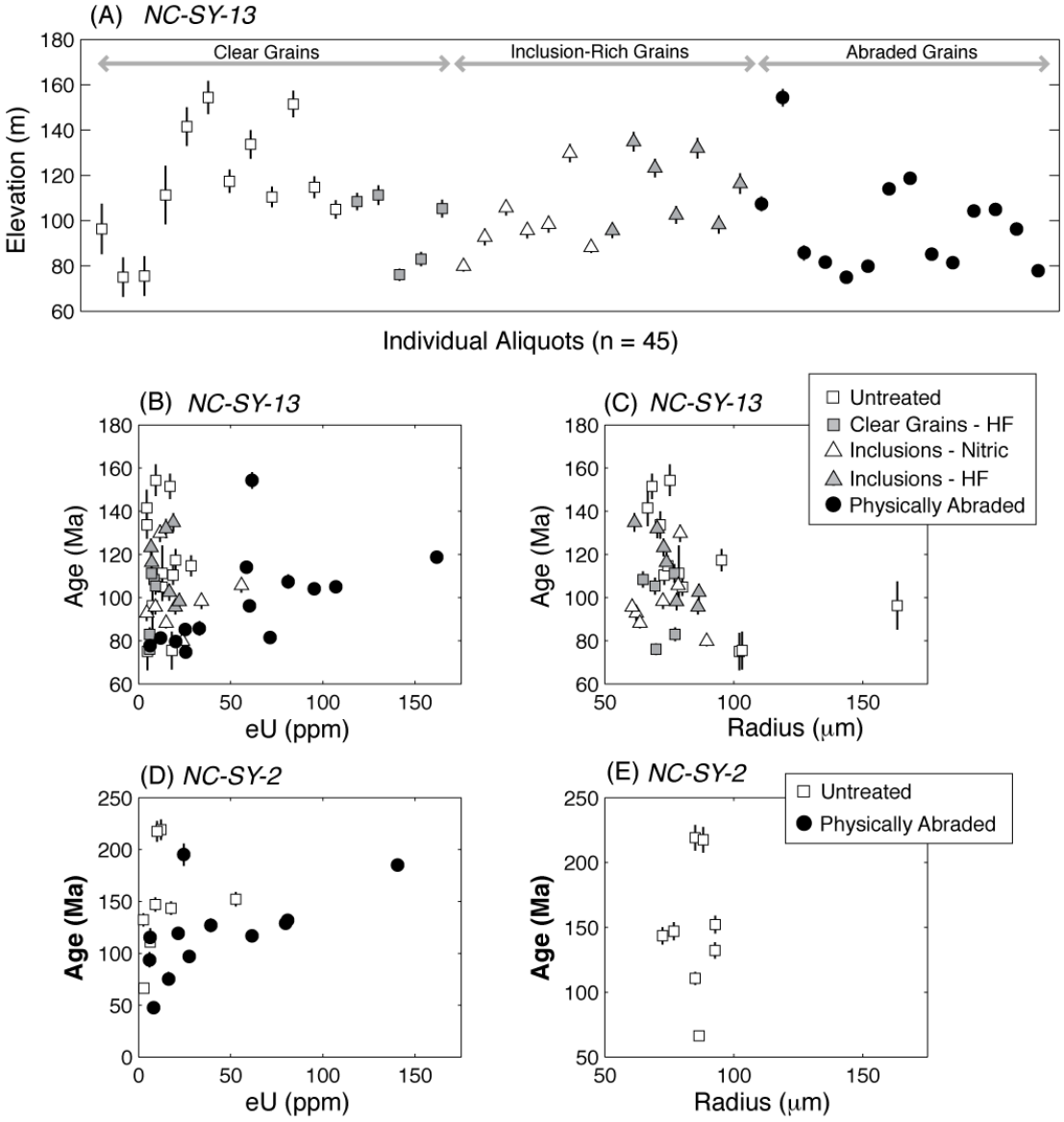

Figure 2.3: Results of inclusion and abrasion experiments for the "bad actor" samples. (A) Results of 45 single-grain aliquots with different treatments from NC-SY-13, boxes represent clear grains appropriate for AHe analysis, triangles represent grains with inclusions, and circles represent physically abraded grains. Light gray shading of boxes and triangles indicates aliquots that received the more rigorous hot HF dissolution protocol to fully digest inclusions. (B and D) Plots showing the lack of correlation between grain size (radius of a sphere of equivalent F_T) and age for all unabraded aliquots for NC-SY-13 (B) and NC-SY-2 (D). (C and E) Plots showing the lack of correlation between eU and age for all unabraded aliquots and the strong positive correlation that is uncovered by physical abrasion for NC-SY-13 (C) and NC-SY-2 (E). For all plots, error bars represent the 2σ propagated uncertainty of He, U, Th, and Sm, measurement and the FT correction (where appropriate), where error bars are not visible, the analytical uncertainty is less than the size of the symbol.

grains digested using hot HF that are representative of the grains selected for all non-inclusion-bearing analyses ranged from 76.1 to 111.2 Ma. Regardless of the presence of inclusions or the dissolution protocol, ages from this experiment displayed no correlation to grain size or eU (Figure 2.3).

2.5 DISCUSSION

2.5.1 U-Th/He Data: Origin of Age Dispersion and Thermochronological Significance

Before turning to landscape evolution, we first need to address the dispersion inherent in some of our samples and assess to what degree our ages can support geologically meaningful interpretations. A key question is whether there is evidence for a single factor that has led to this dispersion, and if this dispersion suggests that the youngest, oldest, or pooled ages are the best representation of each sample's cooling history.

There are at this point quite a number of explanations for why a set of apatite U-Th/He analyses might show dispersion. These explanations range from the analytical and sample-specific to those that reflect a more thorough understanding of the systematics of He accumulation in apatite. We briefly review these here in the context of our samples. Farley (2002), Ehlers and Farley (2003), and Fitzgerald et al. (2006) provided a similar reviews; our review serves as an update.

2.5.1.1 Analytical sources of age dispersion. Clearly there are analytical issues that could impact apatite U-Th/He determinations, and as some of our analyses hail from the earlier days of the method's application, these could in theory pertain. Sample fragments could physically be lost in the transfer from helium-extraction system to U-Th analysis or there could be incomplete sample dissolution or incomplete equilibration of the U and Th spikes with the apatite aliquots. These effects could impact the measured parent/daughter ratio severely, but our reproducibility and experience with the Durango standard makes this unlikely other than an isolated case. Most of our samples were only measured in 2D for the purposes of determining the alpha-loss correction, so any flattening in the third dimension (common in some apatites) would have made some of our F_T values inaccurate, but this effect would only amount to a few percent, and in any case would be insufficient to explain the far larger dispersion we observed in some cases.

2.5.1.2 Internal and external impurities. As stated earlier, dispersion could result from pathologies within the samples themselves. The presence of refractory inclusions of zircon or monazite would significantly impact our results because we used a standard apatite dissolution procedure in nitric acid that would not dissolve such inclusions, resulting in the helium contribution from these inclusions not being supported by the corresponding U and Th from them. However, the similarity of the age dispersion observed from inclusion-bearing grains analyzed with the standard nitric acid dissolution versus the more rigorous hot HF dissolution protocol would suggest that the inclusions in these apatites are not U and Th bearing phases and therefore they are an unlikely source for our observed age dispersion. Similarly, the test group of five inclusion-free grains

that were digested using hot HF showed no dramatic decrease in age dispersion and corroborate the suggestion of Vermeesch et al. (2007) that mirco-inclusions which go undetected during optical selection are not likely to severely impact the age dispersion. Brown et al. (2011) recently pointed out that for slowly cooled samples, analysis of broken grains could result in considerable observed age dispersion since different parts of crystal will contain different portions of the master grain's ^{4}He diffusion profile. However, we were careful to date only unbroken grains, and many of our apatites had complex metamorphic morphologies that would be less prone to mis-identifying a grain parting as a grain termination.

Alternatively, age dispersion could arise from the geological environment of our dated grains. It has been speculated that the presence of a high-U or high-Th neighbor could pollute a grain with high levels of excess ^{4}He (e.g. Spiegel et al. 2009), but this unlucky situation would seem very unlikely to be a common effect. As a variant on this concept, Kohn et al. (2008) noted late fluids percolating along grain boundaries might leave a film high in U and Th, and that this might act in the same way as a bad neighbor; they reported mechanical abrasion results supporting this hypothesis, in which removal of a "skin" equivalent to an alpha-ejection radius led to less dispersed ages. In part our abrasion experiments were motivated by this suggestion.

2.5.1.3 Kinetic variations. Diffusion and retention systematics in apatites provides an additional explanation for age dispersion, particularly for slowly-cooled samples such as ours. The Radiation Damage Accumulation and Annealing Model (RDAAM) of Flowers

et al. (2009; Shuster et al., 2006) shows convincingly that the kinetics of He diffusion are an evolving function that is controlled by the accumulation of radiation damage. This phenomenon is most prevalent in the closure of slowly cooled samples because the increased time spent in the partial retention zone magnifies the differences in He retentivity between grains that experience the same thermal history. Because closure age would then be dependent on U and Th content, dispersion might readily be observed between aliquots and samples, as is commonly seen (e.g Flowers 2007; Flowers, 2009; Ault et al., 2009; Flowers and Kelley, 2011). To a first order, this should manifest itself in a correlation between age and eU. However, in our samples the eU-age correlation is not strong, both between samples and within samples aside for the physically abraded grains where both of our "bad actor" samples display the expected positive correlation between eU and age. Effective diffusion dimension, which in apatite appears to be the physical grain size (Farley, 2000) could also contribute to modest variations in retentivity. For the fairly narrow range in sizes we dated this effect would be equivalent to only a few degrees in closure temperature, but at very cooling rates as low as 0.1C/m.y., this could produce age variation of tens of millions of years (e.g. Reiners and Farley, 2001). However, in our samples, there is no correlation between internal age variations and grain dimension.

2.5.1.4 Thermal structure of the shallow crust. Between samples but not among aliquots from a single sample, the geologic context of the samples could result in dispersion relative to a simplistic explanation that invoked layer-cake cooling-age stratigraphy. In particular, the response of isotherms to paleotopography and the transient lowering or

raising of isotherms relative to the surface during and then after erosion events could complicate age distributions (e.g. Braun, 2002, Ehlers et al., 2006; Olen et al., 2012). Although the response of the temperature field will not be spatially sharp, closure temperatures for helium in apatite are low enough that short-wavelength variations are possible, and in addition, low-temperature isotherms will get up under longer-wavelength topography sufficiently to invalidate assumptions about horizontality and complicate attempts to think about simple kinematic interpretations involving monoclinal tilting. Fluid flow is one other process that might impact the relative ages in an area, because with the low closure interval for apatite of well below 70˚C, even just warm fluids could significantly alter the diffusion process. However, such phenomena cannot explain dispersion internal to samples, and would be mostly limited to more localized and recent resetting rather than alteration of the closure process itself, since it seems unlikely that spatially localized fluid flow would take place over the tens of millions of years involved in slow-cooling closure.

2.5.1.5 Zonation of U, Th, and Sm. Finally, the one other phenomenon that could lead to dispersion of observed ages is zoning of U, Th, and Sm within grains. The problem arises from a mismatch between the alpha-ejection process that occurred and the assumption made in the age-correction process that U and Th are uniformly distributed. The worst-case scenarios would amount to all U and Th being located more than an ejection distance from the grain margin resulting in no alpha loss (effectively an F_T of 1), and all U and Th being located only at the grain boundary (effectively an F_T of 0.5). For these two cases, corrected ages assuming a 80 μm grain radius and uniform distributions of U

and Th would be, respectively, 21% too high, and 39% too low. Extreme zoning could thus explain the magnitude of the scatter seen on our data, however, studies that map the U and Th zonation patterns of a range of apatites from cratonic basement (Farley et al., 2011; Flowers and Kelley, 2011; Ault and Flowers, 2012) suggest that on average the age dispersion resulting from the F_T correction and assumption of homogeneity is on the order of several percent. Zoning has been found to be more the rule than the exception in apatites (Ault and Flowers, 2012), and of significance to our samples, Spotila et al. (2004) noted based on fission-track data that their basement apatites from the southern Appalachians were often zoned. While apatites of igneous origin are sometimes zoned in a systematic fashion which would in turn lead to a systematic mis-correction of U-Th/He ages, the largely metamorphic, polygenetic apatites we dated are more likely to be patchily heterogeneously zoned in U and Th. In this case pooled ages based on multiple grains would give more consistent results, as we observed, because positive and negative mis-corrections would tend to approximately cancel out.

Our working explanation for the excess age dispersion in our data would be a combination of radiation-damage variations in kinetics during slow cooling and patchy zoning in U and Th. In this case it would not be possible to generalize about whether the youngest or oldest ages are most significant, as the eU content and nature of zoning in each grain would need to be known and considered, and this precludes any attempt to build accurate thermal histories.

2.5.1.6 Geological significance of pooled ages. Despite the dispersion we see in aliquots and in some samples, we feel that the pooled ages represent a useful estimate for time of cooling through low temperatures, and our ages are comparable to other results obtained from AHe and AFT dating in the Appalachians. Most significantly, based on these pooled ages (and the data from Spotila et al., 2004), at any locality we studied in the central and southern Appalachians there is no evidence for significant Cenozoic erosionally induced cooling sufficient to be manifested as Cenozoic cooling ages (e.g., cooling of tens of degrees, equivalent to kilometer-scale exhumation as a result of erosional unroofing).

The age-elevation data in the southern Appalachians also do not provide evidence for Cenozoic cooling, nor are they informative about cooling history. Simple thermal models run using Pecube (Braun, 2003) and rules of thumb (e.g, Reiners and Brandon, 2006) suggest that topography having the wavelength observed in the southern Appalachians will most likely have an isotherm structure that is sub-parallel to it, meaning that age-elevation data from surface samples will not be able to sample the true isotherm-normal age-elevation relationship. The only exception to this would be if the entire landscape were carved recently such that the paleoisotherm structure was not in equilibrium with the current topography. This would require recent erosion of significant magnitude at rates far inconsistent with recent cosmogenic measurements (Pavich et al., 1985; Matmon et al., 2003; Hancock and Kirwan, 2007; Portenga and Bierman, 2011). The only slim signature in the age-elevation data takes the form of the few old ages seen at highest elevations; these could be interpreted as representative of an older, very slow-cooling regime, with the younger low-elevation ages, however dispersed, representing a period of

accelerated cooling that exhumed the fringe of a fossil partial-retention zone. Given the low number of old ages and the overall dispersion, it does not seem advisable to press this line of reasoning. Therefore, from the pooled ages we do not find evidence of extensive recent exhumation, but more importantly, we lack the resolution necessary to comment on the steady or unsteady behavior of the evolution of this landscape as it could relate to the observed unsteadiness of sediment deposition rates offshore (Pazzaglia and Brandon, 1996).

2.5.2 Insights from abrasion analysis

2.5.2.1 Sources of age dispersion. The analysis of physically abraded grains from NC-SY-2 and NC-SY-13 produced three key observations that explain the dispersion observed for untreated grains. First, abraded grains produced widely dispersed ages that were similar to untreated grains suggesting that implanted helium from external sources was not a major factor contributing to the observed age dispersion. Second, unlike the untreated grains that tended to have low eU concentrations, the physically abraded grains spanned a wide range of eU concentrations with maximum concentrations nearly three-fold greater than the maximum of the untreated grains. This observation can only occur if there is significant zonation of U, Th, and Sm. The fact that eU concentrations for the abraded grains ranged from 1 to over 100 ppm for both samples suggests that the pattern of zonation is not systematic in these metamorphic apatites and thus neither is the age dispersion resulting from the assumption of U, Th, and Sm homogeneity that is implicit with the F_T correction applied to untreated grains. Third, the positive eU-age correlation

observed for the physically abraded grains is expected given regional evidence for slow cooling (Naeser et al., 2004) and the impact of radiation damage (Shuster et al., 2006); however, the untreated grains did not display this relationship. McKeon et al. (Chapter 1) illustrate how zonation of U, Th, and Sm can mask the eU-age relationship for untreated grains through the combined effect of incorrect application of the F_T correction and the dilution of a high eU and low volume core by the low eU and high volume rim of a grain. Abrasion mitigates this problem by partially removing the low eU rim and the need to correct for alpha-ejection using the F_T correction. Taken together, these observations corroborate our suggestion that the age dispersion observed from untreated grains is rooted in the combined effect of radiation damage-induced variations in closure temperature and zonation of U, Th, and Sm.

2.5.2.2 Inferences about cooling history. Because the variation of diffusion kinetics caused by radiation damage results in grain-specific closure temperatures (Shuster et al., 2006; Flowers et al., 2009), we take advantage of the wide range in eU and age observed for both bad actor samples to infer their low-temperature cooling histories. As stated, the widely dispersed ages for NC-SY-2 and NC-SY-13 were positively correlated with eU concentration, a situation that can only arise as a result of slow cooling through the PRZ. The slower a sample cools through the PRZ, the greater the age dispersion resulting from variations in the concentration of eU will be. We compare our eU-age relationships from the two samples to the regional apatite fission track derived long-term average erosion rate of 20 m/Myr (Naeser et al., 2004) using the diffusion modeling software package HeFTy (Ketcham, 2005) and the RDAAM to forward model the age

dispersion resulting from variations in eU for a grain radius of 80 μm (Figure 2.4). Assuming a stable geothermal gradient of 20 ˚C/km we find that the ridge top sample (NC-SY-2) generally fits the prediction of slow and steady exhumation at a rate of 20 m/Myr, but the valley bottom sample (NC-SY-13) shows distinctly less age dispersion than that predicted by the forward model, suggesting that it cooled through the PRZ at a faster rate.

2.5.2.3 Thermal modeling using abraded grains. To more fully explore the cooling history information stored in the eU-age relationship from our physically abraded datasets we used an inverse modeling approach again using HeFTy and the RDAAM. Aside from parameters that control different aspects of how the model runs, the core input into an inverse model in HeFTy are currently up to 7 eU-age pairs with an analytical uncertainty on the age from different aliquots of a single sample. HeFTy generates random time-Temperature (tT) paths and then uses the RDAAM to calculate what the age should be given a particular eU. As such, HeFTy is not designed to account for sources of age dispersion other than radiation damage and grain size, thus, the model cannot fit thermal histories to moderately dispersed data resulting from other sources because the age dispersion is typically much greater than the analytical uncertainty.

To combat this limitation but still use HeFTy and the RDAAM for the valuable cooling history information that it can elucidate, we fit an exponential regression to the observed eU-age data and then use discrete eU-age points along the regression and the 68.3% C.I bounds (representative of 1σ) on the regression for the age uncertainty as input in the

inverse model (Figure 2.4). We chose to use an exponential regression because it afforded the best compromise between simplicity and accurately fitting the results of RDAAM predicted eU-age relationships for a range of cooling rates. We chose the location of points along the regression to capture both the range of eU concentrations observed and the eU concentrations where the observed data was most densely clustered.

In an attempt to let the inverse model explore the full ramifications of radiation damage, we placed as few constraints on the model as possible. As a result of physical abrasion removing the portion of the grain subject to alpha ejection we turned off both alpha redistribution and ejection from the model and used a standard grain radius of 80 μm to represent the average size of pre-abrasion grains from our Blue Ridge samples. HeFTy allows for radial zonation of U and Th to be input for each age model, however, given that we did not measure the distribution of U and Th within the abraded grains and the evidence for patchy and therefore unpredictable zonation patterns described above, we made the simplifying assumption of homogeneity of parent material within the abraded grains. We applied no constraints to random tT paths other than their starting and ending positions. The starting constraint required paths to begin between 140 - 170˚C at 230 – 250 Ma which was based on regional zircon U-Th/He ages we acquired as part of this study, paths were required to end today at 10˚C which was chosen as an average temperature for the region during the late Cenozoic. For NC-SY-13 (valley bottom sample) we generated 100k random tT paths with the model finding 828 “acceptable” and 288 “good” statistically significant fits to the input data from the exponential regression. For NC-SY-2 (ridge top sample) the greater uncertainty of the exponential regression

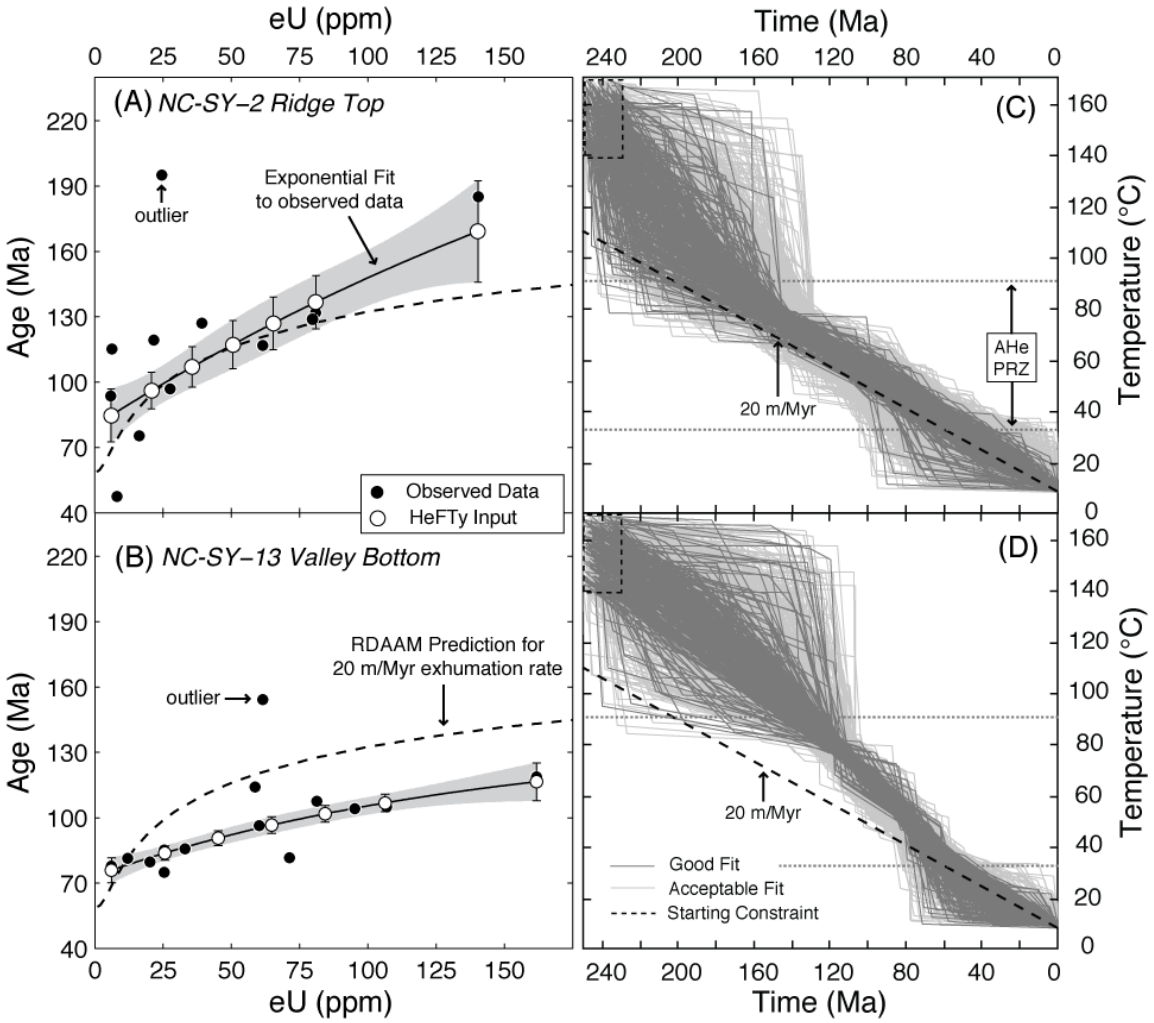

Figure 2.4: Cooling histories derived from inverse modeling of physically abraded grains from NC-SY-2 and NC-SY-13 using HeFTy and the RDAAM. (A and B) Plots showing the observed eU-Age data for the physically abraded grains from both samples (black circles), exponential regressions (solid black lines) and 68.3% confidence intervals (light gray shading) fit to the observed data. The open circles and error bars lying along the exponential regressions indicate the eU-Age data input into the HeFTy inverse models. The eU-Age relationship predicted by the RDAAM for an exhumation rate of 20 m/Myr (assuming a geothermal gradient of 20 ˚C/km) is shown by the dashed lines. (C and D) Results from inverse modeling showing time-temperature (tT) paths yielding acceptable fits (light gray) and good fits (dark gray) to the input eU-Age data points from the exponential regressions. The dashed box indicates the starting constraint for the tT paths and a 20 m/Myr exhumation rate is indicated by the dashed black line. The Partial Retention Zone (PRZ) is indicated to illustrate the temperature range where He diffusion transitions from fully open to fully closed system behavior and indicates where variations in eU between individual aliquots can influence the shape of the tT paths that produce acceptable and good fits for each sample.

resulted in the model finding more statistically significant fits in fewer iterations. To fairly compare the results between the samples we chose to run the inversion for NC-SY-2 until 300 "good" fits were found to match the results of NC-SY-13, this required ~18,000 iterations and generated 752 "acceptable" fits in the process. In HeFTy the statistical significance of a path is determined by applying a goodness of fit test to the predicted age for each of the seven input eU-age pairs and is described in detail in Ketcham (2005).

The results of inverse modeling of the eU-age relationship from abraded grains illustrates the enhanced resolution of the thermal history that is stored in the age dispersion resulting from radiation damage and suggests that both samples have experienced unsteady cooling histories. Figure 2.4 compares the tT path predicted by steady erosion at 20 m/Myr with the tT paths that produced statistically significant fits to the input eU-age data from the exponential regressions. For NC-SY-2, the inverse model suggests relatively rapid cooling from the zircon U-Th/He window to the upper part of the apatite PRZ by ~160 Ma and then steady slow-cooling in line with the 20 m/Myr exhumation rate. The inflection point in the "good" fit tT paths is constrained by the need to quickly cool to fit an age of 170 Ma with an eU concentration of 140 ppm, but then cool slowly through the apatite PRZ to build the wide range of the eU-age relationship observed. For NC-SY-13, the model does not constrain the high temperature cooling history prior to 120 Ma, however, at that point the statistically significant tT paths become narrowly restricted and suggest more rapid cooling than that predicted by the 20 m/Myr long-term average exhumation rate. The tight clustering of "good" fits from 120 to 80 Ma is representative

of the portion of the thermal history that is constrained by the input eU-age data from the exponential regression. For both models, below ~50˚C the RDAAM has reached or exceeded its limit to constrain the very low temperature thermal history, which is manifest in the fanning out of the good fits below these thresholds. Taken together, these results suggest that while the long-term average rate of exhumation has been slow, there is evidence to suggest unsteady exhumation of this portion of the Blue Ridge Mountains.

2.5.3 Appalachian Landscape Evolution

2.5.3.1Interpreted from pooled ages. The patterns of ages that emerge from the our pooled ages constrain the general pattern of Appalachian Landscape evolution, however, age dispersion between and within samples precludes our ability to draw detailed conclusions from this dataset. From the Central Appalachians we find no evidence for significant exhumation in relation to the large increase in sedimentation rates in the Miocene observed offshore (Figure 2.1). Beyond that there is a weak trend of ages getting younger to the west, but the dispersion between the pooled ages is considerable and therefore we hesitate to over-interpret this small and complex dataset. From the southern Appalachians we find older ages at high elevations and also to the far west of our study area, but we also find strong contrasts in cooling ages and their relation to elevation over very short distances between the Sylva and Hornbuckle transects from Waterrock Knob (Figure 2.1). We feel that these two suites of samples are emblematic of the reality using the standard protocols for bulk U-Th/He thermochronology analysis in the Appalachians specifically and slowly eroding landscapes in general. Here we used a

relatively dense sampling strategy to try and combat age dispersion arising from problems associated with the warping of shallow isotherms and transient topography, however, we uncovered a complex series of problems related to grain-specific characteristics which were found to have such a strong impact on the ages derived that we could not address the problem we were trying to solve. As a result we feel that one must interpret the results from our pooled ages very conservatively. As with the Central Appalachian samples, we see no evidence for significant recent exhumation from the rugged landscape of Blue Ridge of western North Carolina, but the specifics of the pace and variability of the cooling history are out of reach of this dataset.

2.5.3.2 Interpreted from radiation damage modeling. By conducting detailed experiments to isolate the source of age dispersion we were able to describe why our untreated grains produced the age dispersion observed and take advantage of the expected dispersion caused by radiation damage to make inferences about the low-temperature thermal history of the Blue Ridge region. Our work with the "rehabilitated" bad actors from the Sylva transect illustrate that until the sources of age dispersion are rooted out, analyzing more grains using the same protocols will not lead to more interpretable data (Figure 2.3). As a result of this observation we suggest that studies interested in using AHe dating in slowly eroding landscapes collect fewer samples, but characterize them more carefully using the techniques that have been developed by Farley et al. (2011) or McKeon et al. (Chapter 1). It is convenient that in slowly eroding landscapes we are typically interested in constraining variations in the thermal history on the order of 10's of Myr, not 1's of Myr, because then the dispersion that remains following attempts at

mitigation through abrasion or otherwise can be tolerated. For example, from our two rehabilitated bad actor samples we find evidence for spatially variable cooling histories form the Appalachian landscape through the difference of the eU-age relationship observed from the abraded grains (Figure 2.3). Though the data from the abraded grains still displayed dispersion that exceeded the analytical uncertainty we were able to interrogate the overall eU-age trends from the two samples by fitting an exponential regression to the data and using the uncertainty of that fit to guide the inverse models (Figure 2.4). From this we infer that cooling from the zircon U-Th/He closure window was initially rapid for NC-SY-2, followed by a long period of generally slow erosion, in line with the long-term estimate of 20 m/Myr from apatite fission track analysis (Naeser et al, 2004). For NC-SY-13, cooling through the PRZ is more rapid, which is expected in order to set the ages observed from the wide range of eU concentrations observed from abraded grains. By isolating the causes of age dispersion for these two samples, we are able to derive much greater resolution of the thermal histories experienced by different points in the landscape. Unlike the pooled ages, we feel that interpretation of the cooling history in context of landscape evolution is permissible with the abraded dataset and with the results of the inverse modeling.

2.5.3.3 Summary from Low-Temperature Thermochronology. The major contribution of our work in the Appalachian landscape has been to illustrate that although the long-term average erosion rate has been slow, the spatial variability of erosion rates through time suggests that landscape evolution has not been uniformly steady. The pooled ages from the central and southern Appalachians corroborate the findings of previous studies and

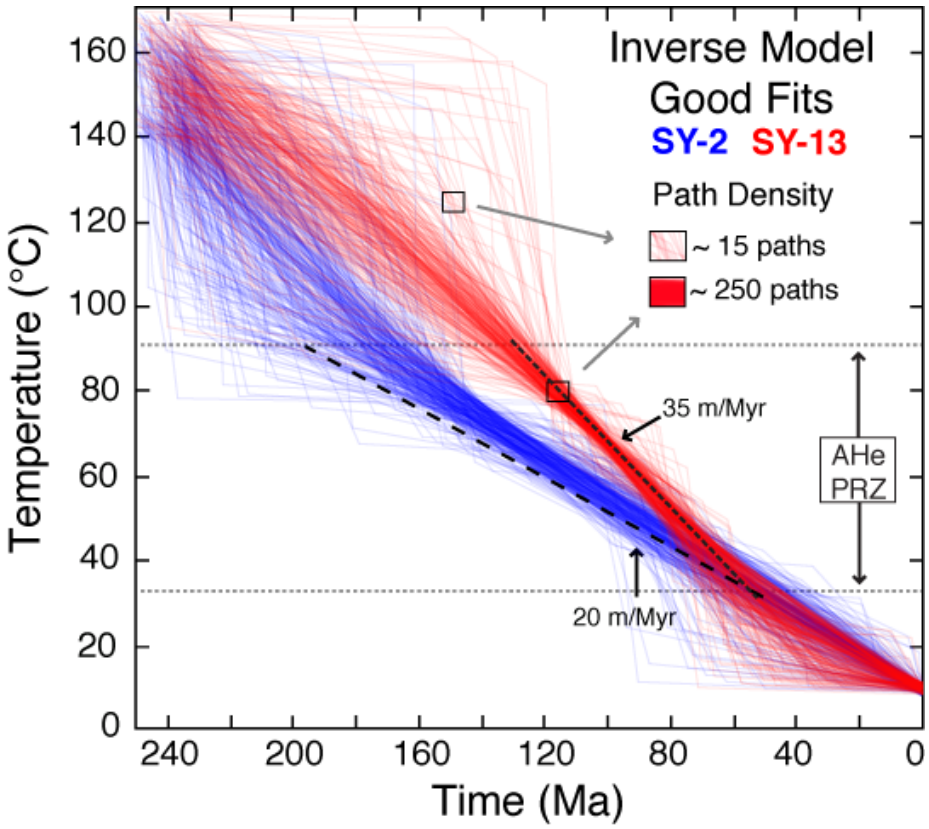

Figure 2.5: Comparison of the results of inverse modeling for NC-SY-2 and NC-SY-13 showing only the time-Temperature (tT) paths that produced statistically good fits to the input data from the exponential regressions. The paths are displayed with 90% transparent lines, thus the darker blue (NC-SY-2) and red (NC-SY-13) colors indicate where the random tT paths overlap. The path density examples show the number of paths that pass through an approximately 5 Ma by 5˚C window to produce the color saturation observed. The dark colors within the PRZ for samples illustrate how the good fits follow dominantly linear cooling paths (approximated by the dashed lines) that suggest the different positions in the landscape represented by the two samples experienced different erosion rates. The ~20˚C offset between the samples prior to 120 Ma corroborates our assumption of the assumed geothermal gradient of 20˚C/Km because the samples are vertically offset by 1.2 km.

give no evidence for significant recent exhumation to explain the observed pulse of rapid sediment accumulation rates observed in offshore basins. Wide age dispersion resulting from the combined effect of several sources precludes meaningful interpretation of the pooled ages from our dataset in the context of landscape evolution, however, detailed investigation of several samples illustrates that the erosive history becomes more complex the closer one looks. Figure 2.5 shows the difference in the cooling rate inferred

from inverse modeling of the abraded grains from the ridge top sample (NC-SY-2) and the valley bottom sample (NC-SY-13), which implies that different positions in the landscape of the Blue Ridge Mountains of western North Carolina experienced different erosion rates during the Cretaceous. Interpreting these results in the context of landscape evolution suggests that the ridge top of Waterrock Knob cooled quickly flowing Triassic rifting and then cooling slowed to the range-wide background erosion rate of 20 m/Myr around ~160 Ma. At that time, the rocks that now comprise the valley floor of the Little Tennessee River were ~20˚C hotter and about 1 km deeper in the crust. Between ~130 Ma and ~60 Ma the ridge top continued to erode slowly at 20 m/Myr, but the valley floor experienced nearly 2X faster erosion, which could be interpreted to reflect headward propagating river incision causing the valley floor to erode more quickly than the ridges, leading to the generation of greater relief. By ~60 Ma, the thermal histories of the two points in the landscape converge at ~40˚C or 1-1.5 km depth in the crust, which is the lower limit of the AHe temperature range. These contrasting cooling histories illustrate spatially unsteady erosion rates during the Cretaceous for the rugged mountains of western North Carolina and provide evidence for relief generation that matches the magnitude of relief in the modern landscape. It should be noted that the entire region cooled from ~40˚C since ~60 Ma and we cannot constrain steady or unsteady nature of the final 1-1.5 km of exhumation that produced the modern landscape. Because our samples are spatially restricted to a small area we feel confident that our contrasting cooling histories are reflective of geomorphic processes acting at different positions in the landscape. However, because we only have detailed thermal histories from a very

small area, we cannot constrain what process is responsible for renewed valley incision during the Cretaceous in this region.

2.5.3.4 The Road Forward. The treatments and modeling approach used for the rehabilitated bad actor samples establish a means to gain useful information about the thermal history from Appalachian bedrock samples, however, it appears that the Cenozoic portion of the thermal history is out of reach of the traditional bulk apatite U-Th/He thermochronology. To fully address the post-orogenic thermal history and thereby make inferences about the processes and drivers controlling Appalachian landscape evolution will require the extremely low-temperature sensitivity of $^{4}He/^{3}He$ thermochronometry (Shuster et al., 2004). This technique enables observation of the natural diffusive ^{4}He concentration profile within an individual apatite grain, the shape of which is very sensitive to the thermal history down to temperatures of ~30˚C at Appalachian cooling rates. Through implementation of this technique and the abrasion and radiation damage modeling technique for bulk AHe dating we feel that an explanation of the paradox of young looking topography and unsteady sedimentation rates in a region that had previously appeared to be the definition of slow and steady erosion is within our grasp.

2.6 CONCLUSIONS

Here we present results of over 250 apatite U-Th/He ages determined on bedrock samples from the central and southern Appalachians of eastern North America. Samples were collected from high-grade polymetamorphic Proterozoic rocks that have experienced slow long-term averaged cooling rates following the close of the Alleghenian Orogeny. Wide age dispersion between and within samples that did not correlate with known sources for age dispersion was observed from both study areas. We address the age dispersion in two ways; first we use pooled ages (Vermeesch, 2008) to compare the widely dispersed aliquots between samples, and second, we conducted detailed experiments using two samples from the southern Appalachians aimed at identifying the sources of age dispersion and take advantage of the thermal history information they provide.

Owning to problems with age dispersion, we interpret the results of the pooled ages very conservatively. From both the central and southern Appalachians there is no evidence of significant recent exhumation to correlate with a large increase of sedimentation rates in Atlantic passive margin basins (Pazzaglia and Brandon, 1996). Beyond this result the pooled ages were too dispersed and their associations too complex to make meaningful interpretations in light of the apparent long-term steadiness of erosion at 20 m/Myr. However, through our efforts to identify the sources age dispersion, we found evidence of irregular and sometimes strong zonation of U and Th through physical abrasion of the outer portion of individual grains. Once this problem was recognized, the ages from

physically abraded grains were found to correlate well with acknowledged age variation caused by radiation damage. From this relationship and inverse modeling of the kinetic effects of radiation damage on He diffusion we were able to infer an unsteady pre-Cenozoic cooling history for the Blue Ridge Mountains of western North Carolina.

The recognition of unsteady cooling histories from our two samples from the southern Appalachians is the first direct evidence of unsteady exhumation from the Appalachian landscape. From our experiences we suggest that future work should concentrate on collecting fewer samples, but concentrating more effort to address the sources of age dispersion.

2.7 ACKNOWLEDGMENTS

This research was supported by a Geological Society of America Student Research Grant and multiple Palmer Research Grants from the Department of Earth and Environmental Sciences of Lehigh University to R.E. McKeon. Support for the field work and lab analysis leading to the pooled age dataset was provided by NSF-EAR 9909393 to P.K. Zeitler, F.J. Pazzaglia, and B.D. Idleman. Richard Ketcham is thanked for thoughtful discussions that improved our use of inverse models of abraded grains in HeFTy. Peter Reiners is thanked for years of U, Th, and Sm analysis and for hosting R.E. McKeon at the University of Arizona. Finally, we thank the contributions of the many previous students at Lehigh University that worked on this project.

2.8 REFERENCES

Ahnert, F., 1970, Functional relationships between denudation, relief, and uplift in large mid-latitude drainage basins: American Journal of Science, v. 268, p. 243–263.

Ault, A.K., and Flowers, R.M., 2012, Is apatite U-Th zonation information necessary for accurate interpretation of apatite (U-Th)/He thermochronometry data?: Geochimica et Cosmochimica Acta, v. 79, no. C, p. 60–78, doi: 10.1016/j.gca.2011.11.037.

Ault, A.K., Flowers, R.M., and Bowring, S.A., 2009, Phanerozoic burial and unroofing history of the western Slave craton and Wopmay orogen from apatite (U–Th)/He thermochronometry: Earth and Planetary Science Letters, v. 284, no. 1, p. 1–11.

Belton, D., Brown, R.W., Kohn, B.P., Fink, D., and Farley, K.A., 2004, Quantitative resolution of the debate over antiquity of the central Australian landscape: implications for the tectonic and geomorphic stability of cratonic interiors: Earth and Planetary Science Letters, v. 219, p. 21–34, doi: 10.1016/S0012-821X(03)00705-2.

Blackmer, G.C., Omar, G.I., and Gold, D.P., 1994, Post-Alleghanian unroofing history of the Appalachian Basin, Pennsylvania, from apatite fission track analysis and thermal models: Tectonics, v. 13, no. 5, p. 1259–1276.

Boettcher, S., and Milliken, K., 1994, Mesozoic-Cenozoic unroofing of the southern Appalachian basin: apatite fission track evidence from Middle Pennsylvanian Sandstones: The Journal of Geology, v. 102, p. 655–663.

Braun, J., 2002, Estimating exhumation rate and relief evolution by spectral analysis of age–elevation datasets: Terra Nova, v. 14, no. 3, p. 210–214.

Braun, J., 2003, Pecube: a new finite-element code to solve the 3D heat transport equation including the effects of a time-varying finite amplitude surface topography: Computers and Geosciences, v. 29, p. 787–794, doi: 10.1016/S0098-3004(03)00052-9.

Brown, R.W., Beucher, R., Roper, S., Gallagher, K., Persano, C., Stuart, F., Fitzgerald, P.G., Swift, D.A., 2011, Exploiting the natural dispersion of single crystal fragment (U-Th)/He age determinations using a new inverse approach to deriving thermal history information, Abstract V31G-06 presented at 2011 Fall Meeting, AGU, San Francisco, CA, 5-9 Dec.

Danišík, M., Sachsenhofer, R.F., Privalov, V.A., Panova, E.A., Frisch, W., and Spiegel, C., 2008, Low-temperature thermal evolution of the Azov Massif (Ukrainian Shield–Ukraine)—Implications for interpreting (U–Th)/He and fission track ages from cratons: Tectonophysics, v. 456, no. 3, p. 171–179.

Davis, W. M., 1889, The rivers and valleys of Pennsylvania: National Geographic Magazine, v. 1, no. 3, p. 184-253.

Davis, W., 1899, The geographic cycle: The Geographical Journal, v. 14, no. 5, p. 481–504.

Dodson, M.A., 1973, Closure temperature in cooling geochronological and petrological systems: Contributions to Mineralogy and Petrology, v. 40, no. 3, p. 259–274.

Ehlers, T.A., and Farley, K.A., 2003, Apatite (U–Th)/He thermochronometry: methods and applications to problems in tectonic and surface processes: Earth and Planetary Science Letters, v. 206, no. 1, p. 1–14.

Ehlers, T.A., Farley, K.A., Rusmore, M.E., and Woodsworth, G.J., 2006, Apatite (U-Th)/He signal of large-magnitude accelerated glacial erosion, southwest British Columbia: Geology, v. 34, no. 9, p. 765, doi: 10.1130/G22507.1.

Farley, K.A., 2002, (U-Th)/He dating: Techniques, calibrations, and applications: Reviews in Mineralogy and Geochemistry, v. 47, no. 1, p. 819–844.

Farley, K.A., 2000, Helium diffusion from apatite: General behavior as illustrated by Durango fluorapatite: Journal of Geophysical Research, v. 105, no. B2, p. 2903–2914.

Farley, K.A., Shuster, D.L., and Ketcham, R.A., 2011, U and Th zonation in apatite observed by laser ablation ICPMS, and implications for the (U-Th)/He system: Geochimica et Cosmochimica Acta, v. 75, no. 16, p. 4515–4530, doi: 10.1016/j.gca.2011.05.020.

Farley, K.A., Wolf, R.A., and Silver, L.T., 1996, The effects of long alpha-stopping distances on (U-Th)/He ages: Geochimica et Cosmochimica Acta, v. 60, no. 21, p. 4223–4229.

Fischer, K.M., 2002, Waning buoyancy in the crustal roots of old mountains: Nature, v. 417, no. 6892, p. 933–936.

Fitzgerald, P., Baldwin, S., Webb, L., and O'Sullivan, P., 2006, Interpretation of (U-Th)/He single grain ages from slowly cooled crustal terranes: A case study from the Transantarctic Mountains of southern Victoria Land: Chemical Geology, v. 225, p. 91–120, doi: 10.1016/j.chemgeo.2005.09.001.

Flowers, R., Shuster, D., Wernicke, B., and Farley, K., 2007, Radiation damage control on apatite (U-Th)/He dates from the Grand Canyon region, Colorado Plateau: Geology, v. 35, no. 5, p. 447, doi: 10.1130/G23471A.1.

Flowers, R.M., 2009, Exploiting radiation damage control on apatite (U–Th)/He dates in cratonic regions: Earth and Planetary Science Letters, v. 277, p. 148–155.

Flowers, R.M., and Kelley, S.A., 2011, Interpreting data dispersion and “inverted” dates in apatite (U-Th)/He and fission-track datasets: An example from the US

midcontinent: Geochimica et Cosmochimica Acta, v. 75, no. 18, p. 5169–5186, doi: 10.1016/j.gca.2011.06.016.

Flowers, R.M., Ketcham, R.A., Shuster, D.L., and Farley, K.A., 2009, Apatite (U-Th)/He thermochronometry using radiation damage accumulation and annealing model: Geochimica et Cosmochimica Acta, v. 73, no. 8, p. 2347–2365, doi: 10.1016/j.gca.2009.01.015.

Green, P., Crowhurst, P., Duddy, I., Japsen, P., and Holford, S., 2006, Conflicting (U–Th)/He and fission track ages in apatite: Enhanced He retention, not anomalous annealing behaviour: Earth and Planetary Science Letters, v. 250, no. 3-4, p. 407–427, doi: 10.1016/j.epsl.2006.08.022.

Hack, J., 1960, Interpretation of erosional topography in humid temperate regions: American Journal of Science, v. 258-A, p. 80–97.

Hancock, G., and Kirwan, M., 2006, Summit erosion rates deduced from 10Be: Implications for relief production in the central Appalachians: Geology, v. 35, no. 11, p. 89–92, doi: 10.1130/G23147A.1.

Hawman, R.B., Khalifa, M.O., and Baker, M.S., 2012, Isostatic compensation for a portion of the Southern Appalachians: Evidence from a reconnaissance study using wide-angle, three-component seismic soundings: Geological Society of America Bulletin, v. 124, no. 3-4, p. 291–317, doi: 10.1130/B30464.1.

House, M., Kohn, B., Farley, K., and Raza, A., 2002, Evaluating thermal history models for the Otway Basin, southeastern Australia, using (U-Th)/He and fission-track data from borehole apatites: Tectonophysics, v. 349, no. 1-4, p. 277–295.

Ketcham, R.A., 2005, Forward and inverse modeling of low-temperature thermochronometry data. in Reiners, P.W., and Ehlers, T.A., (eds.) Low-Temperature themrochronology: Techniques, Interpretations, and Applications, Reviews in Mineralogy and Geochemistry v. 58, p. 315-350.

Ketcham, R.A., Gautheron, C., and Tassan-Got, L., 2011, Accounting for long alpha-particle stopping distances in (U-Th-Sm)/He geochronology: Refinement of the baseline case: Geochimica et Cosmochimica Acta, v. 75, no. 24, p. 7779–7791, doi: 10.1016/j.gca.2011.10.011.

Kohn, B., Spiegel, C., Phillips, D., Gleadow, A., 2008, Rubbing out apatite helium age spread in fast-cooled rocks: In Garver, J.I., and Montario, M.J., (eds.), Proceedings from the 11th International Conference on thermochronometry, Anchorage Alaska, Sept. 2008.

Krogh, T., 1982, Improved accuracy of U-Pb zircon ages by the creation of more concordant systems using an air abrasion technique: Geochimica et Cosmochimica Acta, v. 46, no. 4, p. 637–649.

Matmon, A., Bierman, P., Larsen, J., Southworth, S., Pavich, M., and Caffee, M., 2003, Temporally and spatially uniform rates of erosion in the southern Appalachian Great Smoky Mountains: Geology, v. 31, no. 2, p. 155–158.

Miller, D.S., and Duddy, I., 1989, Early Cretaceous uplift and erosion of the northern Appalachian Basin, New York, based on apatite fission track analysis: Earth and Planetary Science Letters, v. 93, p. 35–49.

Naeser, C.W., Naeser, N.D., Kunk, M.J., Morgan, B.A., Schultz, A.P., Southworth, S.C., Weems, R.E., 2001, Paleozoic through Cenozoic uplift, erosion, stream capture, and depositional history in the Valley and Ridge, Blue Ridge, Piedmont, and Costal Plain provinces of Tennessee, North Carolina, Virginia, Maryland, and District of Columbia: Geological Society of America, Abstracts with Programs, Nov. 7, 2001, paper no. 133-0.

Naeser, N. D., Naeser, C. W., Southworth, C. S., Morgan, B. A., and Schultz, A. P., 2004, Paleozoic to recent tectonic and denudation history of rocks in the Blue Ridge Province, central and southern Appalachians; evidence from fission-track thermochronology: Geological Society of America, Abstracts with Programs, 36, 114.

Nathenson, M., and Guffanti, M., 1988, Geothermal gradients in the conterminous United States: Journal of Geophysical Research, v. 93, no. B6, p. 6437–6450.

Olen, S.M., Ehlers, T.A., and Densmore, M.S., 2012, Limits to reconstructing paleotopography from thermochronometer data: Journal of Geophysical Research, v. 117, no. F1, doi: 10.1029/2011JF001985.

Pavich, M., Brown, L., Valette-Silver, J.N., Klein, J., and Middleton, R., 1985, ^{10}Be analysis of a Quaternary weathering profile in the Virginia Piedmont: Geology, v. 13, no. 1, p. 39–41.

Pazzaglia, F., and Brandon, M., 1996, Macrogeomorphic evolution of the post-Triassic Appalachian mountains determined by deconvolution of the offshore basin sedimentary record: Basin Research, v. 8, p. 255–278.

Poag, C.W., and Sevon, W.D., 1989, A record of Appalachian denudation in postrift Mesozoic and Cenozoic sedimentary deposits of the US middle Atlantic continental margin: Geomorphology, v. 2, no. 1-3, p. 119–157.

Portenga, E.W., and Bierman, P.R., 2011, Understanding Earth's eroding surface with ^{10}Be: GSA Today, v. 21, no. 8, p. 4–10, doi: 10.1130/G111A.1.

Prince, P.S., Spotila, J.A., and Henika, W.S., 2011, Stream capture as driver of transient landscape evolution in a tectonically quiescent setting: Geology, v. 39, no. 9, p. 823–826, doi: 10.1130/G32008.1.

Reiners, P., 2005, Zircon (U-Th)/He thermochronometry: in Reiners, P.W., and Ehlers, T.A., (eds.) Low-Temperature themrochronology: Techniques, Interpretations, and Applications, Reviews in Mineralogy and Geochemistry v. 58, p. 151-179.

Reiners, P., and Brandon, M., 2006, Using thermochronology to understand orogenic erosion: Annual Reviews of Earth and Planetary Science, v. 34: Annual Reviews of Earth and Planetary Science, v. 10, p. 419–466.

Reiners, P.W., and Farley, K.A., 2001, Influence of crystal size on apatite (U–Th)/He thermochronology: an example from the Bighorn Mountains, Wyoming: Earth and Planetary Science Letters, v. 188, no. 3, p. 413–420.

Roden Tice, M.K., and Tice, S.J., 2005, Regional-scale mid-Jurassic to Late Cretaceous unroofing from the Adirondack Mountains through central New England based on apatite fission-track and (U-Th)/He thermochronology: The Journal of Geology, v. 113, no. 5, p. 535–552.

Roden, M.K., 1991, Apatite fission-track thermochronology of the southern Appalachian Basin: Maryland, West Virginia, and Virginia: Journal of Geology, v. 99, p. 41–53.

Roden, M.K., and Miller, D.S., 1989, Apatite fission-track thermochronology of the Pennsylvania Appalachian Basin: Geomorphology, v. 2, no. 1-3, p. 39–51.

Roden, M.K., and Miller, D.S., 1991, Tectono-thermal history of Hartford, Deerfield, Newark and Taylorsville Basins, eastern United States, using fission-track-analysis: Schweizer Mineralogische und Petrographische Mitteilungen, v. 71, p. 187–203.

Roden-Tice, M.K., West, D.P., Jr, Potter, J.K., Raymond, S.M., and Winch, J.L., 2009, Presence of a Long-Term Lithospheric Thermal Anomaly: Evidence from Apatite Fission-Track Analysis in Northern New England: The Journal of Geology, v. 117, no. 6, p. 627–641, doi: 10.1086/605995.

Shuster, D., Flowers, R., and Farley, K., 2006, The influence of natural radiation damage on helium diffusion kinetics in apatite: Earth and Planetary Science Letters, v. 249, no. 3-4, p. 148–161, doi: 10.1016/j.epsl.2006.07.028.

Shuster, D.L., and Farley, K.A., 2004, 4He/3He thermochronometry: Earth and Planetary Science Letters, v. 217, no. 1-2, p. 1–17, doi: 10.1016/S0012-821X(03)00595-8.

Slingerland, R., and Furlong, K., 1989, Geodynamic and Geomorphic Evolution of the Permo-Triassic Appalachian Mountains: Geomorphology, v. 2, p. 23–37.

Spiegel, C., Kohn, B., Belton, D., Berner, Z., and Gleadow, A., 2009, Apatite (U–Th–Sm)/He thermochronology of rapidly cooled samples: The effect of He implantation: Earth and Planetary Science Letters, v. 285, no. 1-2, p. 105–114, doi: 10.1016/j.epsl.2009.05.045.

Spotila, J.A., Bank, G.C., Reiners, P.W., Naeser, C.W., Naeser, N.D., and Henika, B.S., 2004, Origin of the Blue Ridge escarpment along the passive margin of Eastern North America: Basin Research, v. 16, no. 1, p. 41–63.

Stockli, D.F., Farley, K.A., and Dumitru, T.A., 2000, Calibration of the apatite (U-Th)/He thermochronometer on an exhumed fault block, White Mountains, California: Geology, v. 28, no. 11, p. 983–986.

Vermeesch, P., 2008, Three new ways to calculate average (U-Th)/He ages: Chemical Geology, v. 249, p. 339–347, doi: 10.1016/j.chemgeo.2008.01.027.

Vermeesch, P., and al, E., 2007, Alpha-Emitting mineral inclusions in apatite, their effect on (U-Th)/He ages, and how to reduce it: Geochimica et Cosmochimica Acta, v. 71, p. 1737–1746, doi: 10.1016/j.gca.2006.09.020.

Ward, D.J., Spotila, J.A., Hancock, G.S., and Galbraith, J.M., 2005, New constraints on the late Cenozoic incision history of the New River, Virginia: Geomorphology, v. 72, no. 1-4, p. 54–72, doi: 10.1016/j.geomorph.2005.05.002.

APPENDIX B

B1. U-Th/He Analysis Methods

Hand-picked grains were photographed in 2D for use with image-analysis software to determine the alpha-loss correction. Grains were then packaged in high-purity Pt or later Nb microtubes, placed into Pt- or Nb-foil carrier packets, and loaded into an all-metal sample dropper that allowed samples to be introduced to the double-vaccum furnace for heating. Some early samples were heated to only about 960 ˚C, which should be more than adequate to outgas apatites, but the frequent observation of a few percent of refractory ^{4}He in re-extract analyses led us to switch to an 1150˚C-15 minute heating schedule, which appeared to eliminate the re-extract issue. After gettering, the gas was analyzed using a Balzer's Prisma quadrupole mass spectrometer, with abundances being determined two ways: via a ^{3}He spike calibrated for mass discrimination using a 1:1

$^4He/^3He$ mix, and manometrically using the ^4He beam observed in the calibration shots, which were run before, in the midst of, and after the analysis of each batch of unknowns. Agreement between spiked and manometric data was usually within 1%, and where these values deviate, the cause appears to be interference at mass 3 due to the presence of high hydrogen loads. As a result, all data reported in this paper are based on the manometric calibration. After removal from the vacuum system, samples were sent to the University of Arizona for U, Th, and in later years, Sm ICP/MS isotope-dilution analysis at the laboratory of Dr. Peter Reiners.

Table 2.1: Apatite and Zircon U-Th/He data for pooled ages from the central and southern Appalachians

Sample	Age (pooled) (Ma)	Uncertainty ± 2σ (Ma)	Analytical Scatter 2σ (Ma)	eU (pooled) (ppm)	Analyses (used, total)	Elevation (m)	Latitude (DD)	Longitude (DD)
Apatite:								
Central Appalachians								
APL-BUTL-00	126.1	3.5	39	105	4 - 4	126	41.0000	74.3333
APL-CHFD-00	164.1	5.1	79	7	6 - 7	48	39.8708	75.5958
APL-JJ-99	93.8	1.9	28	93	4 - 4	122	40.8583	74.9833
APL-LBCL-00	71.9	1.1	5	235	4 - 4	153	40.4583	75.5500
APL-MORR-00	117.5	3.7	14	37	3 - 3	6	40.2000	74.7708
APL-SCDM-00	183.2	7.4	14	26	4 - 4	15	40.0708	75.3083
APL-SMT-99	155.4	6.5	5	79	3 - 3	229	40.6000	75.3833
APL-VSP-00	116.9	3.7	43	81	3 - 3	183	40.6917	74.9000
Mt. Mitchell Transect								
NC-MM-4a	82.8	1.2	39	11	7 - 7	443	35.7351	82.1026
NC-MM-6	69.7	1.2	45	2	4 - 4	688	35.7512	82.1527
NC-MM-7	88.7	2.9	43	2	3 - 5	794	35.7623	82.1578
NC-MM-9	79.6	1.5	28	3	3 - 5	1044	35.7653	82.1675
NC-MM-16	170.9	7.0	62	8	4 - 4	2034	35.7644	82.2647
Sylva Transect								
NC-SY-2AB	142.7	4.5	88	7	5 - 5	1780	35.4605	83.1441
NC-SY-3	127.7	3.9	90	12	4 - 4	1686	35.4610	83.1274
NC-SY-5	76.9	1.6	45	10	3 - 4	1419	35.4493	83.1044
NC-SY-7	81.3	1.2	57	6	7 - 8	1092	35.4437	83.0833
NC-SY-8	86.8	2.0	5	7	3 - 3	932	35.4632	83.0982
NC-SY-9	75.5	1.1	32	4	6 - 6	808	35.4075	83.1236
NC-SY-10	89.8	1.9	16	10	4 - 4	695	35.3937	83.1780
NC-SY-11	100.2	2.0	29	19	3 - 4	634	35.3224	83.1719
NC-SY-12	169.1	7.7	80	11	3 - 4	520	35.4271	83.4584
NC SY 13	112.4	1.9	38	13	10 - 10	530	35.3722	83.5650
NC-SY-14	162.5	4.8	71	18	7 - 7	402	35.4469	83.8148
Hornbuckle Transect								
H4	92.1	1.5	51	10	7 - 7	1659	35.4678	83.1416
H8	164.0	4.4	75	17	8 - 8	1400	35.4672	83.1512
H9	141.6	3.3	104	14	8 - 8	1227	35.4758	83.1592
H11	144.5	4.0	73	4	6 - 7	933	35.4747	83.1824
H12	155.6	4.4	67	18	7 - 8	757	35.4693	83.2152
CH01	118.2	2.7	73	11	6 - 7	961	35.1059	82.6240
				Total:	160 - 177			
Zircon:								
NC-SY-8	252.4	20.4	17	320	2 - 2	932	35.4632	83.0982
NC-SY-10	212.7	14.5	24	250	2 - 2	695	35.3937	83.1780

Table 2.2: U-Th/He Data for the Inclusion Experiment using single grains from NC-SY-13

Sample	Radius (μm)	^{4}He (mol)	U (mol)	Th (mol)	Sm (mol)	eU[ii] (ppm)	Ft	Raw Age (Ma)	Age corr (Ma)	± 2σ* (Ma)	Th/U
Nitric Acid Dissolution - Apatite Protocol											
Inclusion Bearing Grains											
SY13-Li7	89.5	1.57E-13	1.41E-12	1.69E-12	1.28E-12	23.9	0.837	66.9	79.9	2.4	1.20
SY13-Li5	62.2	1.12E-14	9.54E-14	1.05E-13	1.91E-13	4.5	0.775	71.9	92.8	3.7	1.10
SY13-Li3	78.4	3.52E-13	2.69E-12	1.84E-12	1.15E-12	55.8	0.821	86.8	105.7	3.4	0.69
SY13-Li1	60.6	2.24E-14	2.03E-13	1.20E-13	5.71E-13	9.1	0.771	73.8	95.7	3.5	0.59
SY13-Si5	72.5	1.67E-13	1.56E-12	1.72E-13	8.93E-13	34.1	0.814	80.1	98.4	3.7	0.11
SY13-Si3	79.2	8.67E-14	4.92E-13	5.72E-13	9.93E-13	11.7	0.817	106.1	129.8	4.0	1.16
SY13-Si1	63.6	3.24E-14	1.68E-13	8.85E-13	6.58E-13	15.0	0.758	66.9	88.2	2.5	5.28
Hot Hydrofluoric Acid Dissolution - Zircon Protocol											
Inclusion Bearing Grains											
SY13-Li8	86.1	1.57E-13	1.47E-12	1.08E-13	-	19.9	0.842	80.5	95.6	3.4	0.07
SY13-Li6	61.5	6.02E-14	2.94E-13	6.83E-13	-	18.9	0.762	102.7	134.8	4.3	2.33
SY13-Li4	72.8	3.84E-14	2.09E-13	3.90E-13	-	6.8	0.804	99.1	123.3	4.1	1.87
SY13-Li2	86.4	1.40E-13	1.21E-12	2.08E-13	-	16.7	0.839	86.0	102.5	4.0	0.17
SY13-Si6	70.3	7.39E-14	3.53E-13	8.29E-13	-	14.9	0.792	104.6	132.0	4.5	2.35
SY13-Si4	77.8	1.14E-13	9.92E-13	4.36E-13	-	22.1	0.817	80.2	98.2	4.0	0.44
SY13-Si2	73.9	3.68E-14	2.69E-13	1.37E-13	-	7.1	0.807	94.0	116.4	4.6	0.51
Clear Grains											
SY13-N5	64.8	2.93E-14	2.14E-13	2.22E-13	-	8.5	0.784	85.0	108.4	3.8	1.04
SY13-N4	76.9	3.95E-14	3.21E-13	5.69E-14	-	7.0	0.816	90.8	111.2	4.3	0.18
SY13-N3	69.8	1.81E-14	2.11E-13	7.33E-14	-	6.0	0.801	61.0	76.1	2.7	0.35
SY13-N2	77.2	2.63E-14	2.80E-13	7.60E-14	-	6.0	0.818	67.9	83.0	3.2	0.27
SY13-N1	69.4	3.66E-14	3.18E-13	7.43E-14	-	9.2	0.799	84.1	105.3	4.0	0.23

* Uncertaintyies in ages are two-sigma (Ma); based on propagation of long-term analytical uncertainties in 4He, U, and Th, and 1% uncertainty in Ft factor.

For pooled ages, lowered uncertainties reflect propagation of component uncertainties through summing of measured quantities.

[#] Analytical Scatter - Is a simple 2-sigma standard deviation of measured ages, given as a measure of scatter in the component analyses for the pooled age.

[ii] eU - Values calculated by using Ft factor to determine effective spherical radius to model mass of sample analyzed. Uncertainties of 25% apply.

Table B1: U-Th/He Data for all apatite and zircon analyses from the central and southern Appalachians

Sample	Grains (or mass-mg)	^{4}He (mol)	U (mol)	Th (mol)	Sm (mol)	eU[h] (ppm)	Ft	Age uncorr (Ma)	Age corr (Ma)	± 2σ* (Ma)	Analy. Scatter[#] ± 2σ (Ma)	Th/U
APATITE												
Central Appalachians - Pennsylvania and New Jersey												
CK-10 ap 1 gr	1	2.229E-13	1.326E-12	2.280E-12		70.9	0.762	92.7	121.4	8.5		1.72
D-7 ap 1 gr	1	2.243E-13	1.260E-12	2.435E-12		66.8	0.805	94.8	117.6	8.0		1.93
APL-BUTL-00-1	1	7.884E-13	3.733E-12	1.341E-11		45.1	0.865	89.1	102.9	6.1		3.59
APL-BUTL-00-2	1	1.443E-12	7.243E-12	1.135E-11		48.2	0.885	112.5	127.0	9.4		1.57
APL-BUTL-00 #1	0.3064	2.196E-11	1.348E-10	1.758E-10		136.8	0.850	96.4	113.2	7.4		1.30
APL-BUTL-00 #2	0.3022	1.810E-11	8.622E-11	1.051E-10		87.4	0.850	125.8	147.8	12.7		1.22
POOLED		*4.229E-11*	*2.320E-10*	*3.056E-10*		*104.2*	*0.851*	*107.5*	*126.1*	*3.5*	*38.8*	*1.32*
APL-CHFD-00-1	1	1.858E-13	4.279E-13	2.566E-14		4.2	0.861	322.1	372.4	21.6		0.06
APL-CHFD-00-2	1	1.398E-13	4.802E-13	2.233E-14		2.5	0.890	218.6	245.0	34.8		0.05
APL-CHFD-00-3	1	3.786E-14	1.880E-13	7.060E-14		3.5	0.815	141.8	173.5	17.5		0.38
APL-CHFD-00 #1	0.2197	1.252E-12	6.904E-12	1.353E-12		7.8	0.850	132.9	156.0	14.1		0.20
APL-CHFD-00 4	1	1.179E-13	6.324E-13	7.752E-14	2.712E-12	7.6	0.849	135.9	159.7	14.8		0.12
APL-CHFD-00 5	1	8.275E-14	4.556E-13	6.387E-14	3.005E-12	7.2	0.837	130.5	155.6	14.0		0.14
APL-CHFD-00 6	1	9.334E-14	3.300E-13	1.609E-13	6.956E-13	4.9	0.843	192.0	227.1	29.9		0.49
POOLED		*1.724E-12*	*8.990E-12*	*1.748E-12*	*6.413E-12*	*6.7*	*0.851*	*139.9*	*164.1*	*5.1*	*79.2*	*0.19*
APL-JJ-99-1	1	3.048E-13	2.309E-12	1.242E-12		69.5	0.800	90.3	112.7	7.4		0.54
APL-JJ-99-2	1	3.452E-13	2.491E-12	1.290E-12		78.5	0.795	95.2	119.4	8.3		0.52
APL-JJ-99 #1	0.2575	1.025E-11	9.339E-11	5.296E-11		97.8	0.850	74.7	87.8	4.5		0.57
APL-JJ-99 #2	0.2659	1.093E-11	8.476E-11	6.613E-11		89.8	0.850	84.2	98.9	5.7		0.78
POOLED		*2.183E-11*	*1.829E-10*	*1.216E-10*		*93.1*	*0.848*	*79.7*	*93.8*	*1.9*	*28.3*	*0.66*
APL-LBCL-00-1	1	5.124E-12	3.213E-11	2.611E-11		639.5	0.826	103.2	124.8	9.0		0.81
APL-LBCL-00-2	1	3.222E-12	2.027E-11	1.346E-11		127.2	0.882	105.9	119.9	8.3		0.66
APL-LBCL-00 #1	0.2418	1.169E-11	2.121E-10	1.393E-10		241.0	0.850	37.0	43.5	1.1		0.66
APL-LBCL-00 #2	0.2427	2.246E-11	2.005E-10	1.280E-10		226.2	0.850	75.2	88.4	4.5		0.64
POOLED		*4.249E-11*	*4.650E-10*	*3.069E-10*		*235.6*	*0.849*	*61.2*	*71.9*	*1.1*	*74.8*	*0.66*
APL-MORR-00-1	1	4.019E-13	2.679E-12	1.299E-12		30.4	0.875	103.7	118.3	8.1		0.48
APL-MORR-00-2	1	6.605E-13	4.884E-12	1.564E-12		35.7	0.875	96.8	110.5	7.1		0.32
APL-MORR-00 3	1	6.620E-13	3.937E-12	3.464E-12	4.070E-13	44.3	0.859	107.4	124.8	9.0		0.88
POOLED		*1.724E-12*	*1.150E-11*	*6.327E-12*	*4.070E-13*	*36.8*	*0.869*	*102.2*	*117.5*	*3.7*	*14.4*	*0.55*

APL-SCDM-00-1	1	9.308E-13	4.225E-12	2.181E-13		15.7	0.895	166.1	185.2	19.9		0.05
APL-SCDM-00-2	1	8.488E-13	3.986E-12	8.349E-13		19.6	0.882	155.2	175.6	17.9		0.21
APL-SCDM-00 #1	0.3341	7.767E-12	3.583E-11	2.692E-12		26.0	0.850	162.6	190.8	21.1		0.08
APL-SCDM-00 #2	0.3258	7.868E-12	3.927E-11	2.828E-12		29.2	0.850	150.6	176.8	18.1		0.07
POOLED		*1.741E-11*	*8.331E-11*	*6.573E-12*		*26.0*	*0.854*	*156.8*	*183.2*	*7.4*	*14.4*	*0.08*
APL-SMT-99-1	1	1.607E-12	3.462E-12	2.514E-11		52.2	0.871	133.8	153.4	13.7		7.26
APL-SMT-99-2	1	1.467E-12	3.229E-12	2.202E-11		105.8	0.857	136.1	158.6	14.6		6.82
APL-SMT-99 #2	0.2278	1.329E-11	3.290E-11	1.933E-10		81.8	0.850	132.2	155.3	14.0		5.88
POOLED		*1.636E-11*	*3.959E-11*	*2.405E-10*		*79.0*	*0.853*	*132.7*	*155.4*	*6.5*	*5.2*	*6.07*
APL-VSP-00-1	1	2.905E-12	1.949E-11	2.201E-11		93.5	0.909	91.0	100.1	5.8		1.13
APL-VSP-00-2	1	3.207E-12	1.874E-11	1.524E-11		75.1	0.913	110.7	121.1	8.5		0.81
APL-VSP-00-3	1	1.981E-12	9.923E-12	9.352E-12		73.3	0.877	125.9	143.3	11.9		0.94
POOLED		*8.093E-12*	*4.815E-11*	*4.660E-11*		*81.4*	*0.903*	*105.6*	*116.9*	*3.7*	*43.3*	*0.97*
Southern Appalachians - Mount Mitchell Transect												
NC-MM-4a(sml) #2	18	2.055E-12	2.215E-11	1.298E-12		10.8	0.860	70.5	81.9	3.9		0.06
NC-MM-4a(sml) #2	14	1.759E-12	1.861E-11	1.894E-12		10.5	0.867	71.1	81.9	3.9		0.10
NC-MM-4a 1	1	1.174E-13	1.390E-12	1.269E-13	1.190E-12	14.1	0.857	63.5	74.0	3.2		0.09
NC-MM-4a 2	1	3.200E-13	2.914E-12	1.578E-13	3.798E-12	16.5	0.882	82.8	93.8	5.1		0.05
NC-MM-4a 3	1	3.465E-13	3.131E-12	1.587E-13	3.339E-12	16.8	0.881	83.7	94.9	5.2		0.05
NC-MM-4a 2	2	2.130E-13	2.234E-12	1.652E-13	2.161E-12	21.2	0.816	71.8	87.9	4.5		0.07
NC-MM-4a 4	1	3.213E-14	7.426E-13	4.220E-14	2.683E-13	4.1	0.880	32.9	37.4	0.8		0.06
POOLED		*4.844E-12*	*5.118E-11*	*3.843E-12*	*1.076E-11*	*10.9*	*0.863*	*71.5*	*82.8*	*1.2*	*39.3*	*1.06*
NC-MM-6 #1	8	2.339E-13	2.745E-12	7.903E-13		1.6	0.895	61.6	68.8	2.7		0.29
NC-MM-6 1	1	3.280E-15	4.324E-14	1.379E-14	1.472E-13	3.6	0.757	53.6	70.8	2.9		0.32
NC-MM-6 2	1	5.407E-15	6.878E-14	1.041E-14	2.206E-13	2.9	0.773	57.7	74.5	3.2		0.15
NC-MM-6 3	1	5.167E-15	4.830E-14	9.426E-15	1.915E-13	6.2	0.665	77.3	115.8	7.8		0.20
POOLED		*2.477E-13*	*2.905E-12*	*8.239E-13*	*5.594E-13*	*1.6*	*0.883*	*61.6*	*69.7*	*1.2*	*44.8*	*0.28*
NC-MM-7-1	1	8.736E-13	3.760E-12	1.141E-11		76.4	0.844	105.3	124.6	9.0		3.03
NC-MM-7-2	1	2.854E-13	5.085E-14	7.175E-14		2.0	0.785	2659.3	3231.6	187.4		1.41
NC-MM-7 #1	8	4.531E-13	4.002E-12	1.777E-12		2.3	0.882	79.0	89.5	4.7		0.44
NC-MM-7 3	1	2.263E-14	2.516E-13	7.456E-14	1.066E-12	5.7	0.815	63.6	77.9	3.5		0.30
NC-MM-7 4	1	7.048E-15	7.577E-14	2.166E-14	3.631E-13	1.8	0.817	65.7	80.4	3.7		0.29
POOLED		1.356E-12	8.090E-12	1.328E-11	1.429E-12	5.2	0.856	93.6	109.3	2.9	43.2	1.64
NC-MM-9-1	1	9.192E-13	7.345E-14	3.184E-14		2.0	0.808	5338.2	6109.1	354.3		0.43
NC-MM-9-2	1	7.180E-13	6.248E-14	8.553E-14		1.1	0.830	4637.9	5283.4	306.4		1.37
NC-MM-9 #1	16	6.045E-13	5.228E-12	6.068E-12		2.7	0.880	70.3	79.8	3.7		1.16

NC-MM-9 3	1	7.328E-15	8.007E-14	1.124E-13	9.481E-14	1.9	0.824	53.1	64.4	2.4		1.40
NC-MM-9 5	1	6.644E-15	5.647E-14	6.162E-14	5.549E-14	2.2	0.777	72.2	92.7	5.0		1.09
POOLED		*6.118E-13*	*5.308E-12*	*6.180E-12*	*9.481E-14*	*2.6*	*0.879*	*70.0*	*79.6*	*1.5*	*6181.1*	*1.16*
NC-MM-14-1	1	1.208E-12	2.183E-13	2.880E-13		5.7	0.809	2658.0	3152.8	182.9		1.32
NC-MM-14-2	1	2.748E-12	9.787E-14	8.838E-14		1.5	0.835	8396.5	9238.6	535.8		0.90
NC-MM-16-1	1	1.504E-13	6.276E-13	9.028E-14		7.4	0.853	176.9	206.8	24.8		0.14
NC-MM-16-2	1	4.705E-14	3.051E-13	8.458E-14		8.6	0.830	111.2	133.7	10.4		0.28
NC-MM-16 (3)	1	1.178E-13	6.276E-13	1.690E-13	1.683E-12	8.9	0.841	133.6	158.5	14.6		0.27
NC-MM-16 (3)	1	3.208E-14	1.884E-13	2.026E-14	9.229E-13	5.6	0.796	124.3	155.7	14.1		0.11
POOLED		*3.473E-13*	*1.749E-12*	*3.641E-13*	*2.606E-12*	*7.8*	*0.840*	*143.9*	*170.9*	*7.0*	*61.6*	*0.21*
Southern Appalachians - Sylva Transect												
NC-SY-2AB (2)	1	1.504E-14	1.972E-13	4.628E-14	9.837E-14	3.0	0.838	55.6	66.3	2.6		0.23
NC SY 2AB 200(2)	3	4.628E-13	3.227E-12	1.453E-12		4.6	0.898	99.8	111.0	7.2		0.45
NC SY 2AB 200(1)	3	1.091E-12	6.528E-12	1.746E-12		7.7	0.902	120.6	133.6	10.3		0.27
NC SY 2AB 100(2)	13	5.369E-13	2.925E-12	1.985E-12		7.4	0.804	121.7	151.0	13.2		0.68
NC SY 2AB 100(1)	11	7.916E-13	3.815E-12	9.848E-13		8.6	0.815	149.7	183.1	19.5		0.26
POOLED		*2.897E-12*	*1.669E-11*	*6.215E-12*	*9.837E-14*	*6.8*	*0.857*	*122.5*	*142.7*	*4.5*	*87.7*	*0.37*
NC-SY-3(2)	15	1.016E-12	8.504E-12	6.681E-13		9.2	0.838	90.2	107.4	6.7		0.08
NC-SY-3(1)	10	5.013E-13	4.287E-12	3.509E-13		12.6	0.802	88.2	109.8	7.0		0.08
NC-SY-3 (4)	1	1.552E-13	1.052E-12	7.783E-15	5.261E-14	31.7	0.824	112.9	136.7	10.8		0.01
NC-SY-3 (3)	1	7.201E-13	3.170E-12	2.344E-14	2.987E-12	39.7	0.842	172.1	203.8	24.1		0.01
POOLED		*2.393E-12*	*1.701E-11*	*1.050E-12*	*3.040E-12*	*12.3*	*0.830*	*106.3*	*127.7*	*3.9*	*89.9*	*0.06*
NC-SY-5(1)	2	2.752E-14	5.137E-13	1.452E-13		5.7	0.819	38.8	47.4	1.3		0.28
NC-SY-5 (1)	1	3.182E-14	3.849E-13	4.263E-14	2.031E-12	8.9	0.809	60.5	74.7	3.2		0.11
NC-SY-5 (2)	1	1.145E-13	1.003E-12	4.274E-13	2.667E-12	17.6	0.856	79.0	92.2	4.9		0.43
NC-SY-5 (3)	1	5.954E-13	1.263E-12	2.930E-12	2.403E-12	28.9	0.830	232.9	279.7	45.4		2.32
POOLED		*1.738E-13*	*1.902E-12*	*6.152E-13*	*4.697E-12*	*10.1*	*0.841*	*64.8*	*76.9*	*1.6*	*45.2*	*0.32*
NC-SY-7-2	1	2.734E-14	2.079E-13	1.958E-12		7.4	0.848	32.1	37.9	0.8		9.42
NC-SY-7 (4)	1	6.498E-14	6.581E-13	1.976E-12	3.915E-13	5.8	0.880	45.0	51.2	1.5		3.00
NC-SY-7 (5)	1	9.164E-14	9.974E-13	3.060E-13	1.739E-12	6.0	0.883	65.6	74.2	3.2		0.31
NC SY 7 120(1)	8	4.484E-13	4.175E-12	3.926E-12		6.0	0.853	68.0	79.7	3.7		0.94
NC SY 7 200(1)	6	1.000E-12	9.313E-12	5.419E-12		8.3	0.885	72.9	82.4	3.9		0.58
NC SY 7 80(1)	19	2.416E-13	1.477E-12	4.027E-12		3.5	0.785	77.5	98.6	5.6		2.73
NC-SY-7-1	1	7.979E-14	5.518E-13	7.747E-14		3.8	0.862	107.5	124.5	9.0		0.14
NC-SY-7-3	1	5.399E-13	5.653E-13	2.074E-13		5.9	0.851	644.3	750.0	43.5		0.37
POOLED		*1.954E-12*	*1.738E-11*	*1.769E-11*	*2.130E-12*	*6.3*	*0.862*	*70.2*	*81.3*	*1.2*	*57.4*	*1.02*
	1	1.470E-13	1.463E-12	2.618E-13		11.5	0.866	74.3	85.7	4.3		0.18

NC-SY-8-1												
NC-SY-8-2	1	5.706E-14	5.359E-13	7.354E-14		5.0	0.881	79.4	90.0	4.7		0.14
NC-SY-8-3	1	1.595E-13	1.522E-12	2.550E-13		6.3	0.895	77.6	86.6	4.4		0.17
POOLED		*3.635E-13*	*3.521E-12*	*5.903E-13*		*7.4*	*0.881*	*76.5*	*86.8*	*2.0*	*4.6*	*0.17*
NC-SY-9	1	2.782E-14	1.467E-13	1.485E-12	2.409E-13	11.4	0.794	43.9	55.3	1.8		10.12
NC-SY-9(2)	2	3.144E-14	3.813E-13	1.839E-13		1.1	0.885	57.2	64.6	2.4		0.48
NC-SY-9-3	1	2.411E-14	2.549E-13	9.512E-14		3.5	0.843	67.1	79.5	3.7		0.37
NC-SY-9(1)	2	1.718E-13	1.794E-12	5.464E-13		7.6	0.864	68.9	79.7	3.7		0.30
NC-SY-9-1	1	2.444E-14	1.685E-13	3.383E-13		2.4	0.852	76.5	89.7	4.7		2.01
NC-SY-9-2	1	8.150E-15	6.198E-14	6.276E-14		1.1	0.836	82.1	98.1	5.6		1.01
POOLED		*2.878E-13*	*2.808E-12*	*2.712E-12*	*2.409E-13*	*3.6*	*0.855*	*64.6*	*75.5*	*1.1*	*31.5*	*0.97*
NC-SY-10-1	1	4.658E-14	4.136E-13	2.697E-14		6.9	0.823	85.3	103.5	6.2		0.07
NC-SY-10-2	1	2.215E-13	2.195E-12	3.628E-14		10.2	0.890	77.3	86.8	4.4		0.02
NC-SY-10-3	1	1.781E-13	1.650E-12	1.324E-14		16.6	0.872	82.8	94.9	5.2		0.01
NC-SY-10(1)	3	1.974E-13	2.067E-12	4.203E-14		8.2	0.848	73.2	86.2	4.3		0.02
POOLED		*6.436E-13*	*6.326E-12*	*1.185E-13*		*10.1*	*0.867*	*77.9*	*89.8*	*1.9*	*16.2*	*0.02*
NC-SY-11(1)	3	9.186E-13	7.330E-12	2.639E-12		23.2	0.859	89.0	103.4	6.2		0.36
NC-SY-11(2)	1	5.521E-13	8.058E-15	2.818E-14		0.1	0.892	12307.7	13031.8	755.8		3.50
NC-SY-11 (3)	1	9.638E-14	1.092E-12	1.441E-13	9.076E-13	12.9	0.851	65.7	77.2	3.5		0.13
NC-SY-11 (4)	1	3.448E-14	3.133E-13	9.285E-15	1.020E-12	5.6	0.827	82.7	99.8	5.8		0.03
POOLED		*1.049E-12*	*8.734E-12*	*2.793E-12*	*1.928E-12*	*19.4*	*0.857*	*86.0*	*100.2*	*2.0*	*28.5*	*0.32*
NC-SY-12-1	1	7.583E-14	1.981E-13	8.659E-13		11.8	0.773	146.6	189.2	20.8		4.37
NC-SY-12-2	1	1.856E-13	2.779E-13	3.762E-12		12.2	0.838	125.2	149.2	12.9		13.54
NC-SY-12 (3)	1	5.488E-14	1.287E-13	4.718E-13	8.688E-13	8.4	0.757	174.1	229.2	30.5		3.67
NC-SY-12 (4)	1	1.574E-13	2.257E-13	1.242E-12	2.895E-13	20.4	0.746	234.7	313.2	18.2		5.50
POOLED		*3.163E-13*	*6.047E-13*	*5.099E-12*	*8.688E-13*	*11.4*	*0.807*	*136.7*	*169.1*	*7.7*	*80.0*	*8.43*
NC-SY-13 2	1	5.359E-14	6.060E-13	1.106E-13	7.765E-13	4.9	0.865	65.0	75.0	3.3		0.18
NC-SY-13 3	1	1.183E-13	1.274E-12	4.969E-13	1.174E-12	18.1	0.865	65.4	75.5	3.3		0.39
NC SY 13 200(1)	3	3.777E-13	2.906E-12	3.347E-12		7.4	0.885	79.1	89.3	4.6		1.15
NC SY 13 400(1)	1	4.020E-13	3.425E-12	3.233E-13		7.5	0.916	88.3	96.3	5.4		0.09
NC SY 13 200(2)	3	4.671E-13	3.762E-12	9.643E-13		6.0	0.892	90.1	100.9	5.9		0.26
NC SY 13 100(1)	13	8.046E-13	5.973E-12	6.720E-12		20.2	0.795	82.4	103.4	6.2		1.13
NC-SY-13 1	1	8.887E-14	6.952E-13	1.847E-13	9.921E-13	12.9	0.825	92.0	111.3	7.2		0.27
NC SY 13 100(2)	14	9.605E-13	5.854E-12	1.063E-11		20.8	0.790	89.1	112.6	7.4		1.82
NC SY 13 180(1)	4	1.991E-12	1.189E-11	8.078E-12		24.2	0.877	111.1	126.6	9.3		0.68
NC SY 13 180(2)	5	1.058E-12	5.776E-12	5.902E-12		12.0	0.867	113.9	131.1	10.0		1.02
POOLED		*6.321E-12*	*4.216E-11*	*3.676E-11*	*2.943E-12*	*13.2*	*0.853*	*96.0*	*112.4*	*1.9*	*38.2*	*0.87*

NC-SY-14a 1	1	2.295E-13	1.217E-12	2.566E-12	2.792E-12	53.6	0.786	96.9	123.1	8.8		2.11
NC-SY-14	1	2.577E-13	1.604E-12	8.089E-13	2.574E-12	39.2	0.808	109.7	135.4	10.6		0.50
NC SY 14A	7	2.035E-12	8.810E-12	1.307E-11		18.2	0.854	132.1	154.4	13.8		1.48
NC-SY-14	1	1.505E-14	7.636E-14	3.714E-14	1.386E-12	2.9	0.783	125.5	159.9	14.8		0.49
NC-SY-14a 3	1	8.114E-14	2.552E-13	6.974E-13	2.659E-13	4.0	0.824	149.3	180.8	19.0		2.73
NC SY 14B	3	9.699E-13	3.318E-12	4.576E-12		18.8	0.838	169.7	202.0	23.7		1.38
NC-SY-14a 2	1	1.508E-13	5.637E-13	1.317E-13	1.710E-12	9.1	0.858	190.6	221.5	28.5		0.23
POOLED		*3.739E-12*	*1.584E-11*	*2.189E-11*	*8.728E-12*	*18.0*	*0.841*	*137.0*	*162.5*	*4.8*	*70.8*	*1.38*
Southern Appalachians - Hornbuckle Creek												
CH01	1	9.920E-14	8.393E-13	3.931E-13	3.637E-12	9.6	0.855	80.5	94.1	5.1		0.47
CH01	1	1.991E-13	9.474E-13	2.075E-13	7.036E-12	5.1	0.885	147.7	166.6	16.1		0.22
CH01	1	2.633E-13	1.636E-12	8.202E-13	6.585E-12	15.6	0.858	108.8	126.6	9.3		0.50
CH01	5	3.947E-13	2.604E-12	1.402E-12	1.248E-11	13.8	0.819	101.4	123.6	8.9		0.54
CH01	5	5.793E-13	4.287E-12	1.327E-12	2.025E-11	10.5	0.881	94.8	107.5	6.7		0.31
CH01	1	8.136E-14	6.706E-13	1.654E-13	3.784E-12	13.7	0.810	86.0	105.9	6.5		0.25
CH01	1	4.648E-13	1.236E-12	4.071E-13	7.079E-12	18.0	0.835	257.8	307.4	17.8		0.33
POOLED		*1.617E-12*	*1.098E-11*	*4.316E-12*	*5.377E-11*	*10.8*	*0.857*	*101.4*	*118.2*	*2.7*	*51.0*	*0.39*
H4	1	2.994E-14	4.443E-13	3.320E-14	1.176E-12	16.0	0.814	50.4	61.9	2.2		0.07
H4	1	4.792E-14	6.008E-13	2.624E-14	1.585E-12	8.3	0.843	60.1	71.2	2.9		0.04
H4	5	8.445E-14	1.030E-12	8.663E-14	2.570E-12	9.1	0.776	61.2	78.8	3.6		0.08
H4	1	4.095E-14	4.221E-13	1.107E-13	1.157E-12	15.0	0.816	69.6	85.1	4.2		0.26
H4	5	1.319E-13	1.371E-12	8.498E-14	3.459E-12	10.1	0.782	72.1	92.0	4.9		0.06
H4	1	5.476E-14	3.516E-13	2.926E-14	9.673E-13	11.8	0.783	115.6	147.2	12.6		0.08
H4	1	6.240E-14	3.561E-13	2.215E-14	2.825E-13	8.9	0.835	131.7	157.4	14.4		0.06
POOLED		*4.524E-13*	*4.576E-12*	*3.932E-13*	*1.120E-11*	*10.3*	*0.799*	*73.7*	*92.1*	*1.5*	*75.4*	*0.09*
H8	1	5.197E-14	6.565E-13	3.208E-14	1.488E-12	13.3	0.846	59.6	70.4	2.9		0.05
H8	1	1.511E-13	1.396E-12	6.854E-15	2.087E-12	27.7	0.847	82.5	97.2	5.5		0.00
H8	1	1.453E-14	1.328E-13	1.151E-14	1.322E-13	3.9	0.798	82.1	102.7	6.1		0.09
H8	5	3.615E-13	2.025E-12	4.908E-13	1.392E-12	12.2	0.801	129.1	160.7	15.0		0.24
H8	5	7.374E-13	2.849E-12	9.058E-13	2.882E-12	17.9	0.802	183.0	227.2	30.0		0.32
H8	1	9.627E-14	5.496E-13	8.202E-14	1.388E-13	18.5	0.790	129.5	163.4	15.5		0.15
H8	1	2.038E-13	1.148E-12	3.548E-13	1.337E-12	38.6	0.783	126.3	160.8	15.0		0.31
H8	1	2.765E-14	2.771E-13	5.866E-14	1.992E-13	11.8	0.773	73.0	94.2	5.1		0.21
POOLED		*1.644E-12*	*9.034E-12*	*1.943E-12*	*9.657E-12*	*16.7*	*0.803*	*132.1*	*164.0*	*4.4*	*104.1*	*0.22*
H9	1	1.678E-14	1.733E-13	3.983E-13	2.443E-13	5.9	0.834	48.7	58.3	2.0		2.30
H9	1	3.554E-13	2.144E-12	1.222E-12	8.313E-13	30.8	0.846	112.3	132.5	10.2		0.57
H9	1	6.963E-13	3.224E-12	6.495E-13	1.229E-12	51.8	0.827	157.4	189.7	20.9		0.20
H9	5	4.106E-13	2.826E-12	6.201E-13	1.335E-12	14.9	0.796	105.9	132.7	10.2		0.22
H9	5	2.723E-13	2.070E-12	6.253E-13	1.134E-12	5.0	0.807	94.3	116.6	7.9		0.30

H9		1	5.226E-14	3.306E-13	8.202E-14	1.246E-13	11.6	0.789	114.5	144.7	12.1		0.25
H9		1	6.931E-14	4.478E-13	1.059E-13	2.157E-13	10.6	0.814	112.3	137.7	11.0		0.24
H9		1	2.096E-13	1.407E-12	1.061E-12	3.590E-13	35.8	0.814	97.4	119.5	8.3		0.75
	POOLED		*2.082E-12*	*1.262E-11*	*4.764E-12*	*5.472E-12*	*14.4*	*0.819*	*116.2*	*141.6*	*3.3*	*72.8*	*0.38*
H11		1	3.249E-14	2.005E-13	4.613E-14	2.854E-13	3.4	0.856	117.2	136.7	10.8		0.23
H11		1	3.178E-14	1.515E-13	1.269E-13	1.851E-13	2.7	0.836	134.1	160.0	14.9		0.84
H11		1	1.496E-14	6.757E-14	1.919E-14	1.145E-13	2.0	0.799	157.5	196.4	22.4		0.28
H11		5	1.780E-13	1.230E-12	1.924E-13	1.088E-12	5.6	0.816	106.7	130.5	9.9		0.16
H11		5	9.492E-14	5.581E-13	1.061E-13	7.356E-13	3.9	0.803	124.1	154.1	13.8		0.19
H11		1	2.346E-14	9.575E-14	2.659E-14	2.002E-13	2.4	0.804	174.0	215.6	27.0		0.28
H11		1	8.211E-14	2.620E-13	8.680E-14	3.304E-13	4.0	0.837	220.0	261.9	15.2		0.33
	POOLED		*3.756E-13*	*2.304E-12*	*5.173E-13*	*2.609E-12*	*4.2*	*0.816*	*118.2*	*144.5*	*4.0*	*67.4*	*0.22*
H12		1	4.991E-14	4.148E-13	2.068E-14	9.105E-13	27.2	0.773	90.4	116.7	7.9		0.05
H12		1	3.518E-13	2.424E-12	4.853E-14	4.677E-12	30.9	0.868	109.7	126.2	9.2		0.02
H12		1	1.639E-13	1.072E-12	2.989E-13	1.574E-12	12.1	0.854	109.4	127.9	9.5		0.28
H12		1	1.965E-13	1.361E-12	2.771E-14	2.221E-12	35.2	0.833	109.3	130.9	9.9		0.02
H12		6	4.901E-13	3.287E-12	2.071E-13	5.592E-12	18.1	0.807	111.8	138.2	11.1		0.06
H12		1	2.604E-13	1.446E-12	2.052E-14	3.314E-12	10.5	0.872	135.8	155.4	14.0		0.01
H12		6	7.274E-13	2.922E-12	6.379E-13	5.374E-12	18.3	0.796	179.2	224.2	29.1		0.22
H12		1	5.648E-13	1.861E-12	2.842E-14	3.250E-12	29.4	0.858	227.4	264.2	15.3		0.02
	POOLED		*2.240E-12*	*1.293E-11*	*1.261E-12*	*2.366E-11*	*18.4*	*0.824*	*128.6*	*155.6*	*4.4*	*73.3*	*0.10*
ZIRCON													
	NC-SY-8	1	2.731E-12	8.985E-12	7.288E-12		274.3	0.797	195.3	244.1	34.6		0.81
	NC-SY-8	1	6.134E-12	2.106E-11	3.754E-12		354.1	0.826	212.6	256.4	38.1		0.18
	POOLED		*8.865E-12*	*3.004E-11*	*1.104E-11*		*323.2*	*0.817*	*207.0*	*252.4*	*20.4*	*17.4*	*0.37*
	NC-SY-10	1	3.884E-12	1.616E-11	3.923E-12		186.5	0.852	173.6	203.2	24.0		0.24
	NC-SY-10	1	5.071E-12	2.051E-11	2.346E-12		344.5	0.830	183.5	220.4	28.2		0.11
	POOLED		*8.955E-12*	*3.667E-11*	*6.269E-12*		*249.8*	*0.839*	*179.1*	*212.7*	*14.5*	*24.2*	*0.17*

NOTES

General

* Uncertaintyies in ages are two-sigma (Ma); based on propagation of long-term analytical uncertainties in 4He, U, and Th, and 1% uncertainty in Ft factor. For pooled ages, lowered uncertainties reflect propagation of component uncertainties through summing of measured quantities.

Analytical Scatter - Is a simple 2-sigma standard deviation of measured ages, given as a measure of scatter in the component analyses for the pooled age.

ⁱⁱ eU - Values calculated by using Ft factor to determine effective spherical radius to model mass of sample analyzed. Uncertainties of 25% apply.

For Pooled Ages

Any analyses older than 250 Ma were rejected from pooled age (Gray Text)

Pooled Ft value determined as weighted average, using He concentrations as weights

Pooled ages determined using alpha correction applied to He abundance, before age calcuLation
eU values on pooled ages are for comparison purposes only, as kinetics of component grains could be quite varied and will be non-linear.

CHAPTER 3

SLOW LONG-TERM EXHUMATION OF THE NORTHERN NEW ENGLAND APPALACHIANS FROM DETRITAL APATITE U-Th/He THERMOCHRONOLOGY AND RADIATION DAMAGE MODELING

Ryan E. McKeon[1]*
Peter K. Zeilter[1]
Frank J. Pazzaglia[1]
Bruce D. Idleman[1]
Eva Enkelmann[2]
Jeremy Laucks[1]

[1] Department of Earth and Environmental Sciences, Lehigh University, Bethlehem, PA 18015, USA
[2] Universität Tübingen Institut für Geowissenschaften, Wilhelmstr. 56, 72074 Tübingen Germany
* Corresponding Author: rem208@lehigh.edu

For Submission to *Lithosphere*

Keywords: Apatite U-Th/He, Thermochronology, Detrital Sampling, New England, Appalachians, Radiation Damage

CHAPTER ABSTRACT

The high elevation and considerable relief of the Appalachians of northern New England stand in contrast to the topography of the range to the north and south, making the persistence or rejuvenation of this topography difficult to explain in the context of an old and uniformly decaying orogen. We dated 117 apatite grains using U-Th/He thermochronology on detrital sediment collected from the Connecticut and Merrimack Rivers to compare with extensive apatite fission-track analysis from the region that suggests long-term exhumation rates of ~20 m/Myr. All cooling ages from detrital sediment were pre-Cenozoic and age populations from the two watersheds were indistinguishable, suggesting they experienced similar exhumation histories. The distribution of U and Th (eU) concentrations was large for both watersheds, prompting a forward modeling exercise to assess the impact of closure temperature variation resulting from radiation damage and slow cooling on detrital age populations. We first modeled the age distribution caused only by the observed population of eU concentrations and 0.4˚C cooling rate that reflects the 20 m/Myr erosion rate for a geothermal gradient of 20˚C/km and found that nearly all of the age variation observed could be explained through radiation damage and the variance in eU. When the added complexity of sampling an age-elevation stratigraphy with the hypsometric distribution was added the result was indistinguishable from the radiation damage only model. A sensitivity analysis assessing the relative contribution of cooling rate, radiation damage, and relief was conducted using our New England data set and a published detrital apatite U-Th/He dataset from Inyo Creek of the eastern Sierra Nevada. The dominance exerted on the age

distribution by radiation damage at slow cooling rates was greatly diminished by only modest increases in the cooling rate and relief. Collectively these observations suggest that for slowly cooled regions the long-term exhumation rate could be inferred by fitting models of eU-driven age distributions to measured detrital data. Caution should be used when attempting to infer geomorphic processes from detrital datasets from slowly cooled regions. And lastly, that radiation damage will not significantly impact detrital age populations from regions with cooling rates faster than 1.0˚C/Myr.

3.1 INTRODUCTION

The persistence of rugged topography and considerable relief in the Appalachian Mountains of northern New England is difficult to explain in the context of an old and uniformly decaying landscape. Long-term erosion rate estimates for the region (Roden-Tice et al, 2009) and the Appalachians as a whole (McKeon et al. Chapter 2 and references therein) from low-temperature thermochronometry curiously match short-term estimates from cosmogenic nuclide studies (Portenga and Bierman, 2011 and references therein) with all signals indicating that the pace of erosion has been quite slow, on the order of 20 m/Myr over the last 100 Myr. Within this context of slow and steady erosion of the northern Appalachians is the observation of unsteady sedimentation rates in Atlantic passive margin basins including a large pulse of sediment during the Miocene, the provenance of which is not known, but volumetrically represents 1 km of material eroded off of the Appalachian landscape stretching from Virginia to New Hampshire (Pazzaglia and Brandon, 1996). Additionally the northern Appalachians were overrun by

the southern margin of the Laurentide Ice Sheet and locally accommodated alpine glaciers in the White Mountains of New Hampshire. Here we take advantage of the low-temperature sensitivity of apatite U-Th/He thermochronology applied to detrital samples to constrain the exhumation history of northern New England in the context of these observation and existing regional apatite fission-track data.

The sampling of detrital mineral grains from fluvial sediment and sedimentary rocks has proven to be a useful tool for interpreting thermal histories over a range of spatial and temporal scales (Cerveny et al., 1988; Stock and Montgomery, 1996; Ruhl and Hodges, 2005). The use of detrital sediment has the advantage that it samples broadly from throughout the entire drainage basin and provides a synoptic perspective that would require a large number of point specific bedrock samples to equal. The closure temperature (Dodson, 1973) of the apatite U-Th/He system is dependent upon the cooling rate and the accumulation of radiation damage caused by the decay of U and Th (Shuster et al., 2006), which may be as low as 50˚C for Appalachian cooling rates. It is plausible that the very low-temperature sensitivity could allow detrital apatite grains to record recent exhumation related to the Miocene sediment pulse or Pleistocene glaciation in the form of young cooing ages.

Here we present two new detrital apatite U-Th/He datasets totaling 117 grains derived from large river systems that collectively drain the White Mountains of New Hampshire and the Green Mountains of Vermont. The concentration of U and Th varied widely within each dataset and given the evidence for slow long-term exhumation of the region

we use our age and effective uranium (eU, defined as [U] + 0.235 * [Th]) populations to explore the impact of radiation damage on detrital datasets using forward models. First we illustrate the wide age variation that can be caused solely by radiation damage and slow cooling rates. Next we add the complexity of sampling an age-elevation relationship with the hypsometric distribution of topography within our watersheds. Finally, we conclude with a sensitivity analysis that illustrates the relative influence that cooling rate, radiation damage, and relief impose on detrital apatite U-Th/He datasets.

3.2 STUDY AREA

The northern Appalachians were formed through a series of collisional orogenies during the Paleozoic resulting in a complex history of deformation, polymetamorphism, and plutonism recorded in the bedrock of the northern New England study area. Metasedimentary and metaigneous lithotectonic terranes represent the various stages of sedimentation and tectonic accretion in the region and have been extensively intruded by granitic plutons during Paleozoic orogenesis and more recently in the Mesozoic with the emplacement of the White Mountain magma series and those related to passage over the Great Meteor hotspot (~120 Ma) (Foland and Allen, 1991). (Figure 3.1) Detailed explanations of the geologic units and timing of Paleozoic tectonic events can be found in Hatcher (1989), Rast (1989), and Zartman (1988). Focusing on the watersheds sampled for this study, the Merrimack River sources sediment almost exclusively from the high-grade metasedimentary and intrusive rocks of the Central Maine terrane, including Mesozoic intrusive rocks in central New Hampshire. The Connecticut River sources

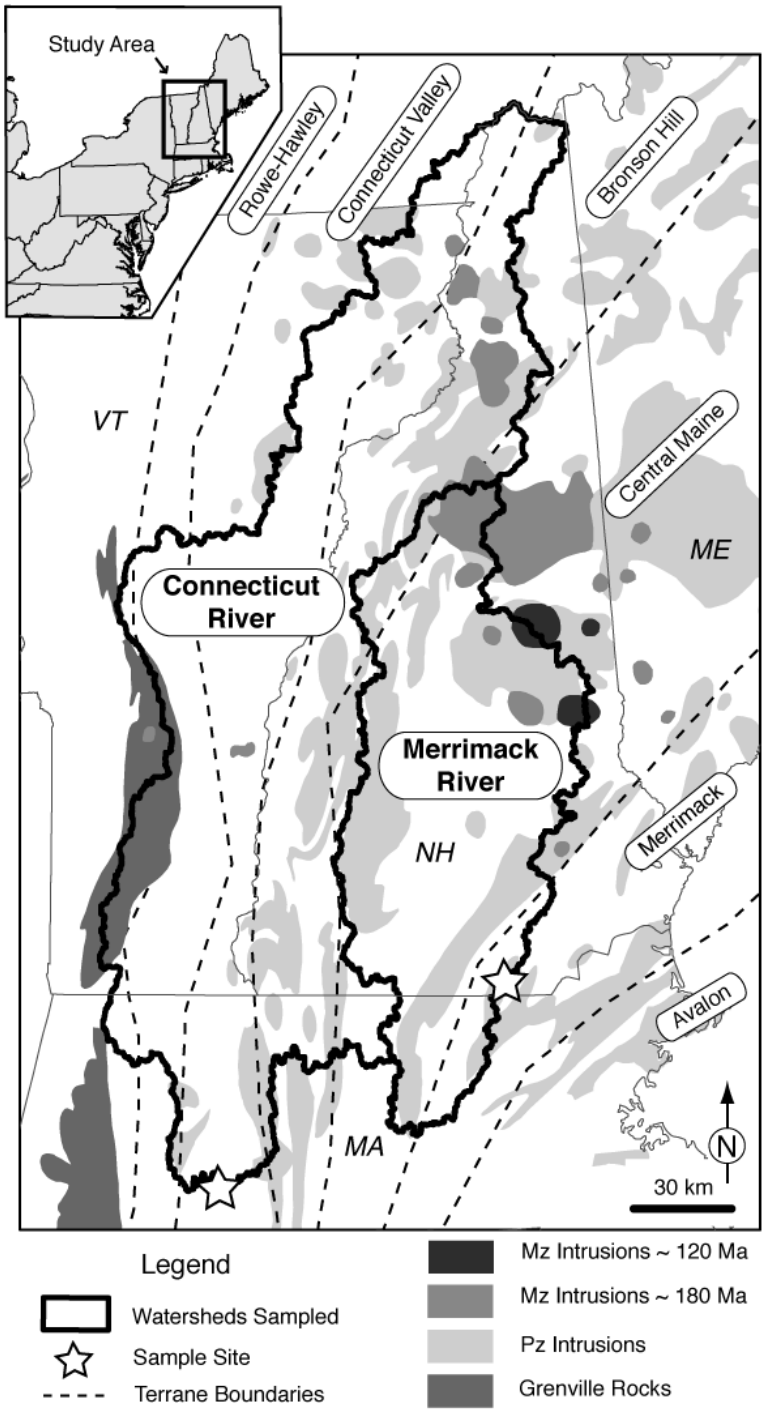

Figure 3.1: Inset map and rectangle show the location of the study area in northern New England. Main map shows the Connecticut and Merrimack River watersheds sampled for this study. The tectonic terranes that correspond to different metamorphic grades and protoliths are separated by the dashed lines and labeled, see Study Area section for a description. Paleozoic intrusive rocks associated with collision and orogenesis are light gray. Mesozoic intrusive rocks of the White Mountain Magma Series (~180 Ma) and resulting from passage over the Great Meteor hotspot (~120 Ma) are indicated in medium gray and darkest gray respectively. Grenville-age rocks that outcrop in the Green Mountains of Vermont are dark gray. State names are abbreviated in italics.

sediment from a more diverse assemblage of tectonic terranes. From east to west it drains the high-grade metaigneous and associated metasedimentary rocks of the Bronson Hill terrane, which are juxtaposed against the low-grade slates and green schists of the

Connecticut Valley terrane by the Ammonoosuc fault, which the modern river follows closely. Further to the west the metamorphic grade increases in the schists of the Rowe-Hawley terrane and Grenville-age metamorphic rocks that outcrop along the spine of the Green Mountains in central Vermont.

Extensive $^{40}Ar/^{39}Ar$ (Harrison et al., 1989; Eusden and Lux, 1994; Zartman, 1988) and apatite fission track (Doherty and Lyons, 1980; Roden-Tice et al., 2009) thermochronologic investigations in northern New England suggest that long-term cooling has been generally slow, but age contrasts against faults suggest localized differential exhumation. Harrison et al. (1989) observed a smooth east to west decrease of biotite $^{40}Ar/^{39}Ar$ ages from 300 to 240 Ma along a transect from central to western New Hampshire that is truncated by the Ammonoosuc fault separating the Bronson Hill and Connecticut Valley terranes where ages jump up to 320-340 Ma. They interpreted this offset to represent post-orogenic tilting of western New Hampshire due to as much as 6-8 km of normal fault movement along a structure that is along strike with the Deerfield Triassic rift basin to the south of the study area. Apatite fission-track (AFT) ages from throughout New Hampshire define a bulls-eye pattern of younger ages (70 – 100 Ma) within the rugged topography of the White Mountains and older ages (100 – 130 Ma) to the south and west, which has been attributed to the presence of a pervasive thermal anomaly associated with the passage of the Great Meteor hotspot (Roden-Tice et al., 2009). The age-elevation relationship of AFT ages spanning 1.5 km of relief from Mt. Washington (at 1916 m the highest elevation in New England) indicate slow long-term average erosion rates of ~20 m/Myr, however, over shorter periods rates may have been

unsteady (Roden-Tice et al., 2012).

The Merrimack River watershed (~10,380 km^2) ranges from 28 to 1524 m above sea level and drains the southwestern portion of the rugged White Mountains in central New Hampshire along with large area of low elevation, low relief rolling topography in southern New Hampshire. The Connecticut River watershed (~21,660 km^2) ranges from 37 to 1904 m and drains the eastern side of the spine of the Green Mountains in Vermont and the northwestern fringe of the White Mountains. The whole region was overrun by the southern margin of the Laurentide Ice Sheet during the Pleistocene and White Mountains accommodated alpine glaciers that cut deep cirques modifying the distribution of relief within the range.

3.3 DETRITAL U-Th/He THERMOCHRONOLOGY

3.3.1 Methods

Here we report 117 single-grain apatite U-Th/He (AHe) ages derived from two detrital samples from the Connecticut and Merrimack Rivers that drain the southern White Mountains and eastern Green Mountains of northern New England. Sand-sized sediment samples from both rivers were collected from the active channels and then sieved to retain grains smaller than 350 μm. Apatites were separated from sieved sediment using standard magnetic and density sorting techniques. The quality of individual apatite grains was assessed using a stereographic microscope and grains were selected for U-Th/He analysis, were unbroken, and optically free of fractures and inclusions, and where

possible, euhedral (e.g. Farley, 2002). It should be noted that although these apatites were derived from detrital sediment, and therefore subjected to weathering and transport processes, the grains that survived to be sampled and selected for analysis did not illustrate the effects of significant physical or chemical abrasion of the grain surface. However, weathering and transport processes have been shown to exert a significant control on the apatite grains that do survive to become part of a detrital sample (Reiners et al, 2007) Apatite grains were measured for calculating the F_T correction (Farley et al., 1996) and loaded individually in Pt micro-tube carries for He, U, Th, and Sm analysis. Sample preparation and He analysis were carried out at the Lehigh Noble Gas Geochronology Lab, U, Th, and Sm concentrations were determined through isotope dilution ICP-MS at Yale University.

Following Ruhl and Hodges (2005), we use normalized synoptic Probability Density Functions (PDFs) to describe the distribution of cooling ages observed for each detrital sample along with their associated analytical uncertainty for comparing the results from the two watersheds, and forward modeling to follow. In detrital sampling every grain is unique, which precludes repeat analyses because the provenance of a grain is unknown. Replicate analyses of bedrock samples from within the sampled watershed have been used to calibrate the uncertainty of detrital datasets (e.g. Stock et al., 2006), but lacking replicate bedrock analyses from the Connecticut and Merrimack watersheds, we used our lab's reproducibility of the Durango apatite age standard (± 3% 1σ) as a measure of analytical uncertainty. This estimate of uncertainty likely underestimates the dispersion of ages derived from replicate analyses of slowly cooled bedrock samples (e.g. McKeon

et al. – Chapter 2), however, it is the impact of that dispersion on detrital datasets that we wished to explore. Therefore we felt that it was better to use a smaller uncertainty that is known and allow the dispersion of ages to be more clearly evident than to guess at a larger uncertainty that would smooth over the complexity we were interested in identifying.

3.3.2 Results

Apatite U-Th/He age populations were found to be quite similar for both watersheds, comprised of primarily Cretaceous cooling ages, and lacking Cenozoic ages that would reflect significant recent exhumation from this rugged landscape (Figure 3.2). For the Connecticut River watershed 54 single-grain ages ranged from 69.5 to 295.4 Ma with the majority falling between 90 and 125 Ma. For the Merrimack River watershed 63 single-grain ages ranged from 66.6 to 400.3 Ma with the majority again between 90 and 125 Ma (Table C1). Interestingly, despite considerable lithologic variation, the distribution of eU concentrations was nearly indistinguishable between the two watersheds, encompassing a wide range from <1 to nearly 150 ppm with the vast majority of grains ranging from 1-50 ppm. Due to the similarity of the age distributions, the hypsometry, and the eU populations we combine the results from the two watersheds into one pooled dataset of 117 grains for use with our forward modeling of the impact of radiation damage on detrital datasets.

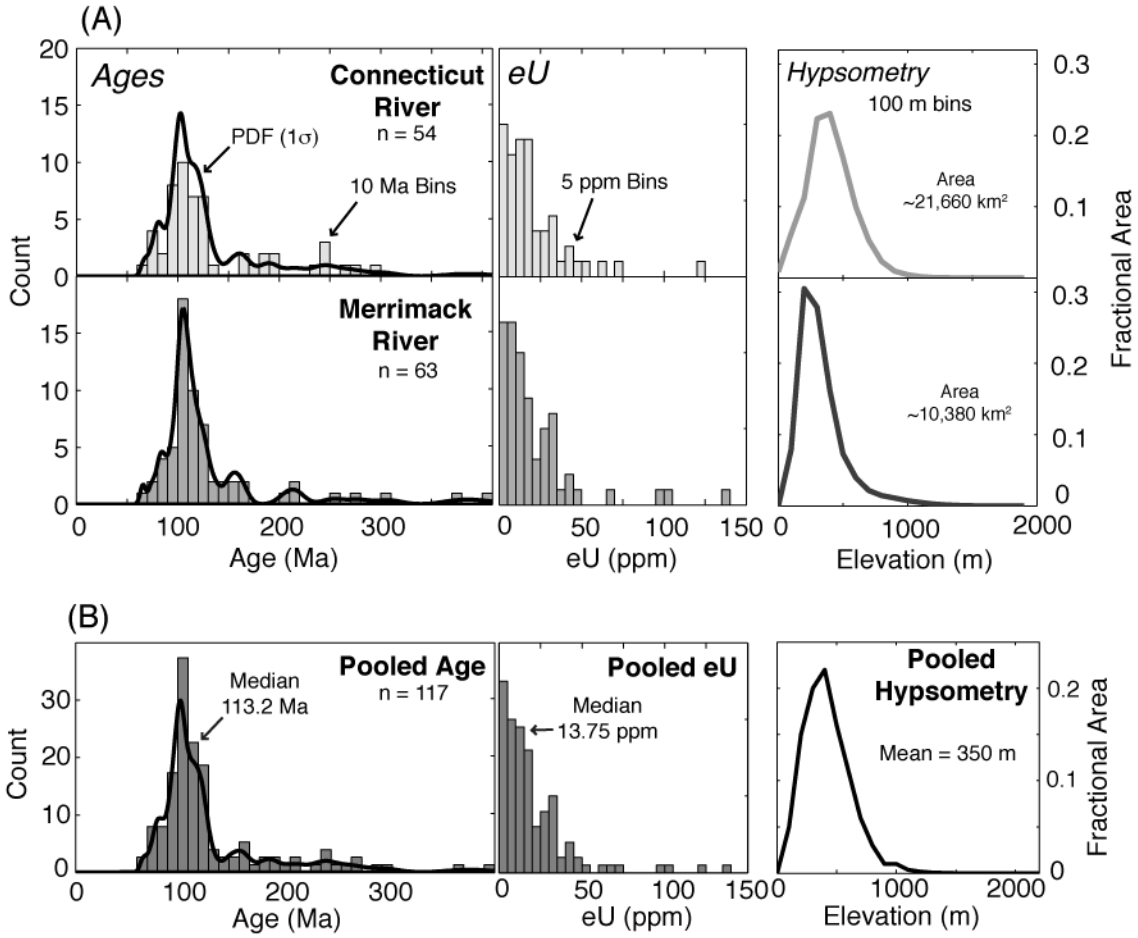

Figure 3.2: (A) Results of detrital apatite U-Th/He thermochronology for the Connecticut and Merrimack River watersheds of Northern New England. Far left plots display age populations for both watersheds, plotted as histograms with Probability Density Functions (PDFs -heavy black lines) that convolve the 1σ analytical uncertainty of the age measurement overlaid. The center plots display the wide, but strikingly similar range of eU concentrations (eU = U + 0.235 * Th, see text for discussion) observed in both watersheds. To the far right are area normalized hypsometric curves from SRTM 90m elevation data sampled in 100 m bins. Of particular note is the similarity of the age and eU data for both watersheds despite sourcing sediment from different tectonic terranes. (B) Radiation damage modeling inputs derived from pooling the Connecticut and Merrimack watershed data into one 117 grain data set.

3.4 RADIATION DAMAGE MODELING

Detrital thermochronology is dependent upon the assumption that cooling ages derived from detrital grains are indicative of the spatial or topographic location from which that grain was derived. Thus, the acknowledgement of grain-specific cooling age dependence

on the accumulation of radiation damage through a combination of cooling rate and the eU concentration has important implications for the application of detrital AHe thermochronology to regions characterized by slow cooling. Given the wide range of eU concentrations observed in the Connecticut and Merrimack detrital populations and the evidence for slow long-term cooling rates, we explore the impact of radiation damage on detrital datasets through forward modeling. We start with a simple model of the distribution of ages resulting solely from the population of eU concentrations we observed from the pooled New England dataset. Next we add the complexity of sampling topography, with a simple age stratigraphy using the hypsometric curve, to the age variation resulting from eU. Finally, we assess the relative impact of the three major factors that control detrital datasets; the cooling rate, the hypsometric distribution and relief, and the range of eU concentrations, using our New England dataset and the detrital AHe dataset from Inyo Creek from the eastern Sierra Nevada of California from Stock et al. (2006).

3.4.1 Radiation Damage Only Model

3.4.1.1 Rationale and Setup. To isolate the effect of radiation damage on the distribution of ages observed we envisioned New England to be flat and for erosion to be accommodated uniformly and simultaneously across the combined watershed resulting in all apatite grains experiencing the same thermal history. We used the Radiation Damage Accumulation and Annealing Model (RDAAM – Flowers et al., 2009) within the thermal modeling software package HeFTy (Ketcham, 2005) to calculate the dispersion of

cooling ages resulting from the range of eU concentrations we observe for different cooling rates. To calibrate different cooling rates we used the median age (113.2 Ma) and eU concentration (13.75 ppm) from our pooled New England dataset (Figure 3.2) as fitting parameters to fix the passage of the cooling history through the AHe Partial Retention Zone (PRZ), where the transition from complete He loss to complete He retention is made and radiation damage induced variations in diffusion kinetics takes effect between ~40 – 80˚C (Stockli et al., 2000). Once the thermal history was calibrated we adjusted the eU concentration to span the range observed from our pooled dataset (0.5 – 140 ppm) to use RDAAM to predict the range of ages expected for a given cooling rate while holding grain size constant at a radius of 85 μm. Finally, we used linear interpolation to derive ages for all of the observed eU concentrations from the pooled dataset for a particular cooling rate. For all models we applied a 3% uncertainty to the modeled ages (as explained above) and generated PDFs to observe the different distributions of cooling ages resulting from different cooling rates in comparison to the observed pooled age population.

3.4.1.2 Results. Through isolating the distribution of ages produced by the range of eU concentrations observed using plausible rates of slow cooling we find that nearly all of the age variation we observed in our detrital dataset can be explained by radiation damage (Figure 3.3). We fit cooling histories to pass through the PRZ ranging from 0.2 to 1.0˚C/Myr assuming a geothermal gradient of 20˚C/km to model long-term erosion rates of 10 – 50 m/Myr. We find that in order to fit the desired cooling rate none of the thermal histories are truly linear; instead they must cool faster or slower to produce the

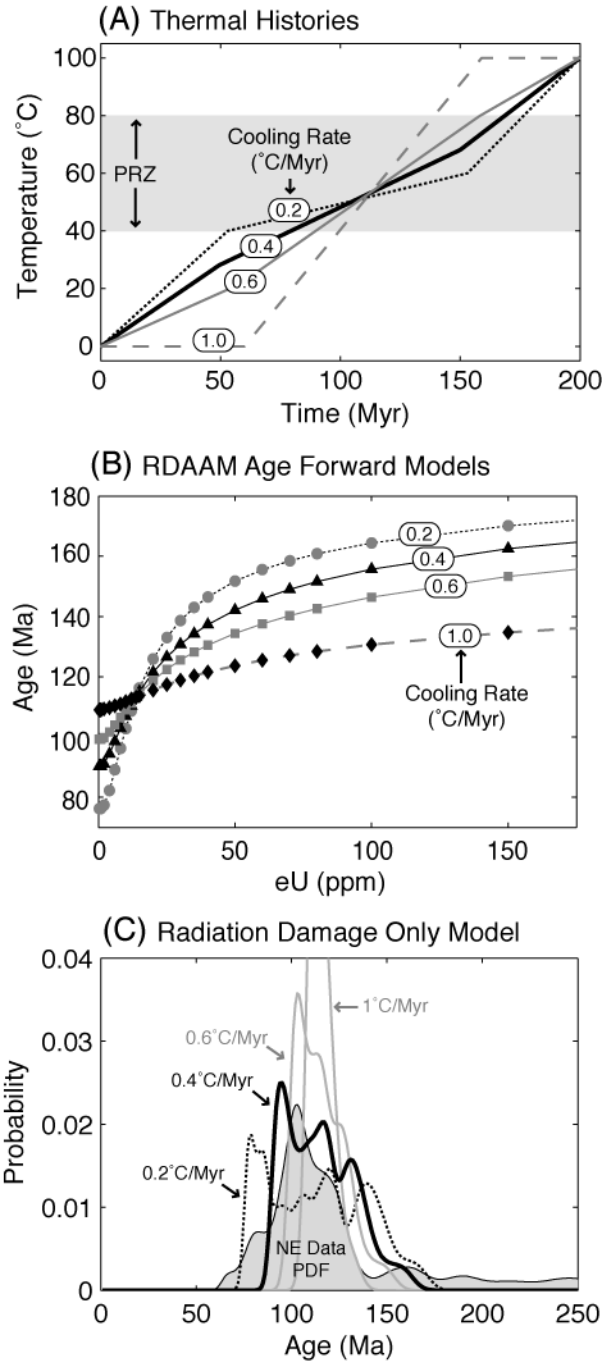

Figure 3.3: Radiation Damage Only model inputs and results. (A) Thermal histories that fit the median age of 113.2 Ma from the pooled New England dataset for an eU concentration of 13.75 ppm. The cooling rates span a range of 10 – 50 m/Myr erosion rates through the AHe Partial Retention Zone (PRZ – gray shading) assuming a geothermal gradient of 20˚C/km. Note that to fit these cooling rates through the PRZ no thermal history was truly linear. (B) Age dispersion as a result of radiation damage predicted by the RDAAM model for the different thermal histories. (C) Results of the Radiation Damage Only model overlaid over the PDF of the pooled New England dataset. The 0.4˚C/Myr population (solid black line) represents a long-term exhumation rate of 20m/Myr that has been suggested by other studies.

target age as outlined above (Figure 3.3). The range of ages predicted by RDAAM for the different cooling rates vary widely, indicating that the amount of variation resulting from radiation damage is quite sensitive to minor variations in the cooling rate (Figure 3). Comparison of PDFs that convolve the range of ages from all 117 eU concentrations

observed from the pooled New England dataset illustrate this point; where relative fast cooling of 1.0˚C/Myr produces a strong, narrow peak centered on the target age of 113.2 Ma, whereas the acknowledged long-term average rate of 0.4˚C/Myr (20 m/Myr) produces a much wider range that closely mimics that of the observed pooled New England dataset (Figure 3.3).

3.4.2.Geologic Model

3.4.2.1 Rationale and Setup. Because real watersheds are not flat, the hypsometric distribution and relief of the landscape impact detrital datasets through the cooling age stratigraphy of the sampling region and the geomorphic processes generating and transporting the sediment. For small watersheds such as Inyo Creek from the Sierra Nevada the age-elevation relationship may be quite simple (Stock et al., 2006) whereas for larger river systems or tectonically active areas the actual relationship is probably more complex due to the warping of shallow isotherms under potentially greater or transient paleo-topography (e.g Braun, 2002; Ehlers et al, 2006). Though we acknowledge these complexities, here our interest was to identify the relative influence of radiation damage and hypsometry on detrital age populations. For the purposes of this modeling exercise, we made the simplifying assumption that all points within the pooled New England watershed contributed equally observed age population and used the hypsometric distribution to weight the sampling of a cooling rate dependent age-elevation stratigraphy. We generated a linear age-elevation relationship using the long-term average erosion rate of 20 m/Myr (Roden-Tice et al., 2012) and calibrated it to our

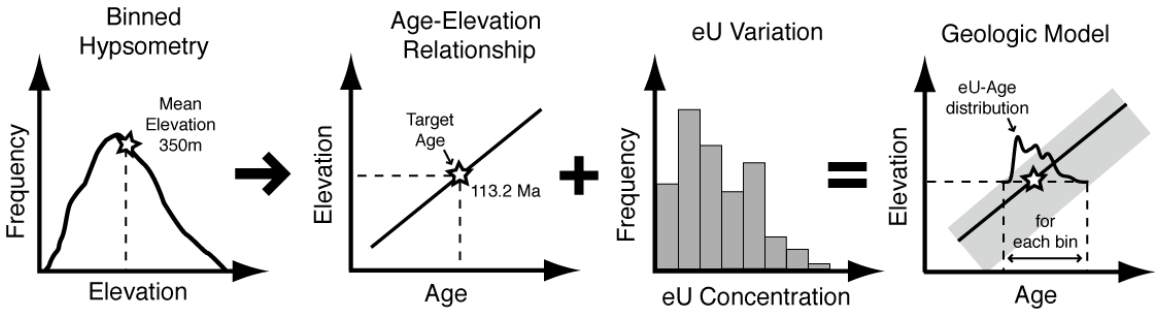

Figure 3.4: Schematic diagram of the input datasets and implications of the Geologic Model. The mean elevation (star) ties the median age from the pooled New England dataset to a linear age-elevation model that is cooling rate dependent. The eU variation and the cooling rate dictate the width of age dispersion on the Geologic Model age-elevation model (gray shaded region) illustrating the range of ages possible for one elevation bin. The output of the Geologic model performs the same process for each 100 m elevation bin and then weights the combined population of possible ages using the hypsometric curve.

watershed by placing the median age (113.2 Ma) at the mean elevation for the pooled watershed (350 m). We divided the hypsometric distribution into 100 m bins for which we then used the linear age-elevation relationship to calculate the cooling age for each bin. Within each bin we used the eU distribution and RDAAM to generate the range of ages at that elevation given the impact of radiation damage as per the Radiation Damage Only model (Figure 3.4). Finally we use the hypsometric distribution to weight the contribution of each bin to the full age variation caused by the age-elevation relationship and radiation damage that is possible within the pooled watershed.

3.4.2.2 Results. The Geologic Model illustrates that at slow cooling rates the added complexity of sampling an age-elevation stratigraphy does not significantly impact the overall distribution of ages predicted by the variation caused by radiation damage alone (Figure 3.5). At a cooling rate of 0.4˚C/Myr (representing a 20 m/Myr erosion rate) the PDFs of the Radiation Damage Only model and the Geologic model are nearly

indistinguishable, suggesting that the age variation introduced by the relatively low relief of the pooled New England watershed is swamped by the influence from radiation damage. Monte-carlo simulations (adapted from Ruhl and Hodges, 2005; and Stock et al., 2006) that subsample the full age distribution of the Geologic model to mimic detrital datasets using a sample population of 50 ages (suggested as a rule of thumb minimum sample size by Hodges et al. (2005)) or 117 ages (suggested by Vermeesch (2004) from statistical analysis) illustrate that the range of ages is likely to be quite similar, but the peak of the distribution will vary between different samples (Figure 3.5). It should be noted that both the Radiation Damage Only model and the Geologic model fail to predict the youngest ages observed from the pooled New England data set, which suggests that our simplifying assumptions and model inputs do not fully capture the reality of the thermal history for the New England study area. However, it is striking how well the Radiation Damage Only model fits the measured data set, despite the obvious over-simplification of what is certainly a complex system by this model.

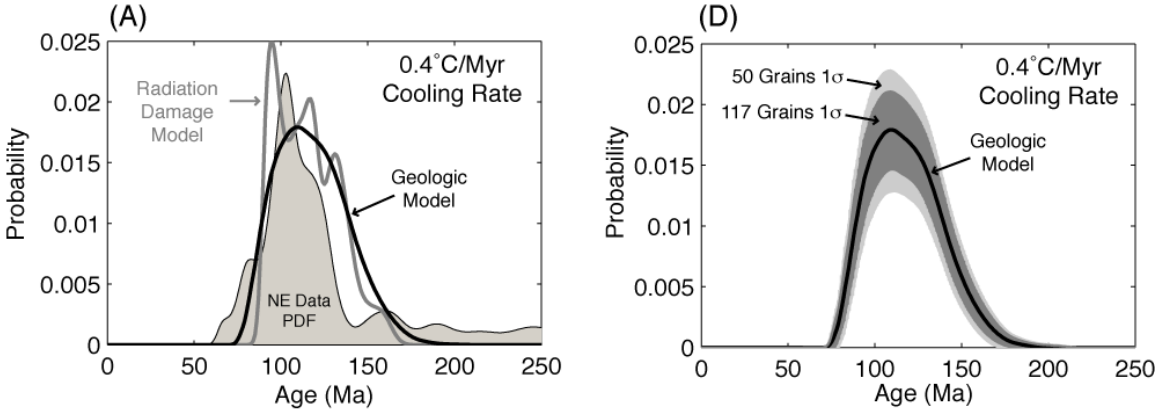

Figure 3.5: (A) Results of the "Geologic Model where both age variation from eU and hypsometric sampling of an age stratigraphy are considered for a cooling rate of 0.4˚C/Myr. The similarity of the Radiation Damage Only and Geologic models suggest that at slow cooling rates the age variation resulting from different eU concentrations dominates the age distribution observed. (B) Results of two monte-carlo simulations where the Geologic Model distribution was randomly subsampled 10,000 times to represent a 50 or 117 grain detrital sample pool.

3.4.3. Sensitivity Analysis

3.4.3.1 Rationale and Setup. Having illustrated that radiation damage can significantly impact a detrital AHe population (Figure 3.5), we use our pooled New England dataset and the Inyo Creek dataset of Stock et al. (2006) to explore how cooling rate, eU variability, and hypsometry collectively control the distribution of ages from detrital sampling. To conduct this sensitivity analysis we use the methodology of the Geologic Model. We use the observed cooling rates for Northern New England (Roden-Tice et al., 2012) and the eastern Sierra Nevada (House et al., 1997; Stock et al. 2006), 0.4˚C/Myr and 1.0˚C/Myr respectively, to represent slow and fast cooling rates. We use three levels of eU variation; no variation, the Durango diffusion model of Farley (2000), moderate variation, the unimodal distribution observed by Stock et al. (2006) from the Sierran Batholith, and high variation, the pooled New England dataset. Lastly, we normalized the hypsometric distributions of Inyo Creek and the pooled New England watershed to assess the role of relief; where Inyo creek is broadly distributed over 2 km of vertical distance and the New England watershed is skewed strongly to elevations below 800 m. Using these three variables we generated 6 predicted PFDs for both input datasets using the Geologic Model to compare to the observed data using a Kuiper goodness of fit statistic (Ruhl and Hodges, 2005).

3.4.3.2 Results. The sensitivity analysis indicates that at slow cooling rates the eU variability exerts the strongest control on detrital datasets, however, that influence disappears as the cooling rate increases to reflect modest cooling rates of 1.0 ˚C/Myr

(Figure 3.6). The suite of models for the New England dataset nicely illustrate the impact of radiation damage on detrital datasets in slowly cooled regions. For all possible eU

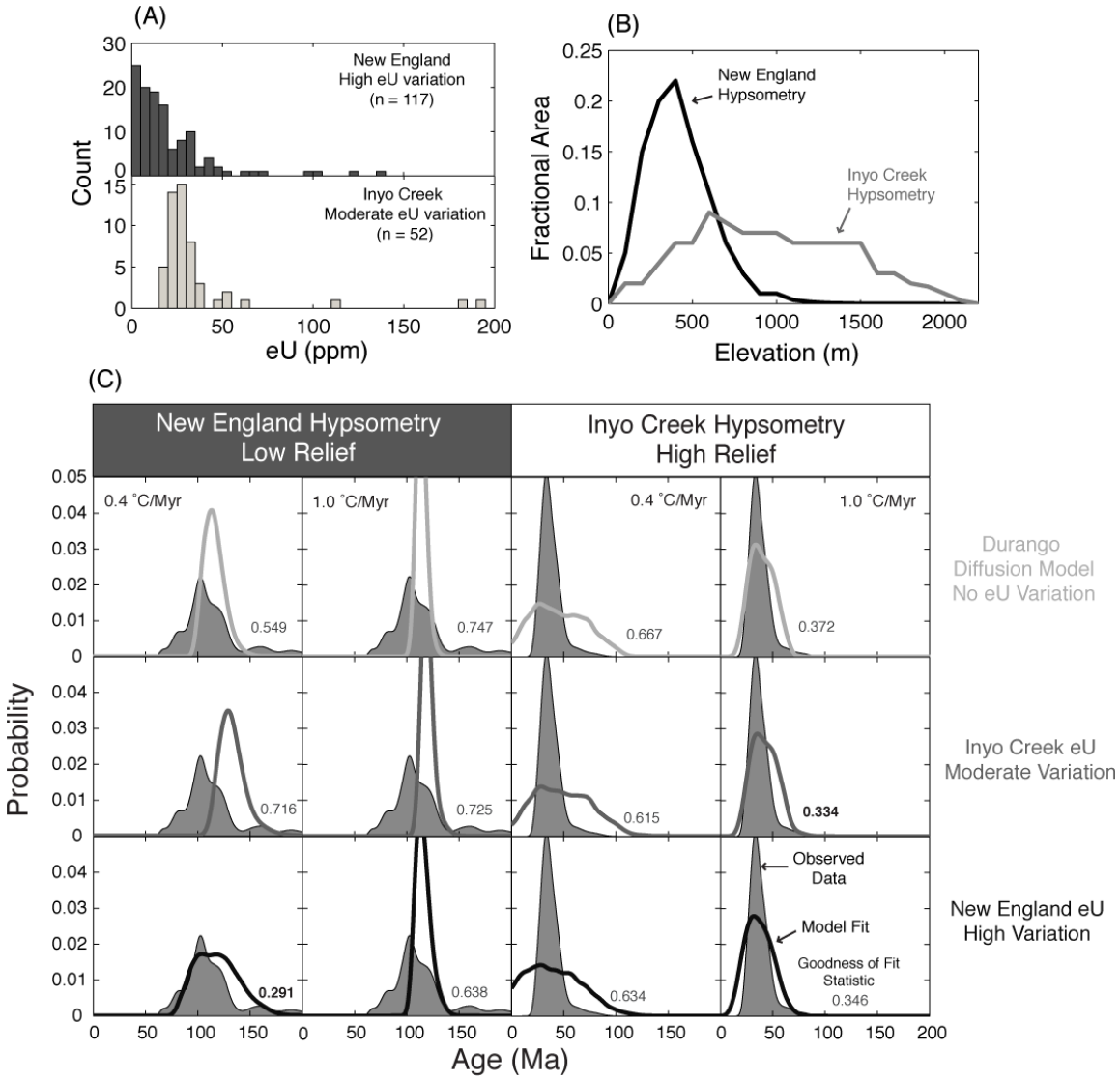

Figure 3.6: Results of the sensitivity analysis that illustrate how the cooling rate, watershed hypsometry, and eU variation impact the shape of detrital age distributions. Panels A and B show the eU and hypsometry data used for the sensitivity analysis from the northern New England watersheds reported here and from Inyo Creek reported by Stock et al. (2006). Panel C compares the observed detrital age populations (gray shaded curves) with the results of forward models (lines) where the cooling rate and eU variability are changed. Plots are arranged vertically by cooling rate and horizontally by the severity of eU variation. The goodness of fit between the model and observed data are measured using a Kuiper test and indicated on each plot. Of particular note is how strongly the eU variation impacts the age distribution in low relief watersheds at slow rates of cooling (New England – 0.4˚C/Myr case), but how that effect diminishes greatly at faster cooling rates.

variations, the predicted PFDs for fast cooling dramatically underestimate the range of ages observed; whereas for slow cooling, the amount of eU variability given to the model strongly impacts the fit between the predicted and observed PDFs with the true case of high eU variability producing a significantly better fit all of the other 5 models (Figure 3.6). From the suite of models using the Inyo Creek dataset, we find that the high relief of this watershed dominates the predicted PDFs for the case of slow cooling regardless of the eU variability (Figure 3.6). For the faster cooling rate, we again find that eU variability plays a minor role in comparison to the hypsometric control on the predicted PDFs and as with the New England models, we again find the best statistical fit of all the Inyo models with the true case of fast cooling and moderate eU variation.

3.5 DISCUSSION

3.5.1 Interpretation of New England Detrital Thermochronology

3.5.1.1 Geologic Implications. From the rugged landscape of northern New England we find no evidence for extensive exhumation during the Cenozoic or for differential exhumation of tectonic terranes since the Cretaceous. Our detrital datasets from the Connecticut and Merrimack Rivers were virtually indistinguishable from one another, with both centered around strong peaks at ~ 110 Ma with tails that skewed to much older ages (Figure 2). The similarity of these two populations indicates that although there is evidence for localized differential exhumation along terrane boundaries during the Cretaceous (Roden-Tice et al., 2009), from the perspective of our large watersheds, the

region as a whole has likely experienced relatively uniform exhumation. It is possible that the few young ages observed, which cannot be explained by either the Radiation Damage model or the Geologic model (Figure 3.5), are sourced from these areas. The presence of ages greater than 200 Ma in both detrital populations is curious given that this region cooled below the $^{40}Ar/^{39}Ar$ biotite and K-spar closure windows around 330 and 220 Ma respectively (Harrison et al., 1989). Either some portion of the landscape cooled very quickly to below the AHe closure window, 15% of our analyses resulted in erroneously high ages while leaving the rest unaffected, or these grains were not sourced from northern New England bedrock, which is the explanation we prefer. Given that this region has been repeatedly overrun by the Laurentide Ice Sheet flowing south over, and transporting material from, the Grenville age and older rocks from Canada, we explain these anomalously old ages as representing far traveled grains that were deposited in our watersheds during the Pleistocene. Taken together these observations suggest that northern New England is not a likely source for the large pulse of sediment deposited in offshore sedimentary basins during the Miocene.

3.5.1.2 Insights from Forward Models. Through forward modeling of the influence that radiation damage and age stratigraphy impose on detrital datasets at different cooling rates we find that our pooled New England dataset is most consistent with slow cooling. The timing of the peak of the observed age distributions is closely aligned with the passage of the region over the Great Meteor hotspot and could perhaps be reflective of exhumation related to thermal doming of the region and river incision which has been suggested for the Mt Washington area based on apatite fission-track analysis (Roden-Tice

et al., 2012). For this pulse of incision to set both AHe and AFT ages to immediately post-date the passage of the hotspot the cooling rate would have to be relatively fast. Though locally this is possible, the wide distribution of ages observed for both watersheds do not fit with fast cooling rates as illustrated by our sensitivity analysis (Figure 3.6). Therefore we feel that the regional average cooling rate was closer to the long-term average of 20m/Myr and that the strong peak at ~110 Ma for both datasets is a product of both locally rapid incision related to the hotspot and the variation caused by radiation damage at slow rates of cooling where low elevation samples can be older and high elevation samples can be younger than that expected by the age-elevation relationship as a result of the grain-specific concentration of eU. Finally, although the similarity between the Radiation Damage and Geologic models might suggest that nearly all age variation can be explained in the context of slow cooling and eU variation, the correlation between eU and age is not absolute (Figure 3.7). There is considerable dispersion around the predicted eU-age trend from the Radiation Damage model, which

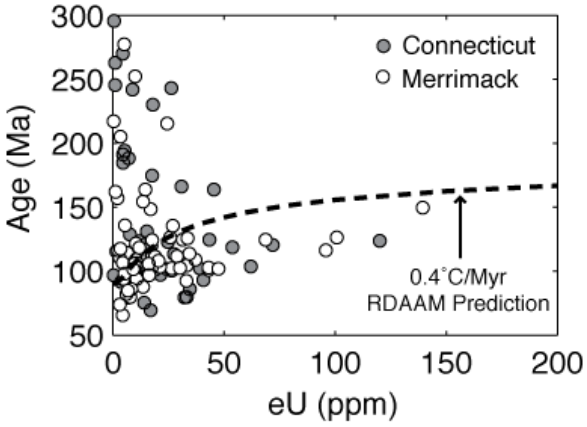

Figure 3.7: The relationship between eU and age for Connecticut and Merrimack River datasets compared to the eU-age prediction from the Radiation Damage model for a cooling rate of 0.4˚C/Myr.

we interpret to be caused by the position in the landscape from which the grain was sourced. In summary we suggest that the models argue for slow cooling since the Cretaceous, but radiation damage does not explain all of the variation that we observe in

the data, which is likely a combination of other factors including hypsometry, geomorphic sampling, and sources of age dispersion within the AHe dating technique (McKeon et al. - Chapter 2).

3.5.2 Radiation Damage and Detrital Thermochronology. The models presented here illustrate the impact that the cooling rate dependence of radiation damage induced age variation can impose on detrital AHe age populations. For regions characterized by slow exhumation rates on the order of 10 – 30 m/Myr, which are typical of post-orogenic landscapes, radiation damage results in significant age variation that can dominate a detrital age population if the range of eU concentrations is wide, especially when watershed relief is low. Given this reality, the Radiation Damage model illustrates that a good estimation of the long-term cooling history of the watershed can be determined by fitting the observed dataset to a predicted distribution of ages, where variation is caused only by differences in the measured eU concentrations. As a result of the strong dependence of the age on the grain-specific concentration of eU, we suggest caution when attempting to use the age as an indicator of provenance for geomorphic or sedimentologic investigations in slowly eroding landscapes. This is especially true for studies investigating paleo-relief using apatite grains from sedimentary deposits (e.g. Stock and Montgomery, 1996) because both the paleo-cooling rate (and therefore the age variation from radiation damage) and the paleo-hypsometry are not known and the relative influence of each on the dataset cannot be discerned. Finally, it is important to point out that the sensitivity analysis clearly indicates the diminishing effect of radiation damage as cooling rate and watershed relief increase. Thus, under the correct conditions,

it is perfectly reasonable to use detrital AHe thermochronology to address geomorphic questions as per the example from Stock et al. (2006).

3.6 CONCLUSIONS

Here we present 117 new U-Th/He ages determined on detrital apatite grains from collected from the Connecticut and Merrimack Rivers of northern New England. All ages were pre-Cenozoic, which places limits on the magnitude of recent exhumation from the rugged White Mountains of New Hampshire and Green Mountains of Vermont despite offshore evidence for a large increase in sedimentation rate during the Miocene and Pleistocene glaciation. Both samples produced wide and impressively similar distributions of the concentration of U and Th, which prompted a forward modeling exercise to explore the influence that radiation damage control of the closure temperature of the apatite U-Th/He system imposes on detrital data sets. We found that nearly all of the age variation observed for our two datasets could be explained solely through the age variation caused by radiation damage at cooling rate equivalent to a long-term erosion rate of 20 m/Myr, corroborating past estimates for the region (Roden-Tice et al., 2012). Further we found that when the added complexity of hypsometric sampling of an age-elevation relationship was added to the age variation caused by radiation damage the result was indistinguishable from the age distribution predicted only from radiation damage. We conducted a sensitivity analysis of the relative influence of cooling rate, radiation damage, and hypsometry and found that at modest cooling rates of 1.0˚C/Myr the impact of radiation damage on detrital age populations diminishes greatly, however,

below that threshold the effect dominates predicted age populations. Given these findings we suggest: 1) For slowly eroding regions the long-term cooling rate can be approximated by fitting models of radiation damage derived age distributions to measured detrital data, 2) caution should be used when attempting to infer geomorphic processes from detrital datasets from slowly cooled regions, and 3) radiation damage will not significantly impact detrital age populations from regions with cooling rates faster than 1.0˚C/Myr.

3.7 ACKNOWLEDGEMENTS

This research was supported by a Geological Society of America Student Research Grant and multiple Palmer Research Grants from the Department of Earth and Environmental Sciences of Lehigh University to R.E. McKeon and as part of NSF-EAR 9909393 to P.K. Zeitler, B.D. Idleman, and F.J. Pazzaglia. Kurt Frankel is thanked for collecting sediment samples from New England. Katharine Huntington and Todd Ehlers are thanked for sharing MATLAB scripts that aided in the monte-carlo analysis employed here.

3.8 REFERENCES

Braun, J., 2002, Estimating exhumation rate and relief evolution by spectral analysis of age–elevation datasets: Terra Nova, v. 14, no. 3, p. 210–214.

Cerveny PF, Naeser ND, Zeitler PK, Naeser CW, Johnson NM. 1988. History of uplift and relief of the Himalaya during the past 18 million years: evidence from sandstones of the Siwalik group. In New Perspectives in Basin Analysis, ed. KL Kleinspehn, C Paola, pp. 43–61. New York: Springer

Dodson, M.A., 1973, Closure temperature in cooling geochronological and petrological

systems: Contributions to Mineralogy and Petrology, v. 40, no. 3, p. 259–274.

Doherty, J., and Lyons, J., 1980, Mesozoic erosion rates in northern New England: Geological Society of America Bulletin, v. 91, p. 16–20.

Ehlers, T.A., Farley, K.A., Rusmore, M.E., and Woodsworth, G.J., 2006, Apatite (U-Th)/He signal of large-magnitude accelerated glacial erosion, southwest British Columbia: Geology, v. 34, no. 9, p. 765, doi: 10.1130/G22507.1.

Eusden, J., Jr, and Lux, D., 1994, Slow late Paleozoic exhumation in the Presidential Range of New Hampshire as determined by the 40Ar/39Ar relief method: Geology, v. 22, no. 10, p. 909–912.

Farley, K.A., 2002, (U-Th)/He dating: Techniques, calibrations, and applications: Reviews in Mineralogy and Geochemistry, v. 47, no. 1, p. 819–844.

Farley, K.A., Wolf, R.A., and Silver, L.T., 1996, The effects of long alpha-stopping distances on (U-Th)/He ages: Geochimica et Cosmochimica Acta, v. 60, no. 21, p. 4223–4229.

Flowers, R.M., Ketcham, R.A., Shuster, D.L., and Farley, K.A., 2009, Apatite (U-Th)/He thermochronometry using radiation damage accumulation and annealing model: Geochimica et Cosmochimica Acta, v. 73, no. 8, p. 2347–2365, doi: 10.1016/j.gca.2009.01.015.

Foland, K., and Allen, J., 1991, Magma sources for Mesozoic anorogenic granites of the White Mountain magma series, New England, USA: Contributions to Mineralogy and Petrology, v. 109, p. 195–211.

Harrison, M.T., Spear, F., and Hiezler, M., 1989, Geochronologic studies in central New England II: Post-Acadian hinged and differential uplift: Geology, v. 17, p. 185–189.

Hatcher, R.D. Jr., 1989. Tectonic synthesis of the U.S. Appalachians, in Hatcher, R.D., Jr., W.A. Thomas, and G.W. Viele, eds., The Appalachian -- Ouachita Orogen in the United States. Geological Society of America, Decade of North American Geology, F2, 29-41.

Hodges, K.V., Ruhl, K.W., Wobus, C.W., Pringle, M.S., 2005, $^{40}Ar/^{39}Ar$ Thermochronology of detrital minerals. in Reiners, P.W., and Ehlers, T.A., (eds.) Low-Temperature themrochronology: Techniques, Interpretations, and Applications, Reviews in Mineralogy and Geochemistry v. 58, p. 239-257.

House, M.A., Wernicke, B.P., Farley, K.A., and Dumitru, T.A., 1997, Cenozoic thermal evolution of the central Sierra Nevada, California, from (U-Th)/He thermochronometry: Earth and Planetary Science Letters, v. 151, p. 167–179, doi: 10.1016/S0012-821X(97) 81846-8.

Ketcham, R.A., 2005, Forward and inverse modeling of low-temperature thermochronometry data. in Reiners, P.W., and Ehlers, T.A., (eds.) Low-Temperature themrochronology: Techniques, Interpretations, and Applications, Reviews in Mineralogy and Geochemistry v. 58, p. 315-350.

Pazzaglia, F.J., and Brandon, M.T., 1996, Macrogeomorphic evolution of the post-Triassic Appalachian mountains determined by deconvolution of the offshore basin sedimentary record: Basin Research, v. 8, no. 3, p. 255–278.

Portenga, E.W., and Bierman, P.R., 2011, Understanding Earth's eroding surface with 10Be: GSA Today, v. 21, no. 8, p. 4–10, doi: 10.1130/G111A.1.

Rast, N., 1989. The evolution of the Appalachian chain, in Bally, A.W.. and A.R. Palmer, eds., The Geology of North America: An Overview. Geological Society of America Decade of North American Geology, A, 323-348.

Reiners, P.W., Thomson, S.N., McPhillips, D., Donelick, R.A., and Roering, J.J., 2007, Wildfire thermochronology and the fate and transport of apatite in hillslope and fluvial environments: Journal of Geophysical Research, v. 112, no. F4, p. 29, doi: 10.1029/2007JF000759.

Roden-Tice, M.K., Eusden, J.D., Jr, and Wintsch, R.P., 2012, Apatite fission-track evidence for the Cretaceous development of kilometer-scale relief and steady-state Tertiary topography in New England: Geomorphology, v. 141-142, no. C, p. 114–120, doi: 10.1016/j.geomorph.2011.12.029.

Roden-Tice, M.K., West, D.P., Jr, Potter, J.K., Raymond, S.M., and Winch, J.L., 2009, Presence of a Long-Term Lithospheric Thermal Anomaly: Evidence from Apatite Fission-Track Analysis in Northern New England: The Journal of Geology, v. 117, no. 6, p. 627–641, doi: 10.1086/605995.

Ruhl, K., and Hodges, K., 2005, The use of detrital mineral cooling ages to evaluate steady state assumptions in active orogens: An example from the central Nepalese Himalaya: Tectonics, v. 24, no. 4, p. TC4015.

Shuster, D., Flowers, R., and Farley, K., 2006, The influence of natural radiation damage on helium diffusion kinetics in apatite: Earth and Planetary Science Letters, v. 249, no. 3-4, p. 148–161, doi: 10.1016/j.epsl.2006.07.028.

Stock, G.M., Ehlers, T.A., and Farley, K.A., 2006, Where does sediment come from? Quantifying catchment erosion with detrital apatite (U-Th)/He thermochronometry: Geology, v. 34, no. 9, p. 725–728.

Stock, J.D., and Montgomery, D.R., 1996, Estimating palaeorelief from detrital mineral age ranges: Basin Research, v. 8, no. 3, p. 317–327.

Stockli, D.F., Farley, K.A., and Dumitru, T.A., 2000, Calibration of the apatite (U-

Th)/He thermochronometer on an exhumed fault block, White Mountains, California: Geology, v. 28, no. 11, p. 983–986.

Vermeesch, P., 2004, How many grains are needed for a provenance study?: Earth and Planetary Science Letters, v. 224, no. 3-4, p. 441–451, doi: 10.1016/j.epsl.2004.05.037.

Zartman, R.E., 1988, Three decades of geochronologic studies in the New England Appalachians: Geological Society of America Bulletin, v. 100, p. 1168–1180.

Table 3.1: U-Th/He Data for Connecticut and Merrimack Detrital Samples

Sample	Radius	^{4}He	^{238}U	^{232}Th	^{147}Sm	eU[ł]	Ft	Raw Age	Age corr	± 2σ*	Th/U
	(μm)	(mol)	(mol)	(mol)	(mol)	(ppm)		(Ma)	(Ma)	(Ma)	
Connecticut River Watershed											
CT-1	63.3	1.614E-14	1.339E-13	3.384E-13	6.110E-12	14.1	0.770	58.0	75.4	2.3	2.53
CT-2	58.2	4.654E-15	5.003E-14	7.166E-15	5.669E-14	3.8	0.763	69.7	91.4	2.7	0.14
CT-3	67.5	1.922E-13	1.522E-12	1.133E-13	2.775E-12	72.0	0.796	95.9	120.4	3.6	0.07
CT-4	74.7	4.633E-14	2.006E-13	1.126E-12	8.391E-12	21.4	0.796	77.4	97.2	2.9	5.61
CT-5	55.8	6.497E-14	5.215E-13	4.830E-14	3.467E-12	43.5	0.754	93.8	124.4	3.7	0.09
CT-6	63.8	1.130E-13	9.344E-13	6.239E-13	7.143E-12	62.1	0.781	80.8	103.4	3.1	0.67
CT-7	64.9	2.109E-14	1.579E-13	2.022E-13	1.927E-12	11.8	0.781	79.5	101.7	3.1	1.28
CT-8	60.5	2.292E-14	4.970E-14	2.105E-13	3.722E-13	8.9	0.745	180.1	241.7	7.3	4.23
CT-9	48.6	3.433E-14	1.527E-13	1.168E-14	3.828E-12	18.1	0.723	166.5	230.3	6.9	0.08
CT-10	52.7	1.406E-14	1.403E-13	2.150E-14	2.473E-12	13.7	0.742	74.0	99.7	3.0	0.15
CT-11	52.5	2.567E-14	1.413E-13	6.948E-13	2.663E-12	40.7	0.709	66.0	93.0	2.8	4.92
CT-12	58.7	1.468E-14	1.160E-13	1.656E-13	7.454E-12	11.8	0.759	71.4	94.0	2.8	1.43
CT-13	47.4	2.599E-14	2.717E-13	2.734E-14	1.812E-12	39.1	0.705	72.1	102.2	3.1	0.10
CT-14	66.8	9.516E-16	8.114E-15	5.839E-15	1.811E-13	0.5	0.794	76.9	96.8	2.9	0.72
CT-15	51.3	1.231E-14	9.533E-14	4.273E-14	2.124E-12	12.0	0.725	89.2	123.1	3.7	0.45
CT-16	64.5	3.600E-14	2.689E-13	5.892E-14	1.112E-11	15.4	0.785	95.7	121.9	3.7	0.22
CT-17	67.5	3.083E-13	2.060E-12	1.622E-12	4.878E-12	120.1	0.792	97.9	123.6	3.7	0.79
CT-18	80.1	6.162E-14	1.487E-13	2.600E-12	1.213E-11	32.3	0.801	63.6	79.5	2.4	17.48
CT-19	71.5	3.732E-14	1.775E-13	3.689E-14	3.473E-12	7.2	0.808	152.1	188.3	5.6	0.21
CT-20	71.0	6.340E-14	5.654E-13	1.335E-13	3.208E-12	24.2	0.805	82.0	101.9	3.1	0.24
CT-21	64.7	2.145E-14	1.766E-13	1.619E-14	7.247E-13	9.4	0.788	91.7	116.4	3.5	0.09
CT-22	52.1	8.024E-15	4.326E-14	8.493E-15	3.767E-13	4.6	0.735	135.8	184.8	5.5	0.20
CT-23	67.6	8.418E-15	6.405E-14	1.072E-13	4.156E-13	4.8	0.785	73.4	93.5	2.8	1.67
CT-24	47.4	1.605E-14	1.182E-13	3.893E-13	4.568E-12	34.6	0.688	59.1	85.9	2.6	3.29
CT-25	59.3	1.069E-14	1.158E-13	2.574E-14	6.101E-12	7.9	0.772	65.6	84.9	2.5	0.22
CT-26	56.4	1.187E-14	8.759E-14	2.680E-14	1.058E-12	7.6	0.755	97.0	128.5	3.9	0.31
CT-27	48.8	1.312E-14	1.158E-13	8.254E-14	7.265E-12	16.6	0.718	72.5	101.0	3.0	0.71
CT-28	74.7	3.425E-14	3.300E-13	1.989E-14	1.388E-12	11.4	0.816	79.0	96.8	2.9	0.06
CT-29	65.8	2.473E-14	1.636E-13	1.809E-13	9.186E-12	10.9	0.787	90.3	114.7	3.4	1.11
CT-30	81.7	6.189E-15	1.744E-14	7.795E-15	7.831E-14	0.5	0.829	244.9	295.4	8.9	0.45
CT-31	79.2	1.004E-13	1.170E-12	1.666E-14	5.570E-12	33.3	0.827	66.1	79.9	2.4	0.01
CT-32	67.6	3.499E-14	1.508E-13	5.954E-13	4.611E-12	17.3	0.778	93.3	120.0	3.6	3.95
CT-33	70.1	2.803E-14	3.615E-13	1.279E-13	2.451E-13	16.9	0.801	55.6	69.4	2.1	0.35
CT-34	66.0	6.262E-14	3.261E-13	9.273E-14	2.787E-12	17.6	0.790	138.0	174.7	5.2	0.28
CT-35	74.3	5.294E-14	4.327E-13	2.941E-13	1.623E-12	18.8	0.810	81.8	101.0	3.0	0.68
CT-36	69.3	3.332E-14	2.296E-13	3.107E-13	1.526E-11	13.8	0.797	82.7	103.7	3.1	1.35

CT-37	64.9	3.406E-15	1.825E-14	4.301E-14	1.599E-12	1.6	0.780	90.0	115.4	3.5	2.36
CT-38	64.0	1.255E-13	4.903E-13	2.876E-14	7.178E-12	26.3	0.787	191.4	243.2	7.3	0.06
CT-39	79.3	7.536E-14	6.128E-13	1.747E-14	8.656E-12	17.2	0.828	93.4	112.8	3.4	0.03
CT-40	73.5	1.816E-13	1.335E-12	5.048E-13	1.513E-11	53.7	0.811	96.0	118.4	3.6	0.38
CT-41	69.7	2.630E-14	1.224E-13	2.043E-14	3.194E-12	5.2	0.804	156.1	194.2	5.8	0.17
CT-42	71.9	1.259E-13	5.889E-13	5.932E-13	5.596E-12	30.9	0.802	133.3	166.2	5.0	1.01
CT-43	76.7	4.238E-14	1.432E-13	9.408E-15	8.208E-13	4.6	0.821	221.7	270.1	8.1	0.07
CT-44	86.0	4.029E-14	1.633E-13	1.269E-13	1.711E-12	4.7	0.836	160.1	191.5	5.7	0.78
CT-45	88.0	2.945E-14	3.199E-13	6.558E-14	9.354E-12	6.8	0.845	66.7	79.0	2.4	0.21
CT-46	99.3	4.915E-14	3.409E-13	2.852E-13	8.163E-12	6.2	0.859	92.2	107.4	3.2	0.84
CT-48	67.3	7.051E-14	5.394E-13	2.500E-14	1.428E-11	24.6	0.798	98.0	122.8	3.7	0.05
CT-50	78.3	2.671E-13	1.482E-12	1.642E-13	5.818E-12	45.4	0.824	134.9	163.7	4.9	0.11
CT-51	132.8	4.081E-13	2.239E-12	5.615E-12	2.198E-11	26.5	0.889	89.3	100.5	3.0	2.51
CT-52	81.5	1.062E-14	3.059E-14	2.258E-14	1.912E-12	0.9	0.831	218.5	262.9	7.9	0.74
CT-53	86.6	5.854E-14	4.132E-13	5.284E-13	6.558E-12	13.2	0.835	84.1	100.7	3.0	1.28
CT-54	60.5	4.784E-14	4.020E-13	8.225E-14	2.801E-12	27.3	0.772	87.5	113.4	3.4	0.20
CT-55	82.4	7.880E-14	4.712E-13	3.680E-13	6.662E-12	15.2	0.829	108.6	131.0	3.9	0.78
CT-56	98.4	1.712E-14	4.262E-14	8.440E-14	1.022E-12	1.1	0.853	209.6	245.7	7.4	1.98
Merrimack River Watershed											
Mer-1	125.7	1.249E-13	9.331E-13	3.370E-13	1.673E-11	7.4	0.890	94.4	106.1	3.2	0.36
Mer-2	94.7	2.479E-13	1.672E-12	2.455E-12	1.361E-11	43.1	0.848	85.6	100.9	3.0	1.47
Mer-3	132.9	1.671E-12	1.138E-11	3.957E-13	7.631E-11	68.7	0.897	111.9	124.7	3.7	0.03
Mer-4	83.9	4.262E-14	3.663E-13	2.306E-13	4.196E-12	10.7	0.833	78.2	93.8	2.8	0.63
Mer-5	70.5	4.711E-14	3.241E-13	3.323E-13	7.485E-12	17.8	0.799	89.9	112.5	3.4	1.03
Mer-6	126.3	1.226E-13	9.386E-13	3.466E-13	8.581E-12	8.5	0.885	92.6	104.6	3.1	0.37
Mer-7	50.5	2.221E-14	1.513E-13	1.884E-14	3.893E-12	17.0	0.729	108.2	148.4	4.5	0.12
Mer-8	98.0	8.635E-14	7.966E-13	3.182E-13	2.487E-11	13.7	0.858	75.3	87.8	2.6	0.40
Mer-9	113.1	4.210E-13	2.925E-12	1.937E-14	7.079E-11	31.4	0.875	108.9	124.5	3.7	0.01
Mer-10	80.5	4.222E-13	3.365E-12	5.069E-14	2.063E-11	95.8	0.827	96.2	116.3	3.5	0.02
Mer-11	66.0	2.500E-14	1.929E-13	3.450E-14	7.354E-13	10.3	0.789	96.0	121.6	3.6	0.18
Mer-12	80.9	1.567E-13	1.281E-12	2.219E-13	1.619E-11	37.2	0.828	90.1	108.9	3.3	0.17
Mer-14	105.5	2.595E-13	2.173E-12	3.280E-13	6.542E-12	26.5	0.871	89.1	102.3	3.1	0.15
Mer-15	91.1	2.033E-13	1.753E-12	4.485E-14	1.364E-11	33.3	0.849	88.6	104.4	3.1	0.03
Mer-16	72.8	2.369E-13	6.674E-13	2.163E-13	1.147E-11	27.8	0.808	248.9	308.0	9.2	0.32
Mer-17	115.7	5.072E-13	4.030E-12	1.264E-12	2.520E-11	43.0	0.878	90.4	103.0	3.1	0.31
Mer-18	97.3	2.215E-13	1.900E-12	1.101E-13	2.692E-11	30.2	0.858	88.0	102.6	3.1	0.06
Mer-19	92.6	1.900E-13	1.838E-12	1.008E-13	8.020E-12	33.1	0.852	78.8	92.4	2.8	0.05
Mer-20	103.6	1.001E-13	8.017E-13	6.714E-14	2.792E-12	10.3	0.868	94.4	108.8	3.3	0.08
Mer-21	94.2	2.713E-14	2.296E-13	1.438E-13	1.171E-12	4.8	0.851	79.8	93.7	2.8	0.63
Mer-22	90.9	1.231E-13	9.902E-13	5.918E-14	2.721E-12	18.9	0.849	94.6	111.4	3.3	0.06
Mer-23	93.2	9.296E-14	2.878E-13	3.981E-14	3.779E-12	5.2	0.853	236.6	277.3	8.3	0.14

Mer-24	80.6	1.421E-14	1.106E-13	2.893E-14	3.247E-12	3.2	0.830	91.8	110.6	3.3	0.26
Mer-25	72.7	3.499E-14	1.861E-13	3.981E-13	1.140E-11	11.8	0.802	94.8	118.2	3.5	2.14
Mer-26	109.0	3.420E-13	2.227E-12	5.478E-13	5.146E-11	25.8	0.874	110.4	126.3	3.8	0.25
Mer-27	105.6	4.927E-14	4.920E-13	1.361E-13	1.415E-11	6.2	0.871	71.5	82.1	2.5	0.28
Mer-28	90.3	6.617E-14	5.580E-13	3.662E-14	1.661E-12	10.9	0.848	90.1	106.3	3.2	0.07
Mer-29	89.2	4.143E-14	3.175E-13	3.822E-14	6.050E-12	6.4	0.847	96.8	114.3	3.4	0.12
Mer-30	91.9	1.891E-13	1.392E-12	6.040E-13	1.861E-11	28.9	0.849	94.7	111.5	3.3	0.43
Mer-31	66.4	1.411E-14	1.443E-13	7.086E-14	8.355E-13	8.3	0.789	67.9	86.0	2.6	0.49
Mer-32	118.6	8.678E-14	4.366E-13	5.372E-13	2.111E-12	5.4	0.879	119.4	135.9	4.1	1.23
Mer-33	82.6	2.371E-14	1.852E-13	3.787E-13	1.080E-11	7.9	0.826	65.7	79.5	2.4	2.04
Mer-34	76.8	7.625E-14	6.845E-13	1.908E-14	6.964E-12	21.3	0.822	85.0	103.4	3.1	0.03
Mer-35	99.6	1.411E-13	1.121E-12	4.000E-13	2.565E-11	17.5	0.862	88.6	102.8	3.1	0.36
Mer-36	70.0	9.941E-14	8.130E-13	9.354E-14	9.904E-12	34.4	0.804	91.3	113.6	3.4	0.12
Mer-37	77.6	1.621E-13	5.383E-13	7.257E-13	7.045E-12	24.5	0.815	175.6	215.5	6.5	1.35
Mer-38	141.9	1.180E-13	2.379E-13	1.122E-12	2.608E-12	3.3	0.893	183.2	205.2	6.2	4.72
Mer-39	196.7	2.125E-13	1.091E-12	3.199E-14	2.600E-11	2.0	0.931	146.2	157.0	4.7	0.03
Mer-40	115.6	1.372E-13	1.877E-13	4.559E-13	8.311E-12	3.2	0.874	349.8	400.3	12.0	2.43
Mer-41	122.2	1.043E-14	3.579E-14	1.236E-14	3.579E-12	0.3	0.891	193.4	217.0	6.5	0.35
Mer-42	94.3	1.921E-14	2.380E-13	1.105E-13	4.117E-12	4.6	0.853	55.9	65.6	2.0	0.46
Mer-43	125.4	8.406E-14	7.251E-13	4.435E-14	9.753E-12	5.2	0.891	87.5	98.3	2.9	0.06
Mer-44	101.7	2.507E-14	1.851E-13	1.505E-14	4.995E-12	2.4	0.867	100.7	116.1	3.5	0.08
Mer-45	106.2	2.076E-14	1.022E-13	2.957E-14	5.233E-12	1.2	0.873	141.5	162.1	4.9	0.29
Mer-46	137.4	2.178E-13	1.740E-12	1.304E-13	4.488E-12	9.7	0.900	95.0	105.5	3.2	0.07
Mer-47	94.5	3.296E-14	2.692E-13	1.451E-14	8.049E-12	4.4	0.857	91.4	106.7	3.2	0.05
Mer-48	72.2	1.746E-14	1.825E-13	2.903E-14	9.439E-12	6.8	0.813	68.9	84.8	2.5	0.16
Mer-49	95.4	3.366E-13	6.338E-13	6.733E-13	1.585E-11	14.0	0.852	319.6	375.2	11.3	1.06
Mer-50	92.4	1.303E-12	7.800E-12	1.916E-13	4.074E-11	139.4	0.852	127.5	149.7	4.5	0.02
Mer-51	84.2	1.286E-13	4.325E-13	6.585E-14	2.211E-11	10.1	0.840	211.8	252.2	7.6	0.15
Mer-52	100.8	7.747E-14	6.708E-13	2.715E-14	7.804E-12	9.1	0.865	87.7	101.4	3.0	0.04
Mer-53	80.1	9.277E-14	5.093E-13	6.827E-14	2.467E-12	14.6	0.828	135.6	163.8	4.9	0.13
Mer-54	90.0	2.366E-13	1.653E-12	2.411E-13	6.689E-12	33.5	0.847	106.7	125.9	3.8	0.15
Mer-55	75.3	5.353E-14	4.673E-13	4.731E-14	1.848E-12	16.1	0.817	86.3	105.7	3.2	0.10
Mer-56	83.0	2.002E-13	1.672E-12	6.577E-13	5.930E-12	47.4	0.832	84.8	101.9	3.1	0.39
Mer-57	109.9	8.845E-13	6.233E-12	2.226E-13	1.446E-11	100.7	0.857	108.4	126.5	3.8	0.04
Mer-58	102.0	3.691E-14	2.590E-13	4.758E-14	1.237E-11	3.4	0.868	102.1	117.6	3.5	0.18
Mer-59	101.4	1.808E-14	2.041E-13	6.182E-14	2.086E-12	3.0	0.864	63.8	73.8	2.2	0.30
Mer-60	86.2	1.016E-13	5.813E-13	9.273E-14	2.426E-12	13.5	0.840	129.5	154.2	4.6	0.16
Mer-61	76.4	1.198E-13	7.998E-13	1.427E-13	1.963E-12	27.1	0.819	110.9	135.4	4.1	0.18
Mer-62	94.7	1.475E-13	1.197E-12	1.392E-13	6.363E-12	20.5	0.855	92.4	108.1	3.2	0.12
Mer-63	86.4	1.089E-13	7.925E-13	4.731E-14	1.192E-12	17.7	0.841	104.6	124.3	3.7	0.06
Mer-64	77.7	5.082E-14	4.372E-13	2.572E-13	1.233E-12	16.1	0.819	79.2	96.7	2.9	0.59

* Uncertaintyies in ages are two-sigma (Ma); based on propagation of long-term analytical uncertainties in 4He, U, and Th, and 1% uncertainty in Ft factor

For pooled ages, lowered uncertainties reflect propagation of component uncertainties through summing of measured quantities.

[#] Analytical Scatter - Is a simple 2-sigma standard deviation of measured ages, given as a measure of scatter in the component analyses for the pooled age.

[ǂ] eU - Values calculated by using Ft factor to determine effective spherical radius to model mass of sample analyzed. Uncertainties of 25% apply.

Ryan E. McKeon
ryan.mckeon@gmail.com
http://www.lehigh.edu/~rem208
Department of Earth and Environmental Sciences
Lehigh University
1 W. Packer Ave.
Bethlehem, PA 18015
work: (610) 758-1242

EDUCATION:

Lehigh University: Bethlehem, PA
Ph.D. candidate, Earth and Environmental Sciences, GPA: 3.94
Dissertation Title: *Apatite U-Th/He Thermochronometry in Slowly Eroding Landscapes: Addressing Age Dispersion to Understand Appalachian Topographic Development*
Advisors: Peter Zeitler and Frank Pazzaglia
Montana State University: Bozeman, MT
Master of Science, Earth Sciences, May 2009, GPA: 4.0
Thesis Title: *The interaction between tectonics, topography, and climate in the San Juan Mountains, southwestern Colorado*
Advisor: David Lageson
The Colorado College: Colorado Springs, CO
Bachelor of Arts, Geology, May 2003, GPA: 3.54
Senior Project Title: *Testing the "glacial buzzsaw" hypothesis in the mountains of the western United States: Geological Society of America*
Advisor: Eric Leonard

APPOINTMENTS:

Graduate Teaching Assistant: Earth and Environmental Sciences Dept. Lehigh University - Fall 2011 to present
College of Arts and Sciences Summer Fellow: Earth and Environmental Sciences Dept., Lehigh University - June to August 2011
Graduate Teaching Assistant: Earth and Environmental Sciences Dept. Lehigh University - Fall 2010 to Summer 2011
Research Assistant: Addressing systematics of age scatter in Apatite U-Th/He Thermochronometry, Advisor Dr. Peter Zeitler, Earth and Environmental Sciences Dept., Lehigh University - Fall 2009 to Summer 2010
College of Arts and Sciences Fellow: Earth and Environmental Sciences Dept., Lehigh University - Fall 2008 to Summer 2009
Graduate Teaching Assistant: Department of Earth Sciences, Montana State University - Fall 2006 to Spring 2008

PUBLICATIONS:

McKeon, Ryan E., Zeitler, Peter K., Idleman, Bruce, 2012, "Effects of physical and chemical abrasion on apatite U-Th/He Thermochronometry". In Preparation for *Geochimica et Cosmochimica Acta*

McKeon, Ryan E., Zeitler, Peter K., Pazzaglia, Frank J., Idleman, Bruce, Enkelmann, Eva, 2012, "Decay of an old orogen: inferences about Appalachian landscape evolution from low-temperature thermochronology". In Preparation for *Geological Society of America Bulletin*

McKeon, Ryan E., Zeitler, Peter K., Pazzaglia, Frank J., Idleman, Bruce, Enkelmann, Eva,

Laucks, Jeremy, 2012, "Slow long-term exhumation of the northern New England Appalachians from detrital Apatite U-Th/He thermochronology and radiation damage modeling". In Preparation for *Lithosphere*

Karlstrom, K.E, Coblentz, D., Dueker, K., Ouimet, W., Kirby, E., Van Wijk, J., Schmandt, B., Kelley, S., Lazear, G., Crossey, L. J., Crow, R., Aslan, A, Darling, A., Aster, R., MacCarthy, J., Hansen, S.M., Stachnik, J., Stockli, D., Hoffman, M., **McKeon, R.,** Feldman, J., Heizler, M., Donahue, M.S., and the CREST working group, 2012, *Mantle-driven dynamic uplift of the Rocky Mountains and Colorado Plateau and its surface response: toward a unified hypothesis.* Lithosphere, 4, 1, p. 3 - 22 DOI: 10.1130/L150.1.

Kulo, V., Bodzin, A., **McKeon, R.,** Anastasio, D., Peffer, T., & Sahagian, D. (in press). *The Isle of Navitas: Towards a better understanding of energy and decision-making using GIS.* In Barnett, MaKinster, & Trautman (Eds.) *Learning Science through the innovative use of Geospatial Technologies: Designing Effective Learning Tools and Programs for K-16 settings*. Dordrecht, Netherlands: Springer.

ABSTRACTS AND PRESENTATIONS (as First Author):

McKeon, Ryan E., Zeitler, Peter K., Pazzaglia, Frank J., Teasing out an unsteady past in the southern Appalachians using apatite U-Th/He thermochronology. AGU Fall Meeting 2011, San Francisco – December 2011 (*talk*)

McKeon, Ryan E., *How old are the Appalachians? Preliminary insights from new applications of apatite U-Th/He thermochronology.* Eastern North America Earthscope and GeoPRISMS Workshop, Bethlehem, PA – October 2011 (*talk*)

McKeon, Ryan E., Zeitler, Peter K., Pazzaglia, Frank J., *Long-Term landscape evolution from apatite U-Th/He thermochronology in slowly eroding landscapes: Problems and potential from the southern Appalachians, U.S.A.* European Geosciences Union General Assembly 2011, Vienna, Austria - April 2011. (*poster*)

McKeon, Ryan E., *How old are the Appalachians? Preliminary insights from new applications of apatite U-Th/He thermochronology.* 2011 Academic Symposium, Lehigh University - March 2011. (poster)

McKeon, Ryan E., Zeitler, Peter K., Pazzaglia, Frank J., *The effect of radiation damage on detrital apatite (U-Th)/He thermochronometry: A case study from New England, USA.* Thermo2010 12th International Conference of Thermochronology, Glasgow, Scotland - August 2010. (*poster*)

McKeon, Ryan E., Zeitler, Peter K., Idleman, Bruce, Enkelmann, Eva, Exploring the potential of whole rock shale (U-Th)/He thermochronometry. American Geophysical Union Fall Meeting, San Francisco, CA - December 2009 (poster).

McKeon, Ryan E., Kulo, Violet, Anastasio, David, Bodzin, Alec, Peffer, Tamara, Sahagian, Dork, *The Isle of Navitas: Towards a better understanding of energy and decision making using GIS*. Geological Society of America Meeting, Portland, OR - October 2009 (*poster*).

McKeon, Ryan E., Kelley, Shari A., Lageson, David R., *The interaction between tectonics, topography, glacial erosion in the San Juan Mountains, southwestern Colorado*. Geological Society of America Meeting, Houston, TX - October 2008 (*poster*).

McKeon, Ryan E., et al., *Structural Style and Sediment Dispersal in an Active Fold-and-Thrust Salient, Sulaiman Range, Pakistan.* Geological Society of America Meeting, Denver, CO - October 2007 (*poster - lead author and presenter for class project*).

McKeon, Ryan E., Leonard, Eric M., Sak, Peter, Testing the "Glacial Buzzsaw" hypothesis in the mountains of the western United States. Geological Society of America Meeting, Seattle, WA - October 2003 (poster).

ABSTRACTS AND PRESENTATIONS (Coauthored):

Pazzaglia, FJ, Berti, C, **McKeon, RE,** Gunderson, K, Semmens, K, Tectonic Geomorphology and EarthScope in eastern North America. Geological Society of America Meeting, Minneapolis, MN – October 2011.

Teletzke, A, Kulo, V, Bodzin, A, Anastasio, D, Sahagian, D, **McKeon, RE**, Designing learning activities to teach "spatially" with web GIS. Geological Society of America Meeting, Minneapolis, MN – October 2011.

Donahue M.S., Karlstrom, K.E., Gonzales, D., Pecha, M., **McKeon, R.E**., Multi-stage uplift of the Rocky Mountains: new age constraints on the Telluride Conglomerate and regional compilation of apatite fission track ages. *Eos Trans. AGU*, Fall Meet. Suppl., 2011.

Pazzaglia, FJ, Zeitler, PK, **McKeon, RE,** Idleman, BD, Berti, C, Unsteady rock uplift and erosion in a decaying orogen in response to surface and dynamic mantle processes (Invited). *Eos Trans. AGU*, Fall Meeting 2010.

Kelley, SA, Karlstrom, KE, Stockli, D, **McKeon, RE,** Hoffman, M, Lee, J, Pederson, J, Coblentz, D, A summary and evaluation of thermochronologic constraints on the exhumation history of the Colorado Plateau- Rocky Mountain region. Colorado River Evolution II Workshop, Flagstaff, AZ – May 2010.

Karlstrom, K., Coblentz, D., Ouimet, W., Kirby, E, Van Wijk, J., Schmandt, B., Crossey, L., Crow, R., Kelley, S., **McKeon, R**., Aslan, A, Darling, A., Dueker, K., Aster, R., Lazear, G., Hilton, D., Dynamic uplift of the Colorado Rockies and western Colorado Plateau in the last 6 Ma driven by mantle flow: Evidence from the Colorado River region, *Eos Trans. AGU*, Fall Meet. Suppl., 2009.

Kelley, SA, **McKeon, RE**, 2009, Thermal and exhumation history of Proterozoic basement and Oligocene plutonic rocks, southwestern Colorado. Geological Society of America Abstracts with Programs, vol. 41, no. 7, p. 136.

AWARDS AND HONORS:

2011

CAS Graduate Student Representative to the 2011 Academic Symposium at Lehigh University
Best Talk - EES Department Graduate Student Symposium

2010

Runner-up Best Student Poster - Thermo2010 12th International Conference of Thermochronology
Runner-up Best Poster - EES Department Graduate Symposium

2009
Student Research Grant Award - Structural Geology and Tectonics Division of the Geological Society of America
Outstanding Mention - Research Grant Proposal, Geological Society of America
2007
Best Poster - Earth Sciences Department, Montana State University, Student Research Colloquium

COURSES TAUGHT (TA):
Lehigh University
EES 115 - Surficial Processes with Frank Pazzaglia (Fall 2011 - 18 students)
EES 341 - Lehigh Field Camp - Director Frank Pazzaglia (Summer 2011 - 30 students)
EES 223 - Structural Geology and Tectonics with David Anastasio (Spring 2011 - 11 students)
EES 004 - Science of Environmental Issues - 1 section (Spring 2011 - 31 students)
EES 115 - Surficial Processes with Frank Pazzaglia (Fall 2010 - 16 students)
Montana State University
GEOL 101 - Physical Geology - Head TA (Fall 2007 and Spring 2008), TA (Spring 2007) 60 students each semester in 3 lab sections.
GEOL 315 - Structural Geology with David Lageson (Fall 2006 - 17 students)
GPHY 111 - Physical Geography - 1 section (Fall 2006 - 19 students)

PROFESSIONAL EXPERIENCE:
Labs Visited -
Berkeley Geochronology Center - Berkeley, CA - Collaborating with David Shuster and Greg Balco on apatite 4He/3He thermochronology of Appalachian samples (July - August 2011).
Arizona Radiogenic Helium Dating Lab - University of Arizona - Tucson, AZ - Collaborating with Peter Reiners on Appalachian bedrock and detrital U-Th/He analyses and learning U and Th dissolution and analysis using ICP-MS (June - July 2010).
KU U-Th/He Laboratory - University of Kansas - Lawrence, KS - Collaborating with Daniel Stockli and Shari Kelley (of New Mexico Tech) on apatite U-Th/He analysis of sample from the San Juan Mountains for my masters thesis.

Mentoring -
Undergraduate Student Thesis – Active in all phases of helping guide an EES major through their thesis, including hypothesis formation, technical and regional background, grant writing, lab techniques, thesis writing, etc.

Session Convener -
American Geophysical Union Fall Meeting 2011 - Title: The Long Road to Flat - Towards understanding the drivers and quantifying change in orogens - Earth and Planetary Surface Processes division - 27 Abstracts submitted.

Seminars Attended -
Teacher Development Seminar Series - Participated and completed the two semester seminar series to improve teaching skills in graduate students and young faculty - Lehigh University (Spring-Fall 2010)
Structural Interpretation of Seismic Data - Exxonmobil Sponsored Short Course offered at the 2009 GSA Meeting in Portland OR.

Departmental Responsibilities -

Student Rep. to Faculty Meetings - Earth and Environmental Sciences Department - Lehigh University (Fall 2011 – Spring 2012)
Student Rep. to the Graduate Instruction Committee - Earth and Environmental Sciences Department Lehigh University: Assisted in reformatting the Qualifying Exam for Ph.D program in EES among other tasks (Fall-Spring 2009-2010)
Tectonics Group Organizer – EES Department Lehigh University (Fall 2009 – Spring 2012) – Weekly seminar where students and faculty lead discussions about their research or recent impactful papers.
Graduate Student Research Symposium - Organizer, Master of Ceremonies, Marketer - EES Department - Lehigh University (Spring 2008 and 2009)
Student Rep. to Faculty Meetings - Earth Sciences Department - Montana State University (Fall 2007 - Spring 2008)
Student Research Colloquium - Organizer, Master of Ceremonies, Session Chair - Earth Sciences Department - Montana State University (Spring 2007 and 2008)

Miscellaneous -
Curriculum Development - Co-Created GIS-based capstone project for energy education curriculum for Lehigh Valley 8th grade students (See Isle of Navitas abstract above) Lehigh University (Spring-Fall 2009)
Visiting Geologist to Elementary Schools - VT (Fall 2003 and Spring 2011), MT (Fall 2007)
Community Education Field Trip Leader to Hyalite Canyon - Bozeman, MT (Fall 2007)
Science Olympiad Event Coordinator - Bozeman, MT (Fall 2006 and Fall 2007)

AFFILIATIONS:
Geological Society of America (2006 to Present)
American Geophysical Union (2008 to Present)
European Geosciences Union (2011 to Present)

FUNDING:
At Lehigh University
Geological Society of America - $3750
Department of Earth and Environmental Sciences Palmer Grant – $6000
At Montana State University
Sigma Xi - $600
Colorado Scientific Society - $1200
American Alpine Club - $1000
Wyoming Geologic Society - $500